

**KU LEUVEN**

DOCTORAL SCHOOL of  
BIOMEDICAL SCIENCES



OMFS  
IMPATH



**UHASSELT**

# Neural and bony changes following oral implant placement



Supervisory Committee:  
Prof. Dr. Reinhilde Jacobs  
Prof. Dr. Ivo Lambrechts

**Dandan Song**

June 2021



KU Leuven  
Biomedical Sciences Group  
Faculty of Medicine  
Department of Imaging & Pathology  
Omfs Impath Research Group



**KU LEUVEN**

DOCTORAL SCHOOL  
BIOMEDICAL SCIENCES

**▶▶ UHASSELT**

# NEURAL AND BONY CHANGES FOLLOWING ORAL IMPLANT PLACEMENT

Dandan SONG

Jury:

Supervisor KU Leuven: *Prof. dr. Reinhilde Jacobs*  
Supervisor University of Hasselt: *Prof. dr. Ivo Lambrichts*  
Chair examining committee: *Prof. dr. Ghislain Opdenakker*  
Chair public defense: *Prof. dr. Tania Roskams*  
Jury members:

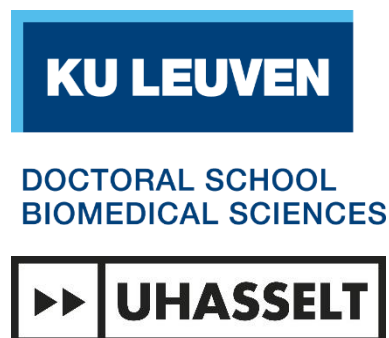
Prof. dr. Constantinus Politis  
Prof. dr. Antoon De Laat  
Prof. dr. Carine Carels  
Prof. dr. Esther Wolfs  
Prof. dr. Krisztian Nagy  
Prof. dr. Ashraf Ayoub

Dissertation presented in partial fulfillment of the requirements for the degree of Doctor in Biomedical Sciences.

June 2021



KU Leuven  
Groep Biomedische Wetenschappen  
Faculteit Geneeskunde  
Department Beeldvorming en Pathologie  
Omfs Impath Onderzoeksgroep



# NEURALE EN BENIGE VERANDERINGEN NA HET PLAATSEN VAN EEN ORAAL IMPLANTAAT

Dandan SONG

Jury:

Supervisor KU Leuven: *Prof. dr. Reinhilde Jacobs*  
Supervisor Universiteit of Hasselt: *Prof. dr. Ivo Lambrechts*  
Voorzitter leescommissie: *Prof. dr. Ghislain Opdenakker*  
Voorzitter openbare verdediging: *Prof. dr. Tania Roskams*  
Juryleden:

Prof. dr. Constantinus Politis  
Prof. dr. Antoon De Laat  
Prof. dr. Carine Carels  
Prof. dr. Esther Wolfs  
Prof. dr. Krisztian Nagy  
Prof. dr. Ashraf Ayoub

Proefschrift voorgedragen tot het behalen van de graad van Doctor in de Biomedische Wetenschappen.



## PREFACE

This doctoral thesis consists of 5 research chapters, preceded by a scientific introduction, and concluded by a general discussion. The research chapters follow the standard IMRAD structure Introduction, Methods, Results and Discussion, and were based on the following peer-reviewed publications:

### **Chapter 1:**

General introduction, Aims and Hypotheses

### **Chapter 2:**

**Song D**, Liang X, Zheng H, Shujaat S, Van Dessel J, Zhong WJ, Ma GW, Lambrichts I, Jacobs R, Peri-implant myelinated nerve fibers: Histological findings in dogs. *J Periodont Res.* 2020;1-7.

### **Chapter 3:**

**Song D**, Huang Y, Van Dessel J, Shujaat S, Orhan K, Vangansewinkel T, Van den Eynde K, Lambrichts I, Roskams T, Politis C, and Jacobs R. Effect of platelet-rich and platelet-poor plasma on peri-implant innervation in dog mandibles. *Int J Implant Dent.* 2019;5(40):1-9.

### **Chapter 4:**

**Song D**, Shujaat S, Huang Y, Van Dessel J, Politis C, Lambrichts I and Jacobs R. Effect of platelet-rich and platelet-poor plasma on 3D bone-to-implant contact: A preclinical micro-CT study. *Int J implant Dent.* 2021;11:1-8.

### **Chapter 5:**

**Song D**, Shujaat S, de Faria Vasconcelos K, Huang Y, Politis C, Lambrichts I and Jacobs R. Diagnostic accuracy of CBCT versus intraoral imaging for assessment of peri-implant bone defect. *BMC Med Imaging.* 2021;21:1-8.

### **Chapter 6:**

**Song D**, Shujaat S, Zhao RT, Huang Y, Shaheen E, Van Dessel J, Orhan K, Vande Velde G, Copopcius R, Pauwels R, Politis C, Jacobs R. In vivo quantification of mandibular bone remodeling and vascular changes in a Wistar rat model: a novel HR-MRI and micro-CT fusion technique. *Imaging Sci Dent.* 2020;50(3):199-208

### **Chapter 7:**

General discussion, Conclusions, and Future perspectives.



## Acknowledgement

*Doing things change things, no doing things, these things are exactly as they were.*

*[House M.D]*

Time flies. Suddenly, I come to the end of this journey of my PhD. While looking back to the journey, so many people stand by my back and support me all the time to whom I would like to express my deepest gratitude at this important time today.

First of all, I appreciate the unique opportunity of undertaking this joint PhD projects in KU Leuven and Hasselt University. I would like to thank Prof. Luc Sels, Rector of KU Leuven, Prof. Bernard Vanheusden, Rector of Hasselt University, Prof. Paul Herijgers, Dean of the Faculty of Medicine of KU Leuven, Prof. Piet Stinissen, Dean of the faculty of Medicine of Hasselt University, Prof. Tania Roskams, chair of the Department of Imaging & Pathology in the KU Leuven allowing me to conduct part of the research in their respective departments.

I am most grateful to those who have made it possible for me to study abroad. In this way, I would like to thank Prof. Reinhilde Jacobs, my main promoter in the KU Leuven, for your continuous support of my PhD study research. I still remember the first day I came to the lab and met you. Although I was very nervous and shy, you were always smiling at me, introduced me to everyone in the team, asked colleague to help me with the accommodation, and encouraged me to talk with others in order to improve my English speaking. Your caring and understanding let me feel incomparable warmth. When I get stuck in my research, your motivation, enthusiasm, patience, and immense knowledge could always help me to overwhelm any challenge. Each time when I make progress towards the goal,

no matter how small step it is, you are always the first one to cheer me on and the happiest one. Your kindness and selflessness impressed me again and again in and out of the lab, which would help me developing myself in the future.

Prof. Ivo Lambrichts, my respected co-promoter in the Hasselt University, helps me open the doors of Hasselt University. I feel so thankful that you always supported me and believed in me through all these years' work even with your busy schedule and your training and teaching in histology will benefit me all of my life.

Here, I would like to specifically offer my thanks to Prof. Xin Liang, my promoter in Dalian Medical University. It's you who opened a new page of my life and changed my life completely. Without your support and help, I would never have thought I could walk out of my country and study abroad. I would never have imagined I could meet so many kind professors and friends. Even though you have left us, your strong mind and positive attitude to life always encourage me. I will keep you in my heart forever.

Besides my promoters, I would like to thank the rest of my thesis committee: Prof. Antoon De Laat, Prof. Constantinus Politis, Prof. Carine Carels, Prof. Ashraf Ayoub, Prof. Krisztian Nagy and Prof. Esther Wolfs for sharing your knowledge, stories, and critical comments. It is a wonderful moment to discuss with you by emails, phones or face-to-face, which I will remember forever. I also gratefully acknowledge Prof. Tania Roskams for chairing the public defense. My sincere gratitude goes to Prof. Annelies Sterckx, Prof. Steven Dymarkowski, Mrs. Bieke Tembuyser, Mrs. Sophie Collart and all the group from Doctoral School Administration for the continue support during these years.

I would like to express my thankfulness to Dr. Yan Huang. It's your help that made the procedure of application of my PhD and even the scholarship more smoothly. And it's your effort in the animal experiment that provided me great data to

conduct my research. And it's your encouragement from the beginning till the end even before the PhD makes me more confidence in research. Wishing you nothing but the best of your life in Belgium.

Sohaib, a special friend and colleague. Your extensive knowledge and perfect writing skills helped me publish my articles efficiently. Every time when I felt depressed or I had some troubles, it was always you who come to help me first and comforted me with your patience and understanding. Your trust brings me a large volume of warmth and happiness. In my mind, you are the best true friend all of my life. I will cherish our friendship in my heart forever.

My heartfelt thanks also goes to every member of the OMFS IMPATH research group for these years' company. I could not have imaged having a better teamwork for my PhD study. Prof. Kaan Orhan, Karla, Mostafa, Emmy, Jeroen, and Yi, many thanks for always being ready to help me. Anna and Myrthel, thank you for offering me the template of the evaluation presentation every year. Fernanda, Ali, Tamara, Clarissa, Francisca, Danieli, Marta, Denise, thanks for sharing the refreshment time, interesting experience with me, help to improve my English and kind suggestion on my research. Although you were only here for months or one year, I will remember those wonderful time we spent together. I am also grateful to Ruiting, Yifei, Jiqing, Hongyang, Xiaotong, Wei, Yan, Yi and so many Chinese friends for their company and for thousands of times that we had parties together.

Special thanks to the Chinese Scholarship Council (CSC) who financially supported this PhD work.

Finally, my grateful heart goes to my beloved family, my parents, my sister, my brother, my brother-in-law, my sister-in-law and all my lovely nephews and nieces. It's your selfless love supporting me spiritually along my way. Also great thanks

to Uncle and Aunt Liang for your caring and praying for me in these years. I hope all of you will be proud of me now! I dedicate this thesis to all of you!

## Table of Contents

|   |     |
|---|-----|
| Preface .....   | I   |
| Acknowledgement.....  | III |
| Table of Contents.....  | VII |
| List of Abbreviations.....  | IX  |
| Chapter 1 - General Introduction, Aims and Hypotheses.....  | 1   |
| 1.1 Innervation of natural teeth.....   | 2   |
| 1.2 Osseoperception.....  | 3   |
| 1.2.1 Evolution of osseoperception.....   | 3   |
| 1.2.2 Evidences of osseoperception.....   | 4   |
| 1.2.2.1 Histological findings of innervation following dental implant treatment.....  | 4   |
| 1.2.2.2 Psychophysical findings in assessment of tactile sensibility following dental<br>implant treatment.....   | 7   |
| 1.2.2.3 Neurophysiological findings in the activation of neurosensory pathway following<br>dental implant treatment.....  | 8   |
| 1.3 Alveolar bone biology.....  | 13  |
| 1.4 Aims and hypotheses.....  | 16  |
| 1.5 References.....   | 18  |
| Chapter 2 - Peri-implant myelinated nerve fibers: Histological findings in dogs.....  | 23  |
| Chapter 3 - Effect of platelet-rich and platelet-poor plasma on peri-implant innervation in dog<br>mandibles.....   | 31  |
| Chapter 4 - Effect of platelet-rich and platelet-poor plasma on 3D bone-to-implant contact: A<br>preclinical micro-CT study.....                                  | 41  |
| Chapter 5 - Diagnostic accuracy of CBCT versus intraoral imaging for assessment of peri-implant<br>bone defect.....   | 51  |
| Chapter 6 - In vivo quantification of mandibular bone remodeling and vascular changes in a Wistar<br>rat model: a novel HR-MRI and micro-CT fusion technique..... | 61  |
| Chapter 7 - General discussion, conclusions and future perspective.....   | 73  |
| 7.1 General discussion.....   | 74  |
| 7.2 Conclusions.....  | 79  |
| 7.3 Future perspectives.....  | 80  |
| 7.4 References.....   | 82  |
| Summary.....  | 88  |
| Samenvatting.....   | 90  |

|  |           |
|--|-----------|
| <b>Scientific Acknowledgement.....</b> | <b>92</b> |
| <b>Personal Contribution.....</b>      | <b>95</b> |
| <b>Conflicts of Interest.....</b>      | <b>96</b> |
| <b>Curriculum Vitae.....</b>           | <b>97</b> |

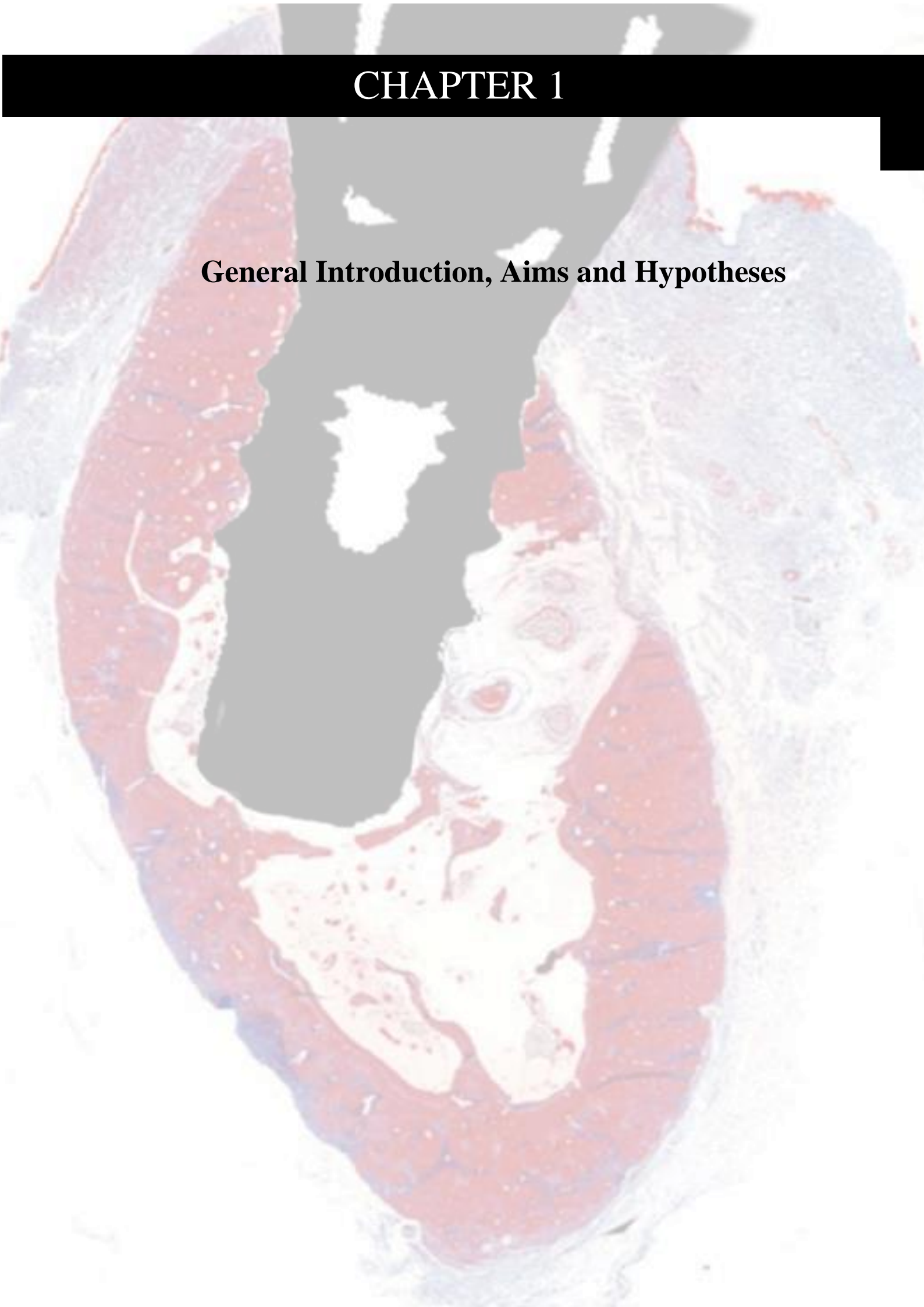
## List of Abbreviations

|      |  |
|------|--|
| PDL  | Periodontal ligament                       |
| AOT  | Anode Oxidized Titanium                    |
| HAC  | Hydroxyapatite-coating                     |
| PIB  | Peri-implant bone                          |
| NPIS | Neurofilament protein immunostaining       |
| TMB  | Thionin methylene                          |
| MTS  | Masson's trichrome                         |
| H&E  | Haemotoxylin and Eosin                     |
| MNF  | Myelinated nerve fibres                    |
| IAS  | Immunoreactive structure                   |
| ATS  | Active tactile sensibility                 |
| PTS  | Passive tactile sensibility                |
| TMJ  | Temporomandibular joint                    |
| SISP | Single-implant-supported prosthesis        |
| MISP | Multi-implant-supported prosthesis         |
| NT   | Natural tooth                              |
| NISP | Non-implant-supported prosthesis           |
| CD   | Complete denture                           |
| OD   | Overdenture                                |
| RL   | Reiz Limen                                 |
| DL   | Difference Limen                           |
| LTS  | Light-touch sensation                      |
| 2PD  | 2-point discrimination                     |
| ATT  | Active tactile threshold                   |
| PTT  | Passive tactile threshold                  |
| TSEP | Trigeminal somatosensory-evoked potentials |
| IOD  | Implant-supported overdenture              |
| BA   | Brodmann's area                            |
| fMRI | Function magnetic resonance imaging        |
| BG   | Basal ganglion                             |
| IIP  | Immediate implant placement                |
| IL   | Immediate loading                          |
| DL   | Delayed loading                            |
| DIP  | Delayed implant placement                  |
| IM   | Intramuscular                              |

|              |   |
|--------------|---|
| EDTA         | Ethylenediaminetetraacetic acid                 |
| ROIs         | Regions of interests                            |
| PRP          | Platelet-rich plasma                            |
| PPP          | Platelet-poor plasma                            |
| TGF- $\beta$ | Transforming growth factor- $\beta$             |
| PDGF         | Platelet-derived growth factor                  |
| TGF          | Transforming growth factor                      |
| IL           | Platelet factor interleukin                     |
| VEGF         | Vascular endothelial growth factor              |
| IGF          | Insulin-like growth factor                      |
| bFGF         | Basic fibroblast growth factor                  |
| NPY          | Anti-neuropeptide Y                             |
| BIC%         | Bone-to-implant contact ratio                   |
| Micro-CT     | Micro-computed tomography                       |
| 2D           | Two-dimensional                                 |
| 3D           | Three-dimensional                               |
| RCF          | Relative centrifugal force                      |
| I.S/TS       | Percent intersection surface                    |
| CBCT         | Cone beam computed tomography                   |
| IO           | Intraoral radiography                           |
| HR-MRI       | High-resolution magnetic resonance imaging      |
| IV           | Intravenous                                     |
| BRONJ        | Bisphosphonate-related osteonecrosis of the jaw |
| ZA           | Zoledronic acid                                 |
| BMD          | Bone mineral density                            |
| MRA          | Magnetic Resonance Angiography                  |
| TOF          | Time-of-flight                                  |
| Tb.Th        | Trabecular thickness                            |
| VOI          | Volume of interest                              |
| BFV          | Blood flow velocity                             |

# CHAPTER 1

## **General Introduction, Aims and Hypotheses**



## 1.1 Innervation of natural teeth

From a microscopic point of view, the nerve fibres innervated in teeth generally come from two parts: pulp and periodontal ligament (PDL) (**Figure 1.1**). First of all, pulp is one only soft tissue in tooth surrounded by dentine and cementum and highly vascularized and innervated<sup>1</sup>. Dental pulp contains pain-related sensation and is innervated by one branch of trigeminal nerves through apical foramen. Two types of fibres were present in the pulp. One is myelinated A-fibres, subclassified by A-delta fibres (90%) and A-beta fibres (10%), which can transmit the low-threshold sensory signals to the brainstem and then to the contralateral thalamus and evoke a sharp pain in the terminate<sup>2,3</sup>. While another is the unmyelinated C-fibres which only can be activated by high threshold stimulation and evoke the slow pain<sup>4</sup>. These sensory functions would disappear following teeth extraction. However, some study reported that nearly a same amount of fibres as natural teeth remains in the inferior alveolar nerve at the bottom of the fresh extraction sockets and vanishes over time<sup>5</sup>.

The periodontal ligament (PDL) is a bundle of specialized connective tissue fibres surrounding the tooth root and attaches to the alveolar bone. The nerve fibres which supply the PDL can be classified based on their functionality as either sensory or autonomic. The sensory nerve fibres are responsible for mechanoreception and nociception, whereas, the autonomic nerve fibres are associated with the vasculature of the periodontal blood vessels.<sup>6,7</sup> The innervation of PDL has been recorded to be most densely at the apex of tooth but sparse toward the cervical margin<sup>8,9</sup>. Both myelinated and unmyelinated nerve fibres are detected in PDL and the large unmyelinated axons are proved as the mechanoreceptive pre-terminals of isolated myelinated axons which have similar location and frequency<sup>8,10</sup>. Afterwards, myelinated axons have also been observed to appear to branch off from the main axon bundles, change direction, and terminate in the cemental portion of ligament. The diameter of myelinated axons is greatest in the apical zone (2-15  $\mu\text{m}$ ) and smaller near to the cervical margin of teeth<sup>8</sup>.

In addition, normal function of stomatognathic system requires perfect anatomic and physiological integration among the jaw bones, teeth, periodontium, and temporomandibular joint through reflex arcs controlled by the neuromuscular system. Proprioceptive feedback plays a significant role in tuning fine motor control and modulating complex mandibular movements, sensory discriminative capabilities, and masticatory protective reflex. In dentate

individuals, this sensory input might be provided by the following two groups of mechanoreceptors. Remote fibres which originate in the temporomandibular joint, oral mucosa, masticatory muscles, periosteum, and even dental pulp, correspond only to discriminating larger particles; whereas, proprioceptors in periodontal ligament can respond to finer stimuli, contributing to specification of direction, magnitude, and the point of attack of the occlusal forces. Removal of proprioceptor fibres in the PDL after tooth extraction might undermine this precision.

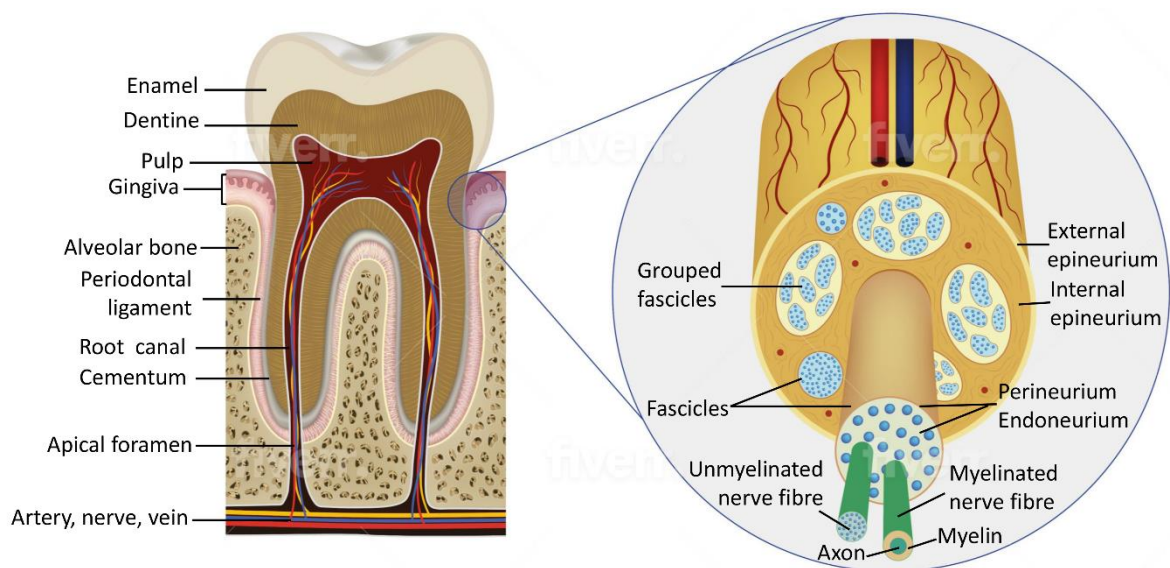


**Figure 1.1.** Structure of tooth and its microscopic innervation and blood supply. Shows typical anatomy of tooth and periodontal tissues.

## 1.2 Osseoperception

### 1.2.1 Evolution of osseoperception

Natural teeth consist of numerous refined tactile sensors known as periodontal mechanoreceptors, and these receptors are responsible for regulation of oral motor function such as chewing and biting based on a sensory feedback pathway signaling to the motor cortex. Following tooth extraction, the PDL may be damaged leading to irreversible damage of the functional mechanoreceptors, thereby affecting the transmission of oral tactile information. This may deteriorate the sensory feedback pathway and sensory-motor interactions, leading to impairment of oral motor function. While oral implants may typically help to replace missing teeth, their role in reactivating the sensory feedback pathway and restoring oral function

remains a matter of debate<sup>11-14</sup>. In general, when comparing conventional fixed and removable prostheses, dental implant and implant-supported prostheses acquire a longer survival rate<sup>15-18</sup> with some improvement but not a complete restoration of oral function, such as tactile function and mastication<sup>11,13,14,19,20</sup>.

Previous studies suggested that bone-anchored prostheses might be capable to improve the (re)innervation pattern in peri-implant region by transmitting mechanical stimuli directly to the bone<sup>21,22</sup>. However, multiple factors, such as low density of nerve fibres, lack of periodontal ligaments and higher tactile threshold levels of implants compared to natural teeth make it difficult for patients to perceive chewing forces and passive occlusal loading. Nevertheless, high chewing force loaded on the implant might cause overload leading to bone resorption and eventual implant failure<sup>21,23,24</sup>. Thus, a proper function is required to maintain the implant longevity and global physiological integration of implant in the human body.

Osseoperception is denoted as the sensory response following mechanical loading evoked by peri-implant mechanoreceptors in absence of functional periodontal ligament mechanoreceptive inputs<sup>25</sup>. The (osseo)mechanoreceptive function should not necessarily come from the bone, yet may also be derived from joint, muscle, mucosa and periosteal tissue which provide mechanosensory information in relation to jaw function and occlusal contact of artificial teeth (**Figure 1.2**)<sup>11,26,27</sup>. The concept of osseoperception initially originated from the studies focusing on restoration of tactile perception in patients with osseointegrated orthopedic artificial limbs following amputation<sup>28</sup>. The first mention on oral function with implants and functional integration of implants dates back to the seventies and eighties when Haraldson and his colleagues pioneered on this problem, after having observed that patients could function quite well with implant supported prostheses despite of the absence of periodontal ligament receptors. They concluded that bite force, masticatory function and tactile function of implant-supported prostheses are somewhat deteriorated yet still within acceptable limits as compared to patients with natural teeth, with considerable improvement over time<sup>29-32</sup>.

## **1.2.2 Evidences of osseoperception**

### **1.2.2.1 Histological findings of innervation following dental implant treatment**

To discover the mechanism of osseoperception, histological studies were performed to

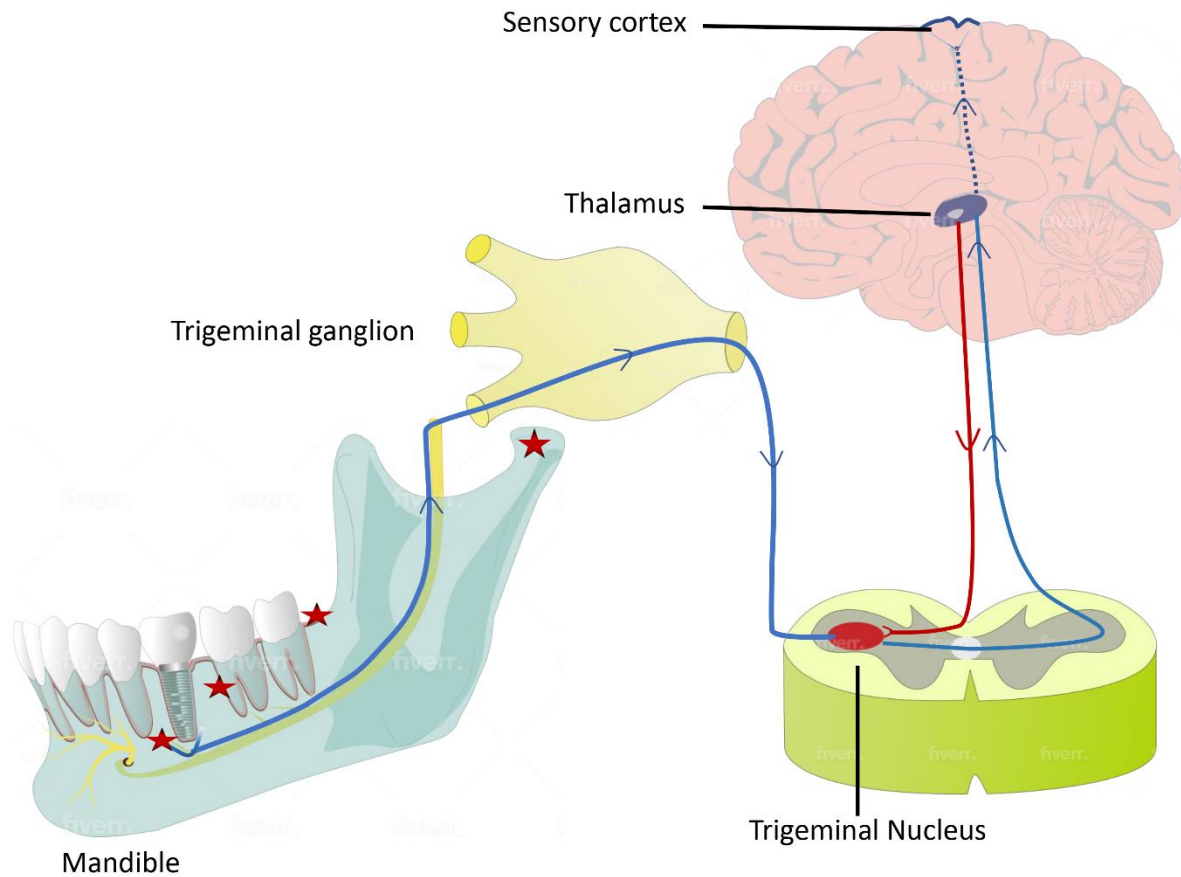


**Figure 1.2. Sensory pathway for tooth/implant stimuli.** Once a stimulus exerted on a tooth, it would activate periodontal sensory endings. This functional mechanoreceptive input might be derived from temporomandibular joint, periosteum, gingiva, periodontal ligaments (PDLs), mucosa, and alveolar bone receptors (red stars), through the trigeminal neurons located at trigeminal ganglion, the signals would be sent to ventral posterior nucleus of thalamus. Lastly, these signals would be replayed to sensory cortex and received by organisms, which eventually forms the complete neurosensory pathway feedback, whereas for implants, some of the mechanoreceptors do no longer play a role.

investigate the pattern of nerve fibres innervated surrounding the implants and the function of mechanoreceptors or axons in the peri-implant tissue. Following the observation of myelinated nerve fibres in the healed extraction sockets<sup>33</sup>, both myelinated and unmyelinated nerve fibres have been observed in the peri-implant bone within a range of 200  $\mu\text{m}$  - 1000  $\mu\text{m}$  from the implant surface in human and animal studies<sup>21,34,35</sup>. The presence of Ruffini mechanoreceptive terminals in peri-implant bone and/or epithelium demonstrate a link with neurosensory

myelinated nerve fibre content<sup>21,36</sup>. Previous animal studies exhibited dense peri-implant bone innervation around loaded implants, whereas a sparsity in innervation was detected in the bone around unloaded implants due to ankylosis with the surrounding bone.<sup>21,35,37</sup> Within a 200~500 µm peri-implant bone perimeter, the density of myelinated nerve fibres was larger in the loaded implant compared to unloaded ones. It was then suggested that immediate implant placement and loading protocol had a positive effect on peri-implant bone innervation<sup>35</sup>. Besides, the greater pattern of nerve fibres mostly observed in the apical region of the endosseous dental implant reinforced this evidence. In addition, the human study quantified nerve fibres in the peri-implant bone, in which the authors collected 12 failed implants from 10 patients and counted both unmyelinated and myelinated nerve fibres. The results added more convincing evidence with regard to the presence of functional nerve fibres in peri-implant bone<sup>35</sup>. Details can be found in Table 1.1. While tooth extraction may lead to damage of the myelinated nerve fibres, remaining functional nerve fibres and their endings in PDL residue might be able to regenerate and recover the sensory feedback. As is common knowledge, axons in the proximal stump randomly produce a large number of collateral and terminal sprouts that advance distally within the initial days or weeks following transection of the nerve trunk<sup>38</sup>. Afterwards, some of these sprouts will approach the proliferation of Schwann Cells in the distal segment or grow into connective tissue in the nerve trunk or some of them will disappear. Thus, it can be assumed that some interference during the process of sprouting plays a critical role in regeneration of nerve fibres in the defect regions<sup>38</sup>.

Literature demonstrates that periodontal mechanoreceptors may remain within the bone after tooth extraction and are successfully stimulated in the healed extraction sockets<sup>33</sup>. The potential to improve this sensory function by boosting the restoration or regeneration of nerve fibres following implant placement has received growing attention. Various methods have been used to reach out this goal, such as changing the type of implant placement and loading<sup>21,35</sup> and modifying implant surface structure<sup>21</sup>.

While assessing different protocols of implant placement and loading, some evidences seemed to support immediate implant placement with immediate loading as hypothetically this concept could allow to leave the damaged nerves to be stimulated and activated by immediate loading, preventing retrograde degeneration of nerve tissue after tooth extraction<sup>35</sup>. Indeed, some

preventing retrograde degeneration of nerve tissue after tooth extraction<sup>35</sup>. Indeed, some evidences revealed that stimulation of functional implants accelerated proliferation of adjacent Schwann cells and detected that loading pressure on regenerated nerve fibres surrounding the implants could conduct axons differentiation and guide sprouting to connect with Schwann cells allowing to reorganise bony innervation<sup>39,40</sup>. However, and even then, it remains unclear whether restored nerve fibres have a sensory function. Besides, there is not enough evidence proving that modification of implant surface structure and application of growth factors increase the amount of nerve fibres. Histological evidence associated with the peri-implant innervation is scarce. Further studies are required with a standardized methodology for evaluating osseoperception within the peri-implant region. In addition, techniques for enhancing regeneration of nerve fibres following implant placement need to be developed and thus improve osseoperception.

#### **1.2.2.2 Psychophysical findings in assessment of tactile sensibility following dental implant treatment**

Psychophysical evidence mainly derived from the evaluation on active tactile sensibility (ATS) and passive tactile sensibility (PTS). Various thin foils with different materials, such as steel, copper, aluminium, and gold, were employed in assessment of the threshold of ATS<sup>14,41-45</sup>. Technically, the foils would be fixed on the occlusal surface of natural teeth or implant-supported prostheses, and then, patients were required to bite onto the foils. The thickness of foil was recorded when patients had given a positive response. The ascending and descending test order for the thickness of foils was adopted and 50% value were commonly recorded as ATS threshold<sup>43,44,46</sup>. In contrast, the pressure exerted by a custom-made stimulator manually or semi-automatically on the natural teeth, implant-supported prostheses, or on the mucosa adjacent to the implant and natural teeth, was detected as PTS threshold<sup>14,20,47-50</sup>. All current outcomes could prove that ATS and PTS have a higher threshold for implant-supported prostheses than for natural teeth, while being considerably lower than the non-implant-supported prostheses. Details are shown in Table 1.2. Specifically, the ATS threshold is 4 to 5 times higher than natural teeth but the PTS threshold is more than 50 times higher than natural teeth. The different receptors activated by active tactile force and passive tactile force can

explain this large discrepancy. Indeed, for ATS some remote mechanoreceptors from the temporomandibular joint (TMJ), muscles, mucosa and periosteum may contribute to ATS, while PTS electively activate periodontal ligament receptors. Nevertheless, all edentulous patients seem to function well after rehabilitation with a bone-anchored prosthesis.

Considering the investigated factors in these studies, such as age, gender, implant surface structure, implant geometry (implant length and diameter), type of implant surface and position of the implant, none of these factors could be convincingly linked to have any positive or negative impact on tactile function<sup>13,14,41,43,44,46,47,49-53</sup>. Although the threshold of tactile sensibility was significantly higher in posterior than that in anterior in natural teeth, which might be understood by the larger number of PDLs and thicker nerve bundles in the posterior region<sup>43</sup>, one study was unable to prove that the position of implants would influence the tactile sensibility. Another study<sup>14</sup> showed some differences in implant surface, albeit not significant. A variety of study designs with a wide range of force intensity, uncontrollable experimental design, unsubstantial sample sizes and a critical influence of the psychophysical set-up are reasons for such inconsistent findings.

### **1.2.2.3 Neurophysiological findings in activation of neurosensory pathway following dental implant treatment**

The analysis of trigeminal somatosensory-evoked potentials (TSEP) was performed in 2 studies with a constant-current stimulator for delivering bipolar electrical square-wave stimuli onto the abutment of endosseous implants<sup>54,55</sup>. In contrast to mechanical stimuli, the electrical stimulus led to direct stimulation of primary afferent axons which bypassed the receptors. The TSEP showed variability in polarity, latency and number of waves. Both researches showed the presence of trigeminal waves and activation of other neural structures in the peri-implant region.

The integrated sensory feedback pathway of the stomatognathic system is constituted of mechanoreceptors, neurons, and primary sensitive cortex. The damage of periodontal ligament after tooth extraction and implant placement induces the loss of the mechanoreceptors and free nerve endings, which results in disruption of the sensory feedback pathway. Evidence for motivation of TSEP in the cortex by electrical stimulation of oral implants makes it acceptable

that the sensory feedback pathway remain function in the patients with osseointegrated implant treatment. Since the healthy periodontal mechanoreceptors were proved to have projections on cortical somatosensory areas, fMRI analysis demonstrated activated areas of primary and secondary sensory-motor cortex in patients with implant-supported prostheses. Though activation was found less than natural teeth but fairly higher than non-implant-supported complete denture<sup>56,57</sup> (Table 1.3). The activated function in patients with single implant-supported prosthesis were closer to those of natural teeth. It could thus be hypothesized that after tooth extraction and implant placement there may be some cortical plasticity involved, often inducing bilateral sensory activations (Table 1.4). Furthermore, the discrepancy in brain cortical plasticity areas in the different groups with various number of implant-supported prostheses could have resulted from the different amount of the adjacent receptors and remote receptors, which possibly exist in the peri-implant bone and the TMJ, mucosa, muscles and periodontium, that were activated by the stimulation during the projection of fMRI. Due to the limited number of studies and the limited sample size, the current findings were not able to provide more convincing evidence regarding the functional mechanoreceptors in the peri-implant bone.

**Table 1.1. Histological evidences for presence of osseoperception through measurement of nerve fibres.**

| Author (year)           | Subjects (N) |     | Implant            |                   |           |                  | Measurement |                    |                     |                      | Outcome                    |  |
|-------------------------|--------------|-----|--------------------|-------------------|-----------|------------------|-------------|--------------------|---------------------|----------------------|----------------------------|--|
|                         | Species      | No. | Surface structure  | Implant placement |           | Loading protocol |             | Region of interest | Staining            | Parameter of testing | Primary                    | Secondary  |
|                         |              |     |                    | Delayed (T)       | Immediate | Delayed (T)      | Immediate   |                    |                     |                      |                            |  |
| Wada S, et al (2001)    | Mongrel dog  | 3   | AOT /HAC           | Y (16 wks)        | —         | Y (10 wks)       | —           | Y                  | NPIS                | MNF (DS)             | DS: Loaded> unloaded       | No difference in surface structure   |
| Huang Y, et al (2014)   | Beagle dog   | 6   | Custom-made thread | Y (8wks)          | Y         | Y (4 wks)        | Y           | —                  | MTS/HIS (NF or NPY) | MNF (DS & DM)        | DS: ISP > NE; DM: NE > ISP | DS: IIP > DIP; IL > DL & gingival > apical > coronal > middle<br>DM: IIP>DIP; DL >IL & middle > coronal > apical> gingival; No difference in regions |
| Corpas LD, et al (2014) | Human        | 10  | ?                  | Y (?)             | —         | Y (?)            | Y           | —                  | TMB                 | (Un) MNF (number)    | MNF: 27 (5.13µm)           | Un-MNF: 7  |

Abbreviation: No: number; T: Time; ?: Unclear; Y: Yes; AOT: Anode Oxidized Titanium; HAC: Hydroxyapatite-coating; PIB: Peri-implant bone; NPIS: Neurofilament protein immunostaining; TMB: Thionin methylene; MTS: Masson's trichrome; H&E: Haematoxylin and Eosin; MNF: Myelinated nerve fibres; DS: Density; Un-MNF: Unmyelinated nerve fibres; DM: Diameter; IAS: Immunoreactive structure.

**Table 1.2. Psychophysical evidences for presence of osseoperception through measurement of threshold level of sensory sensibility.**

| Author(year)            | Population |              |            |            |     |              | Methodology |        |  | Outcome  |  |  |   |
|-------------------------|------------|--------------|------------|------------|-----|--------------|-------------|--------|--|--|--|--|---|
|                         | Test       |              |            | Control    |     |              | Device      | Method | Testing area   | Primary  | Secondary  |  |   |
|                         | No.        | Age (range)  | Situation  |            | No. | Age (range)  |             |        |  |  |  | Situation  |   |
|                         |            |              | SISP (No.) | MISP (No.) |     |              |             |        |  |  |  | NT(No.)  | NIPS (No.)  |
| Jacobs R, et al (1991)  | 25         | 56.6 (29-77) | Y (19)     | Y (6)      | 12  | 28 (18-49)   | Y (12)      | Y (6)  | Foils (Steel)  | RL: method of limits (↑&↓);<br>DL: constant stimuli (thicker or thinner) | 1st premolar   | RL & DL CD/OD > ISP/ISP > ISP/NT > NT/NT                   | No difference in gender & jaw type  |
| Jang KS, et al (2001)   | 30         | 50.8 (?)     | -          | Y (30)     | 20  | 45.6         | Y (10)      | Y (10) | Thickness threshold:<br>Foil / Lateral pressure: tension meter | Method of limit (↑) Test 3x  | Central incisor to the second molar / Labial or buccal surface | CD/CD > ISP/CD > ISP/ISP > NT/NT                           | No difference in regions  |
| Enkling N, et al (2007) | 62         | 46 (19-86)   | Y (62)     | -          | 62  | 46 (19-86)   | Y (62)      | -      | Foils (Copper)   | Method of limits (↑&↓)   | Anterior region/posterior region                               | 50% value ISP/ISP > NT/NT                                  | No difference in regions, surface structure, geometry, period of edentulism, period of prosthesis function & gender |
| Batista M, et al (2008) | 29         | 55.1 (?)     | -          | Y (29)     | 41  | 43.6         | Y (24)      | Y (17) | Foils (Aluminum)   | Method of limits (↓)   | Occlusal surface   | 50% value CD/CD > ISP/ISP > ISP/NT > NT/NT                 | No difference age and period of prosthesis function   |
| Enkling N, et al (2010) | 62         | 45.6 (?)     | Y (62)     | -          | -   | -            | -           | -      | Foils (Copper)   | Computer-assistant design random thickness (Test 10x)                    | Teeth or implant   | 50% value ISP/ISP (20.2 ± 10.9 μm)                         | Surface structure: TPS > Machined > SAE; No difference in age and gender  |
| Enkling N, et al (2012) | 32         | 38.9 (25-63) | Y (32)     | -          | 32  | 38.9 (25-63) | Y (32)      | -      | Foils (Copper)   | Computer-assistant design random thickness (Test 10x)                    | Teeth or implant   | 50% value ISP/ISP (19.7 ± 11.1 μm) > NT/NT (16.1 ± 9.4 μm) | 50% value anterior > posterior (significance in NT/NT but no in ISP/ISP)  |
| Kazemi M, et al (2014)  | 25         | 30.1 (21-66) | Y (50)     | -          | 25  | 30.1 (21-66) | Y (50)      | -      | foils (Gold)   | Computer-assistant design random thickness (Test 5x)                     | Maximum interspation (posterior) and edge-to-edge (anterior)   | ATT: ISP/ISP (30.6 ± 9.15 μm) > NT/NT (21 ± 7.05 μm)       | No difference in regions, surface structure & gender  |

| Jacobs R, et al (1993)        | 31 | 55.7 (24-88) | Y (5)   | Y (26) | 10 | 30 (20-51)   | Y (10)  | -      | Solenoid-driven stimulating   | Method of limits (↑&↓)                               | Incisal edge of teeth or implant in both maxilla and mandible                          | RL: ISP > NT & OD > ISP > NT  | No difference in period of prosthesis function & age                                     |
|-------------------------------|----|--------------|---------|--------|----|--------------|---------|--------|---|--|--|---|--|
| Jacobs R, et al (2001)        | 24 | 51.7 (26-65) | Y (8)   | Y (16) | 16 | 53 (48-64)   | Y (8)   | Y (8)  | LTS: Semmes-Weinstein monofilament sensory testing system; 2PD: Vibrotactile test-modified HC-200 hearing aid | Method of limits (↑&↓)                               | LTS & 2PD: buccal side of the alveolar mucosa; Vibrotactile: upper teeth or prosthesis | LTS: CD > ISP > NT; 2PD: CD > ISP = NT; Vibrotactile: CD > ISP > NT | -  |
| El-Sheikh AM, et al.(2004)    | 20 | 65.1 (50-82) | -       | Y (20) | 20 | 65.1 (50-82) | -       | Y (20) | Custom-made device  | Method of limits (↑)                                 | Impression copings   | ISP 3.1-15.7N   | No difference in period of implant placement, implant separation, geometry, age & gender |
| Habre-Hallage P, et al (2010) | 9  | ? (19-32)    | Y (9)   | -      | 9  | ? (19-32)    | Y (9)   | -      | Von Frey filament   | Method of limits (↑)                                 | Gingival   | LTS: ISP ≈ NT; 2PD: ISP > NT  | No difference in period of implant placement and prosthesis function                     |
| Grieznis L, et al (2010)      | 29 | ? (21-71)    | Y (43)  | -      | 29 | ? (21-71)    | Y (81)  | -      | Computer-controlled custom-made pressure sensitive device   | Method of limits (↑) Test 3x                         | Teeth or implant   | PTT: ISP > NT   | No difference in NT with or without ET & gender  |
| Hsieh WW, et al (2010)        | 10 | -            | Y (10)  | -      | 10 | -            | Y (10)  | -      | Vibrational transducer  | Method of limits (↑)                                 | Adjacent tooth and implant   | VAS: ISP < NT   | High intensity of vibration reduced the difference of ISP & NT                           |
| Negahdari R, et al (2019)     | 45 | -            | Y (135) | -      | 45 | -            | Y (135) | -      | Foils (gold)  | Computer-assistant design random thickness (Test 5x) | Maximum intercuspation (posterior) and edge-to-edge (anterior)                         | ATT: Pontic > ISP > NT  | -  |

Abbreviation: SISP: Single-implant-supported prosthesis; MISP: Multi-implant-supported prosthesis; NT: Natural tooth; NISP: Non-implant-supported prosthesis; CD: Complete denture; OD: Overdenture; RL: Reiz Limen; DL: Difference Limen; LTS: Light-touch sensation; 2PD: 2-point discrimination; ATT: Active tactile threshold; PTT: Passive tactile threshold; Primary outcome: implant(s)-supported prosthesis VS natural tooth (teeth) or non-implant-supported prosthesis; Secondary outcome: Involved outcome

**Table 1.3.** Function brain area with natural dentition (ND), single-implant-supported prosthesis (SISP), implant-fixed denture (IFD), implant-supported overdenture (IOD) and conventional complete denture (CD).

| Brain area                   | BA  | ND | SISP | IFD | IOD | CD |
|------------------------------|-----|----|------|-----|-----|----|
| Postcentral gyrus            | 1   | √  |      |     |     |    |
| Primary somatosensory cortex | 3   | √  |      | √   |     |    |
| Primary motor cortex         | 4   | √  | √    | √   |     |    |
| Precentral gyrus             | 6   | √  | √    |     | √   |    |
| Parietal gyrus               | 7   | √  | √    |     |     |    |
|                              | 9   | √  | √    |     |     |    |
| Prefrontal cortex            | 10  |    |      | √   |     |    |
|                              | 11  |    |      | √   |     | √  |
| Insula                       | 13  | √  |      | √   |     |    |
| Middle temporal gyrus        | 21  | √  |      | √   |     |    |
|                              | 22  | √  |      | √   |     |    |
|                              | 37  | √  |      |     |     |    |
|                              | 39  | √  |      |     |     |    |
| Supramarginal gyrus          | 40  | √  | √    |     |     |    |
| Broca's area                 | 44  |    |      | √   | √   |    |
|                              | 45  | √  | √    | √   | √   |    |
| Prefrontal cortex            | 46  | √  | √    |     |     | √  |
|                              | 47  | √  |      | √   |     | √  |
| Basal ganglion               | BG  |    |      | √   | √   |    |
| Parietal operculum           | OP1 | √  | √    |     |     |    |
|                              | OP2 | √  |      |     |     |    |
|                              | OP3 | √  |      |     |     |    |
|                              | OP4 | √  |      |     |     |    |

Abbreviation: BA: Brodmann's area (blood oxygen level dependent signals)

### 1.3 Alveolar bone biology

Alveolar bone is part of maxilla and mandible which supports the teeth by forming the 'other' attachment for fibres of the periodontal ligament. It consists of two plates of cortical bone separated by spongy bone (**Figure 1.3**). In some areas, the alveolar bone is thin with no spongy bone. The alveolar bone and cortical plates are thickest in the mandible while thinner in the maxilla bone.

The cortical bone was also termed as compact bone, which is a hard-outer layer of bone, composing of compact bone tissue with minimal gaps and spaces. Cortical bone porosity is 5-30% and account for 80% of the total bone mass of an adult skeleton. The spongy bone is termed as the trabecular bone as well, which is composed of an open cell porous network, which makes the overall organ lighter and offers room for blood vessels and marrow. Trabecular bone accounts for the remaining 20% of total bone mass but has nearly ten times of the surface area of compact bone. In comparison

network, which makes the overall organ lighter and offers room for blood vessels and marrow. Trabecular bone accounts for the remaining 20% of total bone mass but has nearly ten times of the surface area of compact bone. In comparison to the other type of osseous tissue, it is softer, weaker, less dense and less stiff with a porosity range of 30-90%. Alveolar bone is constantly being remodeled to adapt to changes in occlusal load. Alterations in resorption or restoration and the interplay of these two phenomena are known as remodeling<sup>58</sup>. Bone remodeling is an active and dynamic process potentiated by the processes of bone deposition by osteoblasts and bone resorption by osteoclasts in a sound balance. There is constant remodeling in all bones of body in response to various stimuli. Undoubtedly, a critical change is going to happen in the alveolar bone following the tooth extraction and implant placement. The loss of tooth can result in the resorption of bone while the loading transmitted by the implants can enhance the regeneration of bone. Unlike the connection between the teeth and bone, the surface of load-carry implant is directly connected to the ordered, living bone, which is termed as implant osseointegration. It has been described that the simultaneous contact and distant osteogenesis at the implant surface and osteotomy wall lead to new bone synthesis and a direct bone to implant contact without inter vening connective tissue<sup>59</sup>.

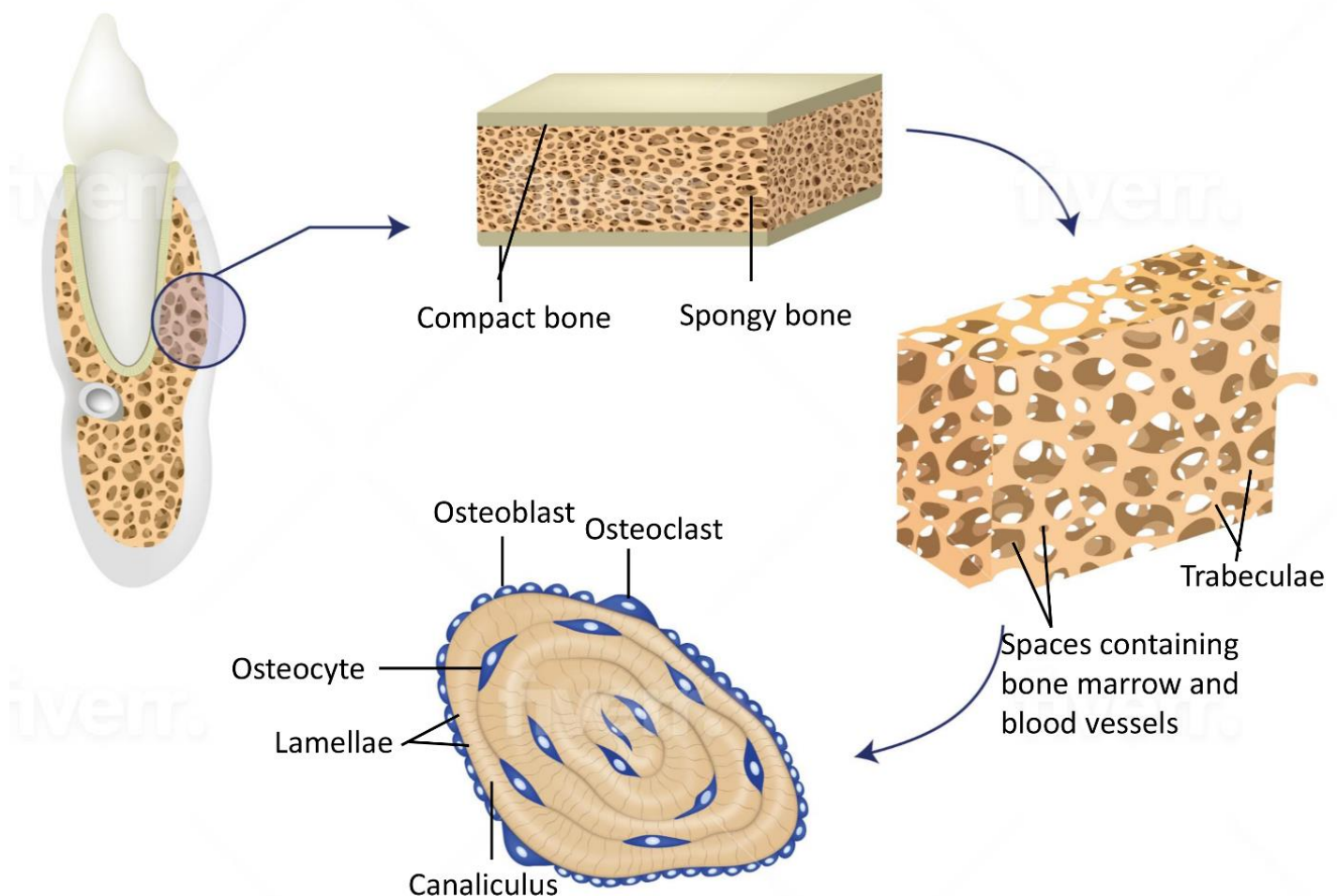


**Figure 1.3. Microscopic compact and spongy bone.**

**Table 1.4. Neurophysiological evidences for presence of osseoperception utilizing function magnetic resonance imaging (fMRI) & trigeminal somatosensory evoked potentials (TSEPs).**

| Author(year)                   | Subjects      |              |            |            |     |               |           |            |  |  | Methodology                    |  |  | Outcome |           |
|--------------------------------|---------------|--------------|------------|------------|-----|---------------|-----------|------------|--|--|--------------------------------|--|--|---------|-----------|
|                                | Testing group |              |            |            |     | Control group |           |            |  |  | Device                         | Method   | Testing area   | Primary | Secondary |
|                                | No.           | Age (range)  | Situation  |            | No. | Age (range)   | Situation |            |  |  |                                |  |  |         |           |
|                                |               |              | SISP (No.) | MISP (No.) |     |               | NT        | NISP (No.) |  |  |                                |  |  |         |           |
| Swinnen A, et al (2000)        | 15            | -            | -          | Y (15)     | 15  | -             | -         | -          | -  | Constant-current stimulator                              | Square-wave stimuli (↑ 2Hz) 2X | Abutments  | Latency peak 9-15ms (channel 1,3,4) prominent and consistent; 2.5-28ms & 19-25ms (channel 2&4) | -       |           |
| Van Loven K, et al (2000)      | 15            | 58 (35-69)   | -          | Y (15)     | -   | -             | -         | -          | Constant-current stimulator  | Square-wave stimuli (↑ 2Hz)                              | Abutments                      | Positive wave 18-25ms (C'6 position); Negative wave 12-17ms; Longer-latency waves 35-42 ms   | -  |         |           |
| Yan C, et al (2008)            | 12            | 58.8 (48-71) | -          | Y (12)     | 8   | 61.5 (48-72)  | -         | Y (8)      | fMRI   | Clenching & Rest (15s) Scanned in the rest position (6X) | Brain                          | ISP: Bilateral SI (BA3) & MI (BA4); Broca's area (BA44,45), PFC BA 11,46,47), the middle temporal gyrus (BA21,22), BG, & the insula (BA13)   | No difference in retention type, the period of prosthesis function, age & gender               |         |           |
| Habre-Hallage P, et al. (2012) | 9             | 39.7 (?)     | Y (9)      | -          | 10  | 34.3          | Y (10)    | -          | 3.0 T fMRI & Von fray filaments & stimulation device with a constant frequency of 1 Hz | Fix force 9300g, 180g & 100g0                            | Brain                          | Lager heterogeneity in the activation pattern in implant group; Contralateral supra-marginal gyrus, inferior frontal gyrus bilaterally and contralateral medial frontal gyrus are unique for ISP | No difference in incisor and canine  |         |           |

Abbreviation: SISP: Single-implant-supported prosthesis; MISP: Multi-implant-supported prosthesis; NT: Natural tooth; NISP: Non-implant-supported prosthesis; fMRI: Functional magnetic resonance imaging; BA: Brodmann's areas; BG: Basal ganglion.

## 1.4 Aims and Hypotheses

The phenomenon of osseoperception following oral implant placement has been previously confirmed by various psychophysical, neurophysiological, and histological studies. However, lack of evidence exists related to the application of different methodologies for enhancing the osseoperception. Therefore, the overall objective of this PhD project was to assess the neural and bony changes following oral implant placement and to investigate a potential method to improve the osseoperception in the peri-implant bone region. **The general hypothesis was that different implant placement and loading protocols and the application of autologous plasma would influence the peri-implant bone innervation and alveolar bone remodeling at the interface of the bone-to-implant contact.** Subobjectives are divided into five chapters, mentioning the respective hypotheses:

### Chapter 2:

Occlusal loading plays a vital role in jaw function with periodontal innervation around the teeth having a crucial role in load transmission and sensory cortex stimulation. However, studies unraveling the potential links between true mechanoreceptive function and their histological presence remains rare. Furthermore, evidence is lacking on how nerve fibers in the peri-implant bone region would be affected by the various loading protocol following dental implant placement.

**Objective:** To study the differential effect of various implant placement and loading protocols on peri-implant innervation.

**Hypothesis:** Immediate implant placement and loading would enhance the peri-implant innervation.

### Chapter 3:

Autologous plasma fractions, such as platelet-rich plasma (PRP) and platelet-poor plasma (PPP) have been employed for stimulating new bone formation, angiogenesis, and peripheral nerve regeneration. It has been revealed that PRP could benefit for the restoration of nerve defect. Nevertheless, studies on the effect of PRP and PPP on the (re)innervation in the peri-implant bone region is rare.

**Objective:** To study the potential effect of adding PRP and PPP to implant placement on peri-implant innervation.

**Hypothesis:** Local application of PRP during implant placement could improve the peri-implant (re) innervation while PPP has no effect.

### Chapter 4:

Various parameters have been reported to influence the BIC levels, such as, implant type and size, implant surface treatment, bone quality and quantity, implant loading conditions, and forces exerted

on implant. Recently, multiple growth factors, most commonly, platelet-derived growth factors have been utilized for enhancing BIC. It is suggested to improve implant stability and earlier osteogenesis with plasma containing higher concentration of platelets. However, there is lack of evidence related to the influence of different platelet-derived plasma concentrations on the 3D BIC at follow-up.

**Objective:** To study the potential effect of adding PRP and PPP to implant placement on peri-implant bone apposition.

**Hypothesis:** Local application PRP during implant placement might enhance the 3D BIC% while PPP has no effect.

### **Chapter 5:**

Since intraoral imaging has certain limitations such as 2D representation of three-dimensional (3D) anatomical structures, geometric distortion, lower spatial resolution, and image magnification which underestimates the defect. Furthermore, their inability to diagnose and distinguish buccally and lingually located defects may lead to an inaccurate representation of the bone defect. Cone beam computed tomography (CBCT) has been proposed and recommended by various studies as a modality of choice for assessment of periodontal bone defects. Nevertheless, only a few studies are available assessing the superiority of CBCT over 2D imaging for the assessment of peri-implant bone defects.

**Objective:** To study the feasibility of using of 3D CBCT imaging for in vivo follow-up of bony changes following implant placement in animals.

**Hypothesis:** 3D CBCT imaging has higher accuracy in the detection of peri-implant bone defect than 2D intraoral (IO) imaging.

### **Chapter 6:**

The potential of utilizing co-registered intermodal imaging for accessing bone structure and micro-vascularization at follow-up remains unclear. Besides, the studies related to bone remodeling assessment and blood flow velocity at follow-up are lacking. Even if histomorphometric analysis is usually considered as gold standard, it prevents assessing the evolution of bone changes over time unless applying a multifold sample size of the animals.

**Objective:** To study co-registration of micro-CT and HR-MRI imaging for in vivo follow-up of bony changes following implant placement in animals.

**Hypothesis:** 3D imaging tools micro-CT and HR-MRI may allow to combine to detect early bony change signs and depict vascular changes.

## 1.5 References

1. Schuh C, Benso B, Aguayo S. Potential Novel Strategies for the Treatment of Dental Pulp-Derived Pain: Pharmacological Approaches and Beyond. *Front Pharmacol.* 2019;10:1068.
2. Abd-Elmeguid A, Yu DC. Dental pulp neurophysiology: part 1. Clinical and diagnostic implications. *J Can Dent Assoc.* 2009;75(1):55-59.
3. Langenbach F, Naujoks C, Smeets R, et al. Scaffold-free microtissues: differences from monolayer cultures and their potential in bone tissue engineering. *Clin Oral Investig.* 2013;17(1):9-17.
4. Yu C, Abbott PV. An overview of the dental pulp: its functions and responses to injury. *Aust Dent J.* 2007;52(1 Suppl):S4-16.
5. Heasman PA. The myelinated fibre content of human inferior alveolar nerves from dentate and edentulous subjects. *J Dent.* 1984;12(4):283-286.
6. Trulsson M. Sensory-motor function of human periodontal mechanoreceptors. *J Oral Rehabil.* 2006;33(4):262-273.
7. Lambrechts I, Creemers J, Van Steenberghe D. Periodontal neural endings intimately relate to epithelial rests of Malassez in humans. A light and electron microscope study. *J Anat.* 1993;182 ( Pt 2)(Pt 2):153-162.
8. Loescher AR, Holland GR. Distribution and morphological characteristics of axons in the periodontal ligament of cat canine teeth and the changes observed after reinnervation. *Anat Rec.* 1991;230(1):57-72.
9. Long A, Loescher AR, Robinson PP. A quantitative study on the myelinated fiber innervation of the periodontal ligament of cat canine teeth. *J Dent Res.* 1995;74(6):1310-1317.
10. Aker FD. Innervation of rat molar teeth: II. A quantitative analysis of primary sensory neurons innervating a mandibular molar tooth. *Anat Rec.* 1987;219(2):186-192.
11. Jacobs R, van Steenberghe D. From osseoperception to implant-mediated sensory-motor interactions and related clinical implications. *J Oral Rehabil.* 2006;33(4):282-292.
12. Van Steenberghe D, Jacobs R. Jaw motor inputs originating from osseointegrated oral implants. *J Oral Rehabil.* 2006;33(4):274-281.
13. Jacobs R, van Steenberghe D. Comparative evaluation of the oral tactile function by means of

- teeth or implant-supported prostheses. *Clin Oral Implants Res.* 1991;2(2):75-80.
14. Jacobs R, van Steenberghe D. Comparison between implant-supported prostheses and teeth regarding passive threshold level. *Int J Oral & Maxillofac Implants.* 1993;8(5):549-554.
  15. Del Fabbro M, Corbella S, Taschieri S, Francetti L, Weinstein R. Autologous platelet concentrate for post-extraction socket healing: A systematic review. *Eur J Oral Implantol.* 2014;7(4).
  16. Gotfredsen K. A 10-year prospective study of single tooth implants placed in the anterior maxilla. *Clin Implant Dent Relat Res.* 2012;14(1):80-87.
  17. Buser D, Janner SF, Wittneben JG, Brägger U, Ramseier CA, Salvi GE. 10-year survival and success rates of 511 titanium implants with a sandblasted and acid-etched surface: a retrospective study in 303 partially edentulous patients. *Clin Implant Dent Relat Res.* 2012;14(6):839-851.
  18. Fischer K, Stenberg T. Prospective 10-year cohort study based on a randomized controlled trial (RCT) on implant-supported full-arch maxillary prostheses. Part 1: sandblasted and acid-etched implants and mucosal tissue. *Clin Implant Dent Relat Res.* 2012;14(6):808-815.
  19. Jacobs R, van Steenberghe D. Qualitative evaluation of the masseteric poststimulus EMG complex following mechanical or acoustic stimulation of osseointegrated oral implants. *Int J Oral Maxillofac Implants.* 1995;10(2):175-182.
  20. Jacobs R, Wu CH, Goossens K, Van Loven K, van Steenberghe D. Perceptual changes in the anterior maxilla after placement of endosseous implants. *Clin Implant Dent Relat Res.* 2001;3(3):148-155.
  21. Wada S, Kojo T, Wang YH, et al. Effect of loading on the development of nerve fibers around oral implants in the dog mandible. *Clin Oral Implants Res.* 2001;12(3):219-224.
  22. Jahangiri L, Hessamfar R, Ricci JL. Partial generation of periodontal ligament on endosseous dental implants in dogs. *Clin Oral Implants Res.* 2005;16(4):396-401.
  23. Ma L, Xiang L, Yao Y, Yuan Q, Li L, Gong P. CGRP-alpha application: A potential treatment to improve osseoperception of endosseous dental implants. *Med Hypoth.* 2013;81(2):297-299.
  24. Weiner S, Sirois D, Ehrenberg D, Lehrmann N, Simon B, Zohn H. Sensory responses from loading of implants: a pilot study. *Int J Oral Maxillofac Implants.* 2004;19(1):44-51.

25. Van Steenberghe D. From osseointegration to osseoperception. *J Dent Res.* 2000;79(11):1833-1837.
26. Klineberg I, Murray G. Osseoperception: sensory function and proprioception. *Advances Dent Res.* 1999;13:120-129.
27. Klineberg I, Calford M, Dreher B, et al. A consensus statement on osseoperception. *Clin Exper Pharmacol Physio.* 2005;32(1-2):145-146.
28. Brånemark P. How the concept of osseoperception evolved. In: Jacobs R, ed. *Osseoperception.* Leuven: Catholic University Leuven.1998:43-46.
29. Haraldson T. *Functional evaluation of bridges on osseointegrated implants in the edentulous jaw.* Goteborg, University of Goteborg; 1979.
30. Haraldson T, Zarb G. A 10-year follow-up study of the masticatory system after treatment with osseointegrated implant bridges. *Scand J Dent Res.* 1988;96(3):243-252.
31. Lundqvist S, Haraldson T, Lindblad P. Speech in connection with maxillary fixed prostheses on osseointegrated implants: a three-year follow-up study. *Clin Oral Implants Res.* 1992;3(4):176-180.
32. Lundqvist S, Haraldson T. Oral function in patients wearing fixed prosthesis on osseointegrated implants in the maxilla. *Scand J Dent Res.* 1990;98(6):544-549.
33. Linden R, Scott B. The effect of tooth extraction on periodontal ligament mechanoreceptors represented in the mesencephalic nucleus of the cat. *Arch Oral Biol.* 1989;34(12):937-941.
34. Corpas Ldos S, Lambrichts I, Quirynen M, et al. Peri-implant bone innervation: histological findings in humans. *Eur J Oral Implantol.* 2014;7(3):283-292.
35. Huang Y, van Dessel J, Martens W, et al. Sensory innervation around immediately vs. delayed loaded implants: a pilot study. *Int J Oral Sci.* 2015;7(1):49-55.
36. Suzuki Y, Matsuzaka K, Ishizaki K, Tazaki M, Sato T, Inoue T. Characterization of the peri-implant epithelium in hamster palatine mucosa: Behavior of Merkel cells and nerve endings. *Biomed Res.* 2006;26(6):257-269.
37. Ishijima M, Tsuji K, Rittling SR, et al. Resistance to unloading-induced three-dimensional bone loss in osteopontin-deficient mice. *J Bone Miner Res.* 2002;17(4):661-667.
38. Lundborg G. Nerve regeneration and repair. A review. *Acta Orthopaed Scand.* 1987;58(2):145-169.

39. Zaminy A, Shokrgozar MA, Sadeghi Y, Noroozian M, Heidari MH, Piryaeei A. Mesenchymal stem cells as an alternative for Schwann cells in rat spinal cord injury. *Iran Biomed J.* 2013;17(3):113-122.
40. Kuhlengel KR, Bunge MB, Bunge RP. Implantation of cultured sensory neurons and Schwann cells into lesioned neonatal rat spinal cord. I. Methods for preparing implants from dissociated cells. *J Comparat Neurol* 1990;293(1):63-73.
41. Jang KS, Kim YS. Comparison of oral sensory function in complete denture and implant-supported prosthesis wearers. *J Oral Rehabil.* 2001;28(3):220-225.
42. Enkling N, Nicolay C, Utz KH, Jöhren P, Wahl G, Mericske-Stern R. Tactile sensibility of single-tooth implants and natural teeth. *Clin Oral Implants Res.* 2007;18(2):231-236.
43. Enkling N, Heussner S, Nicolay C, Bayer S, Mericske-Stern R, Utz KH. Tactile Sensibility of Single-Tooth Implants and Natural Teeth Under Local Anesthesia of the Natural Antagonistic Teeth. *Clin Implant Dent Relat Res.* 2012;14(2):273-280.
44. Kazemi M, Geramipannah F, Negahdari R, Rakhshan V. Active tactile sensibility of single-tooth implants versus natural dentition: a split-mouth double-blind randomized clinical trial. *Clin Implant Dent Relat Res.* 2014;16(6):947-955.
45. Batista M, Bonachela W, Soares J. Progressive recovery of osseoperception as a function of the combination of implant-supported prostheses. *Clin Oral Implants Res.* 2008;19(6):565-569.
46. Enkling N, Utz KH, Bayer S, Mericske-Stern R. Osseoperception: Active Tactile Sensibility of Osseointegrated Dental Implants. *Implantol.* 2012;20(3):285-294.
47. El-Sheikh AM, Hobkirk JA, Howell PGT, Gilthorpe MS. Passive tactile sensibility in edentulous subjects treated with dental implants: A pilot study. *J Prosthetic Dent.* 2004;91(1):26-32.
48. Habre-Hallage P, Abboud-Naaman NB, Reychler H, van Steenberghe D, Jacobs R. Perceptual changes in the peri-implant soft tissues assessed by directional cutaneous kinaesthesia and graphaesthesia: A prospective study. *Clin Implant Dent Relat Res.* 2011;13(4):296-304.
49. Habre-Hallage P, Abboud-Naman NB, Reychler H, van Steenberghe D, Jacobs R. Assessment of changes in the oral tactile function of the soft tissues by implant placement in the anterior maxilla: A prospective study. *Clin Oral Investig.* 2010;14(2):161-168.

50. Grieznis L, Apse P, Blumfelds L. Passive tactile sensibility of teeth and osseointegrated dental implants in the maxilla. *Stomatol.* 2010;12(3):80-86.
51. Enkling N, Nicolay C, Utz KH, Johren P, Wahl G, Mericske-Stern R. Tactile sensibility of single-tooth implants and natural teeth. *Clin Oral Implants Res.* 2007;18(2):231-236.
52. Enkling N, Utz KH, Bayer S, Stern RM. Osseoperception: active tactile sensibility of osseointegrated dental implants. *Int J Oral Maxillofac Implants.* 2010;25(6):1159-1167.
53. Batista M, Bonachela W, Soares J. Progressive recovery of osseoperception as a function of the combination of implant-supported prostheses. *Clin Oral Implants Res.* 2008;19(6):565-569.
54. Swinnen A, Van Huffel S, Van Loven K, Jacobs R. Detection and multichannel SVD-based filtering of trigeminal somatosensory evoked potentials. *Med Biolog Eng Comput.* 2000;38(3):297-305.
55. Van Loven K, Jacobs R, Swinnen A, Van Huffel S, Van Hees J, Van Steenberghe D. Sensations and trigeminal somatosensory-evoked potentials elicited by electrical stimulation of endosseous oral implants in humans. *Arch Oral Biol.* 2000;45(12):1083-1090.
56. Yan C, Ye L, Zhen J, Ke L, Gang L. Neuroplasticity of edentulous patients with implant-supported full dentures. *Eur J Oral Sci.* 2008;116(5):387-393.
57. Habre-Hallage P, Dricot L, Jacobs R, van Steenberghe D, Reyhler H, Grandin CB. Brain plasticity and cortical correlates of osseoperception revealed by punctate mechanical stimulation of osseointegrated oral implants during fMRI. *Eur J Oral Implantol.* 2012;5(2):175-190.
58. Hadjidakis DJ, Androulakis, II. Bone remodeling. *Ann New York Acad Sci.* 2006;1092:385-396.
59. Marco F, Milena F, Gianluca G, Vittoria O. Peri-implant osteogenesis in health and osteoporosis. *Micron.* 2005;36(7-8):630-644.

# CHAPTER 2

## Peri-implant myelinated nerve fibers: Histological findings in dogs

Song D<sup>1,2</sup>

Liang X<sup>1</sup>

Zheng H<sup>1</sup>

Shujaat S<sup>2</sup>

Van Dessel J<sup>2</sup>

Zhong WJ<sup>1</sup>

Ma GW<sup>1</sup>

Lambrichts I<sup>3</sup>

Jacobs R<sup>2,4</sup>

<sup>1</sup>Department of School of Stomatology, Dalian Medical of University, Dalian, China

<sup>2</sup>OMFS IMPATH research group, Department of Imaging & Pathology, Faculty of Medicine, KU Leuven, and Oral & maxillofacial Surgery, University Hospitals Leuven, Leuven, Belgium

<sup>3</sup>Morphology Group, Biomedical Research Institute, Hasselt University, Diepenbeek, Belgium

<sup>4</sup>Department of Dental Medicine, Karolinska Institute, Stockholm, Sweden.

Published in *Journal of Periodontal Research* 2020;00:1-7

# Peri-implant myelinated nerve fibers: Histological findings in dogs

Dandan Song<sup>1,2</sup>  | Xin Liang<sup>1</sup> | Hui Zheng<sup>1</sup>  | Sohaib Shujaat<sup>2</sup>  |  
Jeroen Van Dessel<sup>2</sup>  | Weijian Zhong<sup>1</sup>  | Guowu Ma<sup>1</sup>  | Ivo Lambrichts<sup>3</sup>  |  
Reinhilde Jacobs<sup>2,4</sup> 

<sup>1</sup>Department of School of Stomatology, Dalian Medical University, Dalian, China

<sup>2</sup>OMFS IMPATH research group, Department of Imaging & Pathology, Faculty of Medicine, KU Leuven and Oral & Maxillofacial Surgery, University Hospitals Leuven, Leuven, Belgium

<sup>3</sup>Morphology Group, Biomedical Research Institute, Hasselt University, Diepenbeek, Belgium

<sup>4</sup>Department of Dental Medicine, Karolinska Institute, Stockholm, Sweden

## Correspondence

Reinhilde Jacobs, OMFS IMPATH research group Department of Imaging & Pathology, Katholieke Universiteit Leuven, Campus Sint-Rafaël, Kapucijnenvoer 33, BE-3000 Leuven, Belgium.  
Emails: reinhilde.jacobs@kuleuven.be; reinhilde.jacobs@uzleuven.be

## Funding information

China Scholarship Council, Grant/Award Number: 201708210187; Fonds Wetenschappelijk Onderzoek, Grant/Award Number: 11.ZU.117N; National Natural Science Foundation of China, Grant/Award Number: 81370026

## Abstract

**Background and Objective:** While osseointegration following various dental implant placement protocols has been extensively investigated, the neurohistological integration has received little attention. The primary aim of this study was to compare the myelinated nerve fibers density in peri-implant bone tissue following various implant placement protocols. The secondary aim assessed the effect of follow-up on peri-implant nerve fibers density.

**Methods:** Ten beagle dogs randomly received 68 commercially pure titanium implants in the mandibular premolar or molar region bilaterally following extraction utilizing one of the six treatment protocols: (a) immediate implant placement (IIP) and immediate loading (IL); (b) IIP and delayed loading (DL); (c) IIP and left unloaded (UL); (d) delayed implant placement (DIP) and IL; (e) DIP and DL; and (f) DIP and UL. Histomorphometric analysis of the peri-implant myelinated nerve fibers was performed in a 300 µm peri-implant zone at the cervical, middle, and apical level following implant placement. The follow-up assessment involved longitudinal observation at 3 months following each implant treatment protocol and at 6 months for IIP+IL and IIP+DL protocols.

**Results:** The influence of different treatment protocols, including the fixed effects of implant groups (IIP+IL, IIP+DL, IIP+UL, DIP+IL, DIP+DL, DIP+UL) and regions (cervical, middle, apical), was examined via a linear mixed model. The IIP+IL group showed a significantly higher myelinated nerve density compared to the IIP+UL and DIP+UL group. Peri-implant nerve re-innervation was significantly higher ( $P = .002$ ) in the apical region compared to the cervical region. After immediate implant placement, the IL group showed a significantly ( $P = .03$ ) higher density of myelinated nerve fibers compared to DL. No significant ( $P = .19$ ) effect of follow-up on nerve density was observed.

**Conclusion:** The immediate implant placement and loading protocol showed most beneficial effect on peri-implant innervation with highest myelinated nerve density in the apical region. A longer loading time had no influence on the peri-implant nerve density.

## KEYWORDS

dental implants, histology, immediate dental implant loading, myelinated, nerve fibers

## 1 | INTRODUCTION

The periodontal mechanoreceptors are somatosensory receptors which provide an essential tactile information to refine oral motor behavior.<sup>1,2</sup> While tooth extraction results in the loss of these receptors causing disruption in the sensory-motor interaction,<sup>3</sup> dental implant rehabilitation allows partial restoration of the oral neurosensory function. Edentulous patients rehabilitated with bone-anchored oral prosthesis have been shown to have an improved tactile sensation. This phenomenon of partial tactile function recovery with improved sensory awareness is denoted as “osseoperception”.<sup>4</sup> While psychophysical evidence confirms tactile threshold recovery following dental implant treatment,<sup>5-7</sup> there is still a lack of evidence concentrating on the source of origin of these receptors.<sup>1,8</sup>

Several histological studies evaluating the bone healing process following dental implant placement have verified the presence of mechanoreceptors and their associated nerve fibers in the gingiva, mucosa, muscle, and periosteum.<sup>9-11</sup> Nevertheless, nerve fibers found in the peri-implant region play the most vital role in restoration of the sensory function. The nerve density in peri-implant bone is less than that of the alveolar bone around natural teeth.<sup>12</sup> Previous animal experiments and clinical studies have shown that different implant placement and loading protocols exert a differential effect on the peri-implant nerve fiber regeneration.<sup>13,14</sup> Some histological studies have indicated that the immediate implant placement and loading protocol shows a higher myelinated nerve fiber density compared to delayed and unloaded implants,<sup>14</sup> while others have found no significant difference.<sup>13</sup> Evidence also suggests inconsistent findings in relation to follow-up time after loading. Some studies indicated an increased nerve density following longer follow-up periods, whereas others suggested decreased number and density of nerve fiber following loading.<sup>15,16</sup>

To address the ambiguity related to previous findings, the primary aim of this study was to histomorphometrically evaluate the impact of different implant placement and loading protocols on the myelinated nerve fibers density in peri-implant trabecular bone tissue. The secondary aim was to assess the effect of follow-up on peri-implant nerve density. The null hypothesis was that the nerve fibers density would be similar, regardless of the implant placement and loading protocol, and a longer follow-up period would show no difference in nerve density.

## 2 | MATERIAL AND METHODS

The study protocol was approved by the ethical committee of Dalian Medical University (Protocol No. 21100370000896). A randomized design using six dental implant treatment protocols in 10 healthy adult male beagle dogs was used (Figure 1). Randomization was performed using the Rand function in Microsoft Excel (Microsoft Excel 2016, Microsoft Corp.) To reduce the number of animals used in the experiment, a sample size calculation was carried out based on a previous study on dogs with similar design.<sup>14,17</sup> A priori power analysis

in G\*power 3.1 suggested a minimum sample size of 4 specimens per treatment protocol when assuming 80% power and a significance level of 5% ( $\alpha = .05$ ). All dogs (weight: 10.0-14.0 kg) were individually housed and were free of any oral lesion or systemic disease. The dogs were fed according to the general feeding program at the Experiment Animal Center of Dalian Medical University, China.

### 2.1 | Surgical procedure

The dogs received 1 week of intramuscular prophylactic antibiotic (gentamicin sulfate 1 600 000 U/d, Lingrui Pharmaceutical Co., Ltd.). A 12-hour fasting period was applied to prevent possible vomiting during surgery. All surgical procedures were performed under general anesthesia with application of xylazine hydrochloride (Lumianlin 0.1 mL/kg, Changchun Military Academy of Medical Sciences, Changchun, China) and local anesthesia (2-4 mL lidocaine 2% with epinephrine 1:100 000, Tianjin Pharmaceutical Co., Ltd) at the surgical site. Following tooth extraction and implant placement, all animals were administered with intramuscular (IM) antibiotics (gentamicin sulfate 1 600 000 U/d, Tianjin Pharmaceutical) and ibuprofen (IM, 5-8 mg/kg, Tianjin Pharmaceutical) for a period of 3 days to control post-operative infection and pain.

Following anesthesia, bilateral extraction of mandibular 2nd, 3rd, and 4th premolar and 1st molar was performed with closure of the extraction site using a 5.0 resorbable suture under sterile conditions. Periapical radiographs were taken before tooth extraction to observe the root shape, after tooth extraction to ensure that no roots tips were left behind and following implant placement to confirm correct positioning of dental implant. Sixty-eight titanium implants (3.8 mm × 8 mm for 2nd premolars, 3.8 mm × 10 mm for 3rd and 4th premolars, 4.5 mm × 12 mm for 1st molars, DIO implant system, Dong Seo Ltd. company) were randomly assigned to one of the six treatment protocols (Figure 1): (a) immediate implant placement and immediate loading (IIP+IL); (b) immediate implant placement and delayed loading (3 months after implant placement) (IIP+DL); (c) immediate implant placement and unloaded (IIP+UL); (d) delayed implant placement (3 months after extraction) and immediate loading (DIP+IL); (e) delayed implant placement (3 months after extraction) and delayed loading (DIP+DL); and (f) delayed implant placement (3 months after extraction) and unloaded (DIP+UL). Table S1 describes the random allocation of treatment protocol for each site in individual dogs.

One experienced surgeon (HZ) performed the surgical procedure. All implant sites were prepared with a starter drill followed by drill depths of 2.5 mm × 8 mm and 3 mm × 8 mm. The final preparation was made with 3.5 mm and 4.2 mm width increasing drills. Implants were placed using a low-speed protocol (800 rpm) while being cooled with sterilized saline. A torque of 45-50 N/cm was applied to ensure a good primary stability with an implant shoulder at the marginal bone level. Nickel-titanium (NiTi) alloy-based crowns were placed on the loading site using resin cement (RelyX, Unicem, RX, 3M ESPE). The crowns involved in the immediate loading

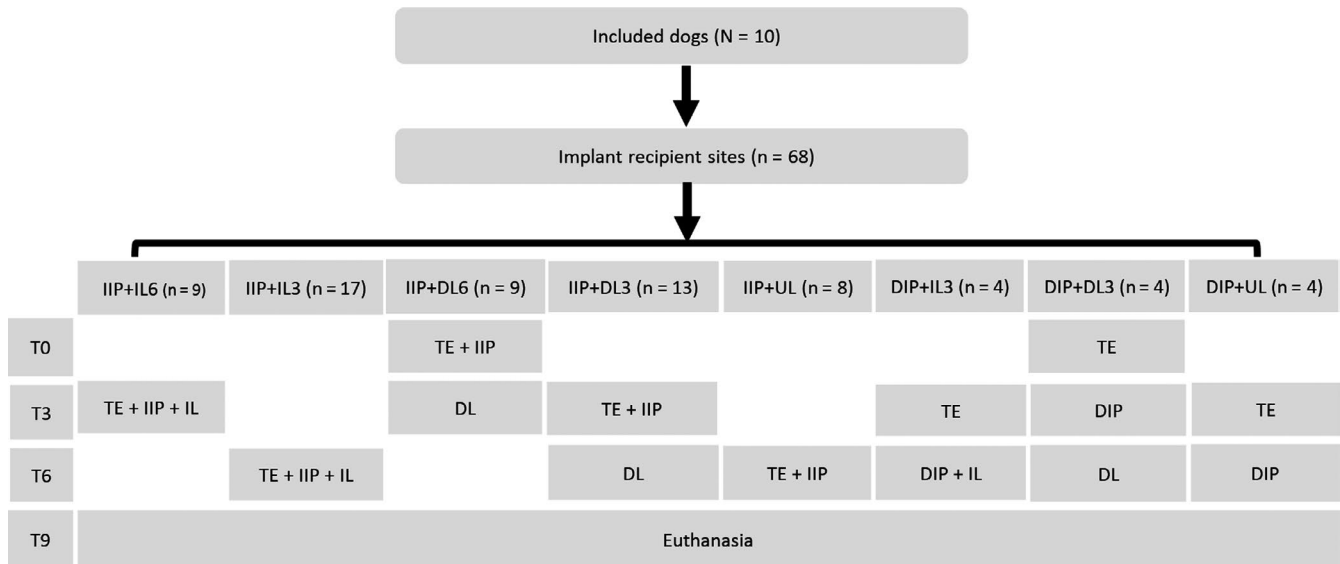


**FIGURE 1** Flowchart of the implant placement and loading protocols. DIP, delayed implant placement; DL, delayed loading; DL3 or IL3, 3 mo loading protocol; DL6 or IL6, 6 mo loading protocols; IIP, immediate implant placement; IL, immediate loading; T0, baseline; T3, 3 mo; T6, 6 mo; T9, 9 mo; TE, tooth extraction; UL, unloaded

protocols were set within 2 hours and for the delayed loading protocols 3 months after implant placement. For the dogs having a delayed loading treatment protocol, the restoration procedure was performed under general anesthesia with the application of xylazine hydrochloride (Lumianlin 0.1 mL/kg, Changchun Military Academy of Medical Sciences) 3 months after implant placement.

In the group IIP+IL3 and DIP+IL3, the implant was placed and loaded at 6 months. The IIP+DL3 and DIP+DL3 treatment protocols involved implant placement at the third month and loading at sixth month. In group IIP+UL and DIP+UL, the implant was placed at the sixth month without loading. In group IIP+IL6, the implant was placed and loaded at the third month, whereas, in group IIP+DL6, the implant was placed at the baseline time point and loaded at third month. All animals were euthanized at the same time point of 9 months. The aforementioned treatment strategies at various time points before euthanization allowed the follow-up assessment at a 3-months period for six treatment protocols (IIP+IL3, IIP+DL3, IIP+UL, DIP+IL3, DIP+DL3, DIP+UL) and 6-months only for two treatment protocols (IIP+IL6 and IIP+DL6).

## 2.2 | Histological preparation

All animals were euthanized with an excess amount of xylazine hydrochloride intramuscularly and immediately perfused with 4% paraformaldehyde and 0.0125% glutaraldehyde in 0.1 mol/L phosphate buffer (pH 7.4) through the external carotid arteries. The jawbones were removed, defleshed, and trimmed into bone blocks with a bone width of 3–5 mm from the dental implant surface in the mesial and distal regions. Samples were decalcified in 0.5 mol/L ethylenediaminetetraacetic acid (EDTA) and phosphate-buffered saline (pH 7.4) for 10 months at 4°C; thereafter, the implants were easily removed

using surgical forceps. The specimens were neutralized with 5% sodium sulfate, dehydrated by a graded series of increasing ethanol concentration, and were then embedded in paraffin. Tissue blocks were serially cut into 4–6 µm thick sections using a microtome in a vertical plane perpendicular to the long axis of the implant-removed socket. Sections were stained with hematoxylin and eosin staining (H&E staining).

## 2.3 | Histomorphometric analysis

Each bone block was separated into three parts (cervical, middle, apical), and three serial sections from each sample were digitized using MiraxScan (Carl Zeiss) at ×100 magnification. All digital slide files were viewed on a 17-inch LCD monitor (Dell) using an image software package (Panoramic Viewer) at three root levels (1, 5, and 9 mm from the apex, respectively). One experienced observer, who was blinded to treatment protocol allocation, analyzed the myelinated nerve fibers density (N/mm<sup>2</sup>, number of myelinated nerve fibers per area) with an automated digital image analysis system linked to histomorphometry software (Leco Instruments) following the protocol based on a previous study.<sup>18</sup> This system displayed the microscopic image on a video monitor calibrated to 0.125 mm/pixel. Each section was measured three times at an interval of 1 week between measurements, and a mean value was generated for minimizing the intra-observer variability. The histomorphometric analysis of myelinated nerve density was based on a protocol previously described by Huang et al,<sup>14</sup> which involved assessment of a 300 µm wide peri-implant zone at 2 mm height for three regions of interests (ROIs), that is, cervical, middle, and apical levels (Figure 2). A 300 µm wide peri-implant zone was selected as this region is most widely influenced by the dental implant's loading transmission.<sup>19</sup> The single

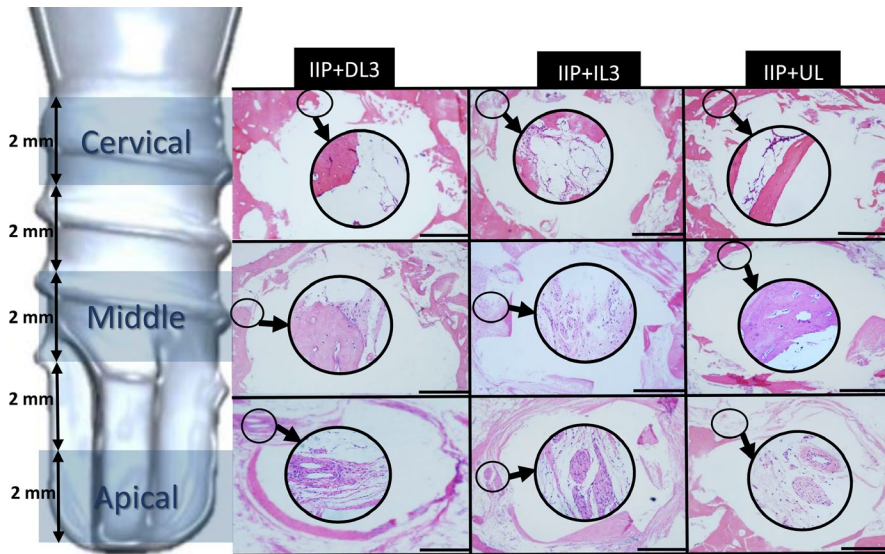


**FIGURE 2** Illustration of comparative histological analysis for three treatment protocols. The histological slices present myelinated nerve fibers magnified ( $\times 20$ ) in the circle (black). The Bar is 500  $\mu\text{m}$

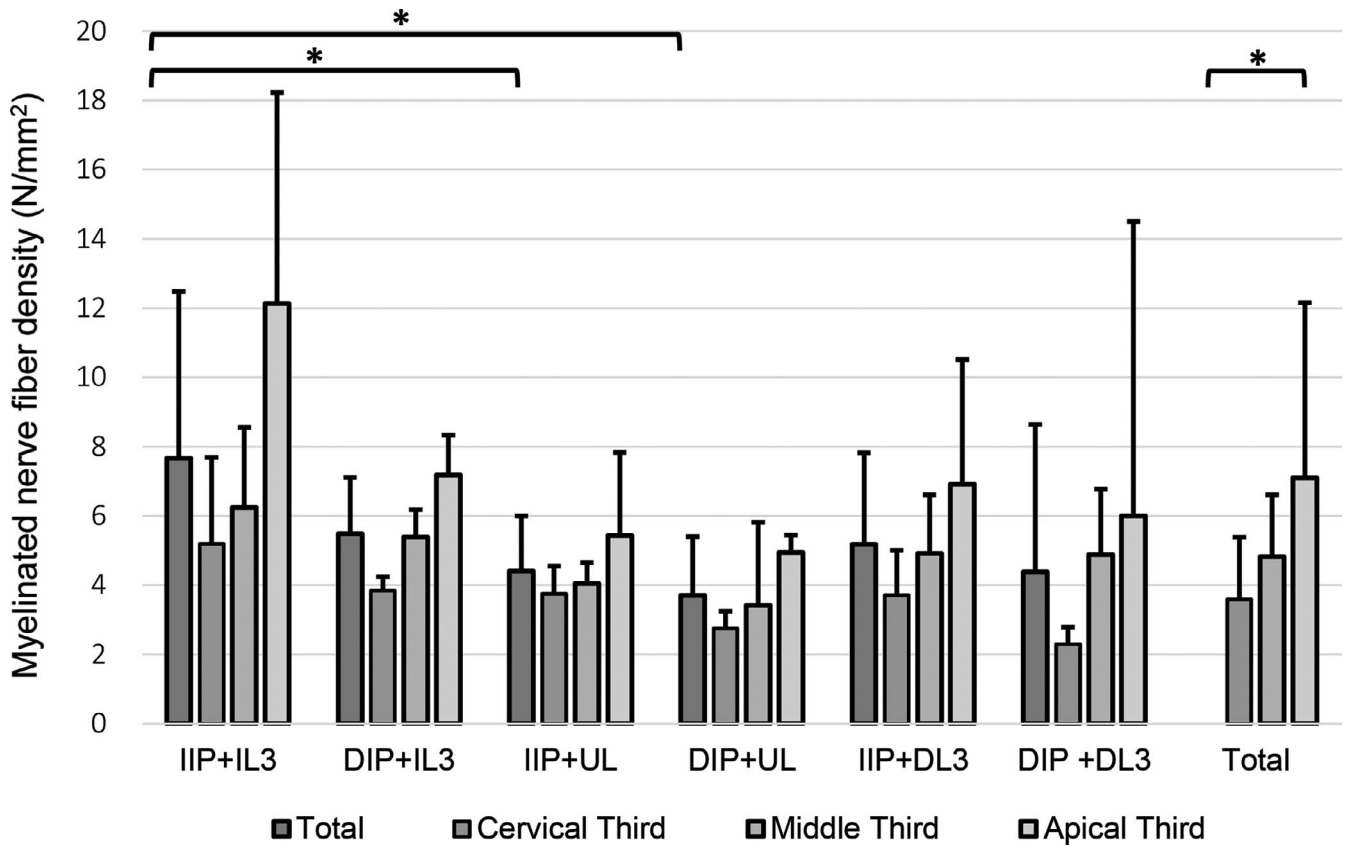


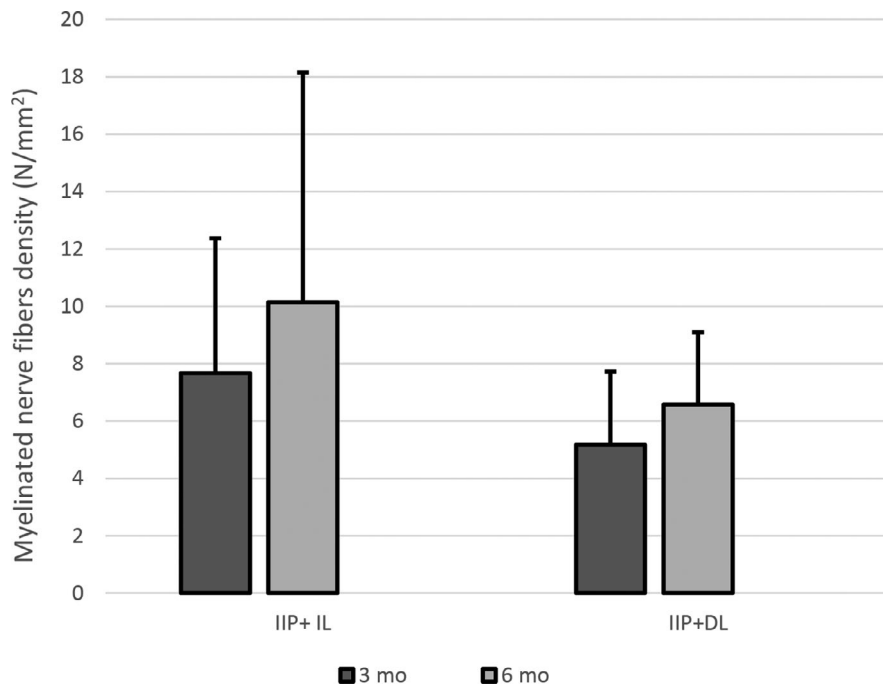
**FIGURE 3** Chart showing myelinated nerve fiber density of treatment protocols in relation to region of interest.  $*P < .05$  shows the significant difference

myelinated nerve fibers were measured, which always existed individually and were situated mostly in the peri-implant bone. A single myelinated nerve axon was defined as the nerve axon around which there was no more than one axon in a 20  $\mu\text{m}$  range. The partial fibers at the borderline of an ROI were excluded. An interleaved gap of 1 mm for the 8 mm implants and 2 mm for the 10 mm implants between the 3 ROIs was set.

## 2.4 | Statistical analysis

Two separate linear mixed models were defined to fully consider the effect of the randomized design. The first model was applied to examine the influence of the different treatment protocols, including the fixed effects of implant groups (IIP+IL, IIP+DL, IIP+UL, DIP+IL, DIP+DL, DIP+UL), regions (cervical, middle, apical), their two-way interaction

**FIGURE 4** Mean density of myelinated nerve fibers at 3- and 6-month follow-up in IIP+IL and IIP+DL groups. DL: delayed loading; IIP: immediate implant placement; IL: immediate loading.



effect, and the random effects of dogs. The second model evaluated the effect of follow-up, including group (IIP+IL, IIP+DL), follow-up time (3 months, 6 months), their two-way interaction effect, and the random effect of dogs. Bonferroni-corrected post hoc *t* tests were used to examine significant main and interaction effects. All statistical testing was performed in SPSS (IBM) at a significant level of  $\alpha = .05$ .

### 3 | RESULTS

All animals remained in good health throughout the whole experimental period. Six implants failed due to local peri-implantitis (4 implants: IIP+DL3 group, 1 implant: IIP+DL6 group, 1 implant: IIP+IL3 group) and were excluded from further analysis.

#### 3.1 | Effect of implant placement and loading protocols

There was a main effect of treatment protocol ( $F = 4.1$ ;  $P = .01$ ) and region ( $F = 6.9$ ;  $P = .002$ ; Figure 3). Post hoc test showed significant differences between the IIP+IL3 group and IIP+UL ( $P = .02$ ), and DIP+UL ( $P = .010$ ; Figure 3). Myelinated nerve fiber density was significantly higher in the apical region compared to the cervical region ( $P = .002$ ; Figures 2 and 3). There was no interaction between treatment protocol and region ( $P = .77$ ).

#### 3.2 | Effect of follow-up after IIP+IL and IIP+DL

Myelinated nerve density after immediate loading was significantly higher compared to delayed loading ( $F = 5.0$ ;  $P = .03$ ; Figure 4). The

immediate loading group showed a 53% higher amount of myelinated nerve fibers compared to delayed loading after immediate implant placement. While there was a tendency that the myelinated nerve fibers density increased slightly over time in both IIP+IL group and IIP+DL group (Figure 4), no significant difference was found between 3 and 6 months of follow-up ( $F = 1.7$ ;  $P = .19$ ).

### 4 | DISCUSSION

The present study was carried out to assess the effect of different implant placement protocols on nerve density at the cervical, middle, and apical peri-implant region. In addition, the influence of follow-up period after loading was also investigated in a randomized controlled animal experiment. These findings might be of importance for further understanding the underlying mechanism of osseoperception and for guiding a treatment design. In our study, immediate implant placement and loading protocols showed increased peri-implant re-innervation with highest nerve density in the apical region, and a longer follow-up led to an increase in density of myelinated nerves. Therefore, the null hypothesis was rejected.

In order to minimize the potential bias related to implant position and dynamic loading forces among experimental animals, a randomized design was applied. Each of the six treatment protocols was randomly distributed in both anterior and posterior mandibular region. Following 10 months of complete decalcification process, the presence of myelinated nerve fibers in peri-implant bone was confirmed. The myelinated nerve fibers were histologically observed as rounded structures with dark-blue color at the periphery and light blue at the center, concentrated under the screw thread, bone marrow, and haversian canals in the ROIs.

In the present study, density of myelinated nerve fibers at a region of 300  $\mu\text{m}$  from the implant interface was found to be highest in the IIP+IL group, while lowest in DIP+UL group. These results suggested that the immediate implant placement and immediate loading were more beneficial in relation to improved regeneration of nerve fibers compared to delayed implant placement and delayed loading. Our findings were in accordance with Huang et al's study, which also showed increased mean nerve density of myelinated axons in the IIP+IL group compared to DIP+DL and DIP+IL protocols.<sup>14</sup> The loaded group showed increase in nerve fibers compared to the unloaded group which was also consistent with the previous findings.<sup>13,19</sup> Our findings suggested that the ability of the nerve fibers regeneration is linked to the time point of when the implant is inserted and the prosthesis is loaded.

Previous studies showed high concentration of nerve fibers in the apical region of natural teeth, as the periodontal ligament in this region receives the most loading.<sup>18,20</sup> Based on this fact, our findings suggested increased nerve fiber density in the apical region of dental implant. Wada et al<sup>13</sup> also found proliferation of the neurofilament protein (NFP)-positive nerve fibers in apical region of implant.

The present study indicated no beneficial effect of longer post-experimental loading time on the density of nerve fibers. Although the density of nerve fibers increased slightly at 6-month follow-up, there was no significant difference when compared with 3-month follow-up. The re-innervation in the peri-implant bone after 3 months tended to be stable. This outcome was consistent with the findings of Zhu and Lin,<sup>21</sup> which also showed an improvement of nerve fiber regeneration within 3-month post-loading. This evidence proved that early implant stimulation was beneficial for peri-implant nerve fibers regeneration. Upon implant loading, the signals from activated nerves and/or dedifferentiated Schwann cells might promote the regeneration of peri-implant nerve fibers.

The limitations of the present study included failure of six dental implants due to peri-implantitis and non-osseointegration during the healing period. The most susceptible site for implant failure was second premolar region potentially related to a thin cortex. However, based on a randomized design with implant recipient site and protocol allocation, implant failure did not exert a negative effect on the results.

It should also be mentioned that the present study assessed neurohistology, but this does not enable us to link the current histological findings to the function and origin of the nerve fibers. Further studies should focus on discovering the origin of the regenerating nerve fibers and combining the accumulated neurophysiological, psychophysical, clinical, and histological evidence to better understand the neurosensory function as a keystone in osseoperception, oral function, and neurophysiological integration of the implant in the bone.

In conclusion, while immediate implant placement resulted in increased nerve fiber density, immediate loading contributed to a further increase as compared to delayed implant loading. Also, peri-implant innervation had the highest myelinated nerve density in the apical region. No significant difference was observed between nerve densities and between 3- and 6-month follow-up of implant loading.

## ACKNOWLEDGMENTS

The authors thank the laboratory technicians from Dalian Medical of University and Translational Cell & Tissue Research of KU Leuven for their valuable help during this animal research. Financial support from the National Nature Science Foundation of China (No. 81370026) to Dr LX, China Scholarship Council (No. 201708210187) to SD, and FWO-research fellow (No. 11.ZU.117N) to JVD is greatly appreciated.

## CONFLICT OF INTEREST

The authors declare no conflict of interest.

## ORCID

Dandan Song  <https://orcid.org/0000-0001-5394-6746>

Hui Zheng  <https://orcid.org/0000-0001-7516-5705>

Sohaib Shujaat  <https://orcid.org/0000-0002-6250-2650>

Jeroen Van Dessel  <https://orcid.org/0000-0001-5084-8710>

Weijian Zhong  <https://orcid.org/0000-0002-1284-0539>

Guowu Ma  <https://orcid.org/0000-0002-7564-5028>

Ivo Lambrichts  <https://orcid.org/0000-0001-7520-0021>

Reinhilde Jacobs  <https://orcid.org/0000-0002-3461-0363>

## REFERENCES

1. Jacobs R, VanSteenberghe D. From osseoperception to implant-mediated sensory-motor interactions and related clinical implications. *J Oral Rehabil.* 2006;33(4):282-292.
2. Abarca M, VanSteenberghe D, Malevez C, Jacobs R. The neurophysiology of osseointegrated oral implants. a clinically underestimated aspect. *J Oral Rehabil.* 2006;33(3):161-169.
3. Klineberg I, Murray G. Osseoperception: sensory function and proprioception. *Adv Dent Res.* 1999;13:120-129.
4. Bränemark P-I. How the concept of osseoperception evolved. In: Jacobs R, ed. *Osseoperception.* Leuven: Catholic University Leuven;1998:43-46.
5. Enkling N, Utz KH, Bayer S, Stern RM. Osseoperception: active tactile sensibility of osseointegrated dental implants. *Int J Oral Maxillofac Implants.* 2010;25(6):1159-1167.
6. El-Sheikh AM, Hobkirk JA, Howell PG, Gilthorpe MS. Changes in passive tactile sensibility associated with dental implants following their placement. *Int J Oral Maxillofac Implants.* 2003;18(2):266-272.
7. Yan C, Ye L, Zhen J, Ke L, Gang L. Neuroplasticity of edentulous patients with implant-supported full dentures. *Euro J Oral Sci.* 2008;116(5):387-393.
8. Bhatnagar VM, Karani JT, Khanna A, Badwaik P, Pai A. Osseoperception: an implant mediated sensory motor control – a review. *J Clin Diag Res.* 2015;9(9):18-20.
9. Suzuki Y, Matsuzaka K, Ishizaki K, Tazaki M, Sato T, Inoue T. Characterization of the peri-implant epithelium in hamster palatine mucosa: Behavior of Merkel cells and nerve endings. *Biomed Res.* 2006;26(6):257-269.
10. Garzino M, Ramieri G, Panzica G, Preti G. Changes in the density of protein gene product 9.5-immunoreactive nerve fibres in human oral mucosa under implant-retained overdentures. *Archs Oral Biol.* 1996;41(11):1073-1079.
11. Jacobs R, van Steenberghe D. Qualitative evaluation of the masseteric poststimulus EMG complex following mechanical or acoustic stimulation of osseointegrated oral implants. *Int J Oral Maxillofac Implants.* 1995;10(2):175-182.
12. Marco Garzino GR, Panzica G, Preti G. Changes in the density of protein gene product 9.5-immunoreactive nerve fibers in human

- oral mucosa under implant-retained overdentures. *Archs Oral Biol.* 1996;41:1073-1079.
13. Wada S, Kojo T, Wang YH, et al. Effect of loading on the development of nerve fibers around oral implants in the dog mandible. *Clin Oral Implants Res.* 2001;12(3):219-224.
  14. Huang Y, van Dessel J, Martens W, et al. Sensory innervation around immediately vs. delayed loaded implants: a pilot study. *Int J Oral Sci.* 2015;7(1):49-55.
  15. Wang Y-HKT, Ando H, Nakanishi E, et al. Nerve regeneration after implantation in peri-implant area. A histological study on different implant materials in dogs. In: Jacobs R, ed. *Osseoperception*. Leuven: Catholic University Leuven;1998;3-11.
  16. Masahito Sawada HK, Sato O, Maeda T, Takano Y. Histological investigation on chronological changes in peri-implant tissues, with special reference to responses of nerve fibers to implantation. *J Jpn Prosthodont Soc.* 1993;37(1):144-158.
  17. Huang Y, VanDessel J, Liang X, et al. Effects of immediate and delayed loading on peri-implant trabecular structures: a cone beam CT evaluation. *Clin Implant Dent Relat Res.* 2014;16(6):873-883.
  18. Huang Y, Corpas LS, Martens W, Jacobs R, Lambrichts I. Histomorphological study of myelinated nerve fibres in the periodontal ligament of human canine. *Acta Odontol Scand.* 2011;69(5):279-286.
  19. Weiner S, Klein M, Doyle JL, Brunner M. Identification of axons in the peri-implant region by immunohistochemistry. *Int J Oral Maxillofac Implants.* 1995;10(6):689-695.
  20. Trulsson M. Sensory-motor function of human periodontal mechanoreceptors. *J Oral Rehabil.* 2006;33(4):262-273.
  21. Zhu Y, Lin Y. Electrophysiological study of peripheral neurophysiologic mechanism in osseoperception phenomena [ol]. 2012;12-24.

#### SUPPORTING INFORMATION

Additional supporting information may be found online in the Supporting Information section.

**How to cite this article:** Song D, Liang X, Zheng H, et al. Peri-implant myelinated nerve fibers: Histological findings in dogs. *J Periodont Res.* 2020;00:1-7. <https://doi.org/10.1111/jre.12744>

# CHAPTER 3

## Effect of platelet-rich and platelet-poor plasma on peri-implant innervation in dog mandibles

Song D<sup>1</sup>

Huang Y<sup>1,2</sup>

Van Dessel J<sup>1</sup>

Shujaat S<sup>1</sup>

Orhan K<sup>1,3</sup>

Vangansewinkel T<sup>4</sup>

Van den Eynde K<sup>5</sup>

Lambrichts I<sup>4</sup>

Roskams T<sup>5</sup>

Politis C<sup>1</sup>

Jacobs R<sup>1,6</sup>

<sup>1</sup>OMFS IMPATH research group, Department of Imaging & Pathology, Faculty of Medicine, KU Leuven, and Oral & maxillofacial Surgery, University Hospitals Leuven, Leuven, Belgium

<sup>2</sup>State Key Laboratory of Oral Diseases, West China College of Stomatology, Sichuan University, Chengdu, China

<sup>3</sup>Department of Dentomaxillofacial radiology, Faculty of Dentistry, University of Ankara, Ankara, Turkey

<sup>4</sup>Morphology Group, Biomedical Research Institute, Hasselt University, Diepenbeek, Belgium

<sup>5</sup>Department of Translational Cell and Tissue Research, University Hospitals Leuven, Leuven, Belgium

<sup>6</sup>Department of Dental Medicine, Karolinska Institute, Stockholm, Sweden.

RESEARCH

Open Access



# Effect of platelet-rich and platelet-poor plasma on peri-implant innervation in dog mandibles

Dandan Song<sup>1\*</sup> , Yan Huang<sup>1,2</sup>, Jeroen Van Dessel<sup>1</sup>, Sohaib Shujaat<sup>1</sup>, Kaan Orhan<sup>1,3</sup>, Tim Vangansewinkel<sup>4</sup>, Kathleen Van den Eynde<sup>5</sup>, Ivo Lambrechts<sup>4</sup>, Tania Roskams<sup>5</sup>, Constantinus Politis<sup>1</sup> and Reinhilde Jacobs<sup>1,6</sup>

## Abstract

**Background:** Autologous plasma fractions, such as platelet-rich plasma (PRP) and platelet-poor plasma (PPP), contain growth factors that can enhance neural cell survival and are therefore likely to have the ability to promote nerve regeneration. The present study compared the effect of PRP and PPP application on myelinated nerve density and diameter in the peri-implant bone region. In addition, the effect of healing time on nerve regeneration was assessed.

**Materials and methods:** Nine beagle dogs randomly received 54 dental implants in the bilateral mandible according to a split-mouth design. Each implant was randomly assigned to one of three implant protocols: delayed implant placement with delayed loading (DIP + DL) with local application of PRP, DIP + DL with local application of PPP and DIP + DL without any plasma additive. The animals were euthanized at 1, 3, and 6 months after loading (3 dogs per time point). Block biopsies were prepared for histomorphometry in the peri-implant bone within 500  $\mu\text{m}$  around the implants.

**Results:** Myelinated nerve fibers were identified in the trabecular bone and in the osteons near the implants surface. The nerve fibers in the PRP group (median  $\pm$  IQR;  $2.88 \pm 1.55 \mu\text{m}$ ) had a significantly ( $p < 0.05$ ) greater diameter compared to the PPP ( $2.40 \pm 0.91 \mu\text{m}$ ) and control ( $2.11 \pm 1.16 \mu\text{m}$ ) group. The nerve diameter after 6 months healing ( $3.18 \pm 1.58 \mu\text{m}$ ) was significantly ( $p < 0.05$ ) greater compared to 1 ( $2.08 \pm 0.89 \mu\text{m}$ ) and 3 ( $2.49 \pm 1.22 \mu\text{m}$ ) months. No significant difference was found for myelinated nerve density between groups and healing time.

**Conclusions:** The present study showed that the healing time significantly influenced the diameter of the myelinated nerve fibers in peri-implant bone. PRP exerted a significant effect on the diameter of the myelinated nerve fibers as compared to PPP. Large-scale animal studies and longer follow-up periods are needed to confirm these findings and to verify whether platelet plasma can facilitate nerve regeneration process.

**Keywords:** Platelet-rich plasma, Platelet-poor plasma, Dental implant, Histomorphometry, Myelinated nerve fibers, Innervation

## Background

Dental implant surgery is one of the most widely accepted procedures for replacing missing dentition without harming the neighboring healthy teeth. The survival of the dental implant is dependent on successful osseointegration, defined as the direct structural and

functional connection between vital bone and dental implant surface under a functional load. If optimal osseointegration is not achieved, biological failure and consequent implant loss can occur [1]. The residual alveolar ridge constantly undergoes modeling and remodeling following tooth extraction [2].

Maxillary and mandibular alveolar bone contains multiple nerve fibers, which are responsible for detecting mechanical loading-induced signals through the mechanosensitive cells known as mechanoreceptors [3, 4]. These receptors are responsible for transmitting information

\* Correspondence: [dandansong9015@gmail.com](mailto:dandansong9015@gmail.com)

<sup>1</sup>OMFS IMPATH Research Group, Department of Imaging and Pathology, Faculty of Medicine, KU Leuven and Oral and Maxillofacial Surgery, University Hospitals Leuven, Campus Sint-Rafaël, Kapucijnenvoer 33, BE-3000 Leuven, Belgium

Full list of author information is available at the end of the article

from nerve endings on the magnitude, direction, and rate of occlusal load for sensory perception and neuromotor control. The mechanism of such receptors involves the transmission of sensitivity and pain when natural teeth are in hyperocclusion. Degeneration of the alveolar structure or periodontal ligaments (PDLs) can lead to the impairment of these receptors, hence effecting the neurosensory pathway [5]. As osseointegrated dental implants are highly susceptible to occlusal overload, the damaged receptors can directly result in the loss of fine exteroception [6]. The existing mechanoreceptors in the bone and periosteum play a significant role in tactile function following implant loading. The threshold level of active tactile force in implant-supported prostheses has been suggested to be lower than the complete denture but similar to that of the natural tooth [7–10].

Previous studies reported a partial restoration of peripheral sensory feedback pathway following implant placement. However, the underlying mechanism of this phenomenon remains unknown [11, 12]. Furthermore, neurophysiological and psychophysical evidence confirms peripheral receptor activation after active or passive loading of the implant. It is assumed that the latter could cause activation of endosseous and/or periosteal receptors in the peri-implant tissue [13]. In addition, histomorphological studies showed the presence of functional mechanoreceptors in the peri-implant region which might have been originally located in the periodontal ligament and neighboring periosteum [14, 15].

Myelinated nerve fibers are the most effective sensory signal transporters responsible for carrying these mechanoreceptors [16]. Several treatment strategies have been utilized for the regeneration of mechanoreceptors around osseointegrated dental implant which include, reconstruction of the peri-implant ligament [17], transplantation of Schwann cells (SCs) [18], injection of neuropeptides (e.g., calcitonin gene-related peptide- $\alpha$ ) [19], and application of various implant placement and loading protocols [20]. Nevertheless, the clinical application of these therapies in implant surgery remains ambiguous.

Autologous plasma fractions, such as platelet-rich plasma (PRP) and platelet-poor plasma (PPP) have been utilized in dental implantology for stimulating new bone formation [21], angiogenesis [22], and peripheral nerve regeneration [23]. PRP is obtained by differential centrifugation of peripheral blood which divides the plasma, platelets, and leukocytes from red blood cells to form an upper plasma layer and intermediate buffy coat. The upper layer and superficial buffy coat are centrifuged for a second time to form the final PRP product, whereas, PPP is the residual plasma once the PRP is extracted [24]. The clinical potential of platelet concentrates depends on the number of platelets and the concentration of growth factors. Various growth factors, such as

transforming growth factor- $\beta$  (TGF- $\beta$ ), platelet-derived growth factor (PDGF), transforming growth factor (TGF), platelet factor interleukin (IL), vascular endothelial growth factor (VEGF), insulin-like growth factor (IGF), and basic fibroblast growth factor (bFGF), contained in the alpha-granules of platelets have been known to be responsible for PRP-related effects. Although recent studies showed that PRP and PPP have comparable effects on bone [21] and blood vessel formation [22], no evidence is available comparing the effect of these two fractions on nerve innervation in the peri-implant bone. Therefore, the purpose of this study was to assess the effect of PRP and PPP on myelinated nerve density and diameter following delayed implant placement and delayed loading. In addition, the effect of healing time on peri-bone innervation was evaluated following 1, 3, and 6 months after loading.

## Materials and methods

### Study design

The study was approved by the Bioethics Committee of Sichuan University (reference number: WCCSIRB-D-2014-010). A split-mouth randomized study was designed in nine healthy male beagle dogs. The housing and feeding condition for all experimental dogs strictly followed the general program at Experimental Animal Center of Laboratory of Biotherapy.

### Sample size calculation

The minimum required sample size was calculated using the discrepancy in myelinated nerve diameter for delayed implant placement with delayed loading ( $1.07 \pm 0.18 \mu\text{m}$ ) and natural socket healing ( $1.23 \pm 0.19 \mu\text{m}$ ) obtained from a study with similar design [25]. An a priori power analysis in G\*power 3.1 recommended minimum sample size of 18 peri-implant bone samples when assuming 80% power and  $\alpha$  of 0.05 [26].

### Surgical procedure

All animals (average weight 15.3 kg) received 1 week of prophylactic antibiotic therapy prior to and after surgery (Gentamycin Sulphate 300 mg, Tianjin Pharmaceutical, Tianjin, China). Bilateral extraction of mandibular third premolar, fourth premolar, and first molar was carried out. All surgeries were performed by the same oral and maxillofacial surgeon. After 1 month of natural healing, six dental implants without surface spiral burr (Beijing Leiden Biomaterial implant system, diameter 3.3 mm/length 8 mm) obtained from Leiden Biomaterial Limited Company, (Beijing, China) were placed bilaterally in the mandible of each dog. The surgical procedures were performed under general anesthesia with Sumianxin (0.1 ml/kg xylazine hydrochloride, Changchun Military Academy of Medical Sciences, Changchun, China) and

local anesthesia (2–4 ml lidocaine 2% epinephrine, Tianjin Pharmaceutical Co. Ltd, Tianjin, China) was used at the surgical sites. The implant body part which was buried into alveolar bone was coated with a thin layer of plasma-sprayed hydroxyapatite (HA). Each implant was randomly assigned to one of the three implant protocols: delayed implant placement with delayed loading (DIP + DL) with a local application of PRP, DIP + DL with local application of PPP and DIP + DL without any plasma additive (Fig. 1). The surgeon was blinded to the allocation process during tooth extraction but aware of the exact position of implant placements. A crown was fabricated and attached to each implant at one month following surgery.

**Preparation and application of PPP and PRP**

A double-centrifugation protocol was followed as suggested by Lee et al. [27]. Five milliliters of fresh whole blood was withdrawn from the foreleg vein of each dog and transferred into a sterile syringe, containing 1 ml of sodium citrate anticoagulant solution. The whole blood was first centrifuged (Allegra X 30R centrifuge, CA, USA) at 700 g for 8 min and then separated into four layers. Thereafter, supernatant plasma with a buffy coat was separated and transferred to a new centrifugation

tube. It underwent a second centrifugation at 1600 g for 8 min. Finally, 1 ml of PPP and PRP were obtained separately and each implant in test groups was dipped in PPP and PRP solution prior to insertion in the alveolus.

**Occlusion restoration**

The surgical condition and occlusion restoration were kept similar for all groups. All tissue-level implants were placed with their shoulders parallel to the level of marginal bone. Customized posts with resin crown (flowable resin composite under halogen light-curing unit for 20 s) were prepared with a resin cement (RelyX, Unicem, RX, 3M ESPE, St. Paul, USA). Occlusal contacts were kept edge-to-edge between implants and opposing natural teeth. The contacts were checked with an articulating paper (20 µm thick, Accufilm II, RX, 3M ESPE, St. Paul, USA).

**Animal sacrifice and histology**

All dogs were healthy with clinically stable implants and normal surrounding soft tissue before sacrifice. Three dogs were randomly chosen utilizing a direct sampling technique at 1, 3, and 6 months' time points (T1, T3, and T6). They were sacrificed using an overdose of xylazine hydrochloride (intravenous injection)

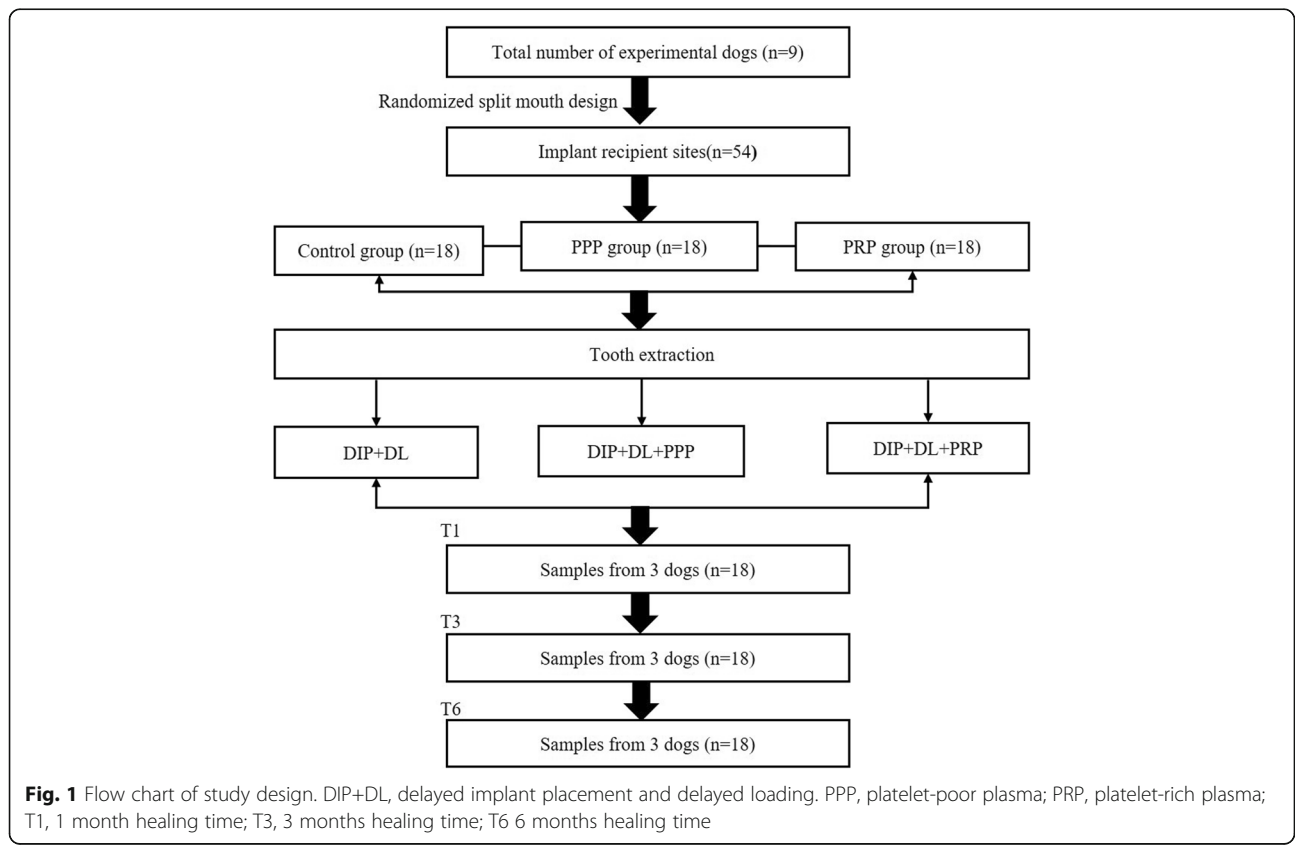


**Fig. 1** Flow chart of study design. DIP+DL, delayed implant placement and delayed loading. PPP, platelet-poor plasma; PRP, platelet-rich plasma; T1, 1 month healing time; T3, 3 months healing time; T6 6 months healing time

and immediate perfusion of 4% paraformaldehyde and 0.0125% glutaraldehyde in 0.1 M phosphate buffer (pH 7.4). Specimen blocks were immersed in 0.5 mol/L ethylenediaminetetraacetic acid (EDTA) phosphate-buffered saline (pH 7.4) at 4 °C for 10 months, enabling easy removal of the implants using surgical forceps without damaging the samples. After dehydrated and fully infiltrated by paraffin, thin serial sections (~6 μm) were obtained by cutting in a buccal-lingual direction. All collected sections were then stained with Masson trichrome stain for histological analysis and detection of myelinated nerve fibers.

**Immunohistochemistry**

The presence of myelinated nerve structures was confirmed with immunohistochemistry (IHC) by applying a labeled avidin-biotin method [28]. Sections were deparaffinized and microwaved using a 10-mm citrate buffer (pH 6.0). Thereafter, 0.5% H<sub>2</sub>O<sub>2</sub> was applied to suppress endogenous peroxidase activity for reducing background staining. The unoccupied binding sites were blocked with 10% normal goat serum. Staining of the sections was carried out with primary antibody mouse monoclonal anti-neuropeptide Y (NPY, Santa Cruz Biotechnology, CA, USA, 1:50) followed by pretreatment with citrate (pH 6.0).

**Histomorphometric analysis**

Digitization and evaluation of three serial sections from every sample was performed with MiraxScan (Carl Zeiss, Göttingen, Germany). A single observer (DS), who was blinded to implant groups, evaluated the density (number of myelinated nerves/mm<sup>2</sup>) and outer diameter of myelinated fibers (μm) on a ×100 magnified image using Fiji software (LOCI in Madison, WI, USA). A region of interest (ROI) with a distance of 500 μm away from the implant surface was selected (Fig. 2), which is most likely to be influenced by the pressure from dental implant [29]. The partial fibers at borders of selected ROIs, myelinated nerve bundles and isolated axons in inferior alveolar nerve canal were excluded from evaluation.

**Statistical analysis**

Normality in the distribution of data was assessed graphically and with the Shapiro-Wilk test. Non-parametric statistical tests were chosen by means of small sample size and non-linear data distribution. The descriptive analysis expressed data as median and interquartile range. The Kruskal-Wallis test was used to compare nerve density and shortest diameter values between implant protocols (control, PPP and PRP group) and time points (T1, T3, and T6). Dunn-Bonferroni corrected post hoc tests were used to explore significant interaction effects. A significance level α of 5% was

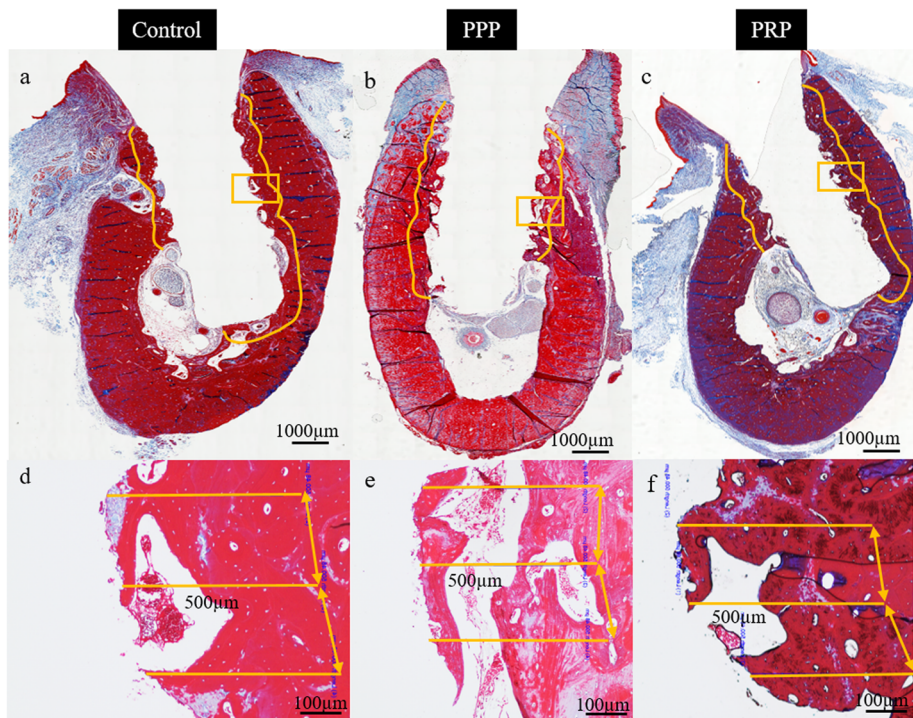


**Fig. 2** Region of interest selection 500 μm away from the implant surface on histological sections stained with Masson's trichrome stain for control (a, d), platelet-poor plasma (b, e), platelet-rich plasma (c, f) group. All sections were after 6 months healing time and taken with a light microscope at ×10 (upper row) or ×40 magnification (bottom row)

considered for all tests. Statistical analysis was performed in SPSS (IBM, NY, USA).

### Results

All animals recovered well after implant placement and loading procedures without any clinical signs of infection or inflammation. All implants were clinically stable until euthanasia. Histological observation showed myelinated nerve fibers in the osteons near the implant surface and trabecular bone around the implant (Fig. 2). Nerve fibers were primarily dispersed perivascular and oriented according to the axis of the blood vessels. No difference was observed in the myelinated nerve density between the three groups ( $p = 0.58$ ) and time points ( $p = 0.29$ ) (Figs. 3 and 5). However, there was a significant ( $p < 0.001$ ) difference between the three implant groups related to nerve diameter (Figs. 3 and 5). The nerve fiber diameter in the PRP group was greater than in the PPP ( $p = 0.02$ ) and control ( $p < 0.001$ ) group (Fig. 5). Overall, healing time significantly ( $p < 0.001$ ) influenced myelinated nerve fiber diameter (Figs. 4 and 5). An increase in nerve diameter was observed at 6 months healing time compared to 1 ( $p < 0.001$ ) and 3 ( $p = 0.002$ ) months (Fig. 5).

### Discussion

The periodontal mechanoreceptors are an important component of the stomatognathic system. Tooth extraction leads to impairment of osseoperception by damaging these receptors [30]. The application of PRP has been demonstrated and proven to be beneficial for repairing damaged nerve fibers and receptors [31, 32]. Evidence suggests successful application of PRP for inducing nerve regeneration when the traumatic gaps of nerve structures are less than 3 cm long [33]. While the fact that the defects around dental implants are normally not as large as peripheral nerve defects might make the regeneration of peri-implant nerve fibers more feasible. Based on this fact, the present study was conducted to quantify the density and diameter of myelinated nerve fibers in peri-implant bone following local application of PRP and PPP. Moreover, the study focused on the clinical hypothesis that PRP contains numerous growth factors for promoting nerve growth.

The amount of growth factors in platelet plasma vary widely amongst different species. Van den Dolder et al. demonstrated in a comparative study that humans had a higher concentration of growth factors compared to other animal models [34]. Considering these differences amongst species, we applied regular double centrifugated protocol and separately transferred both the low

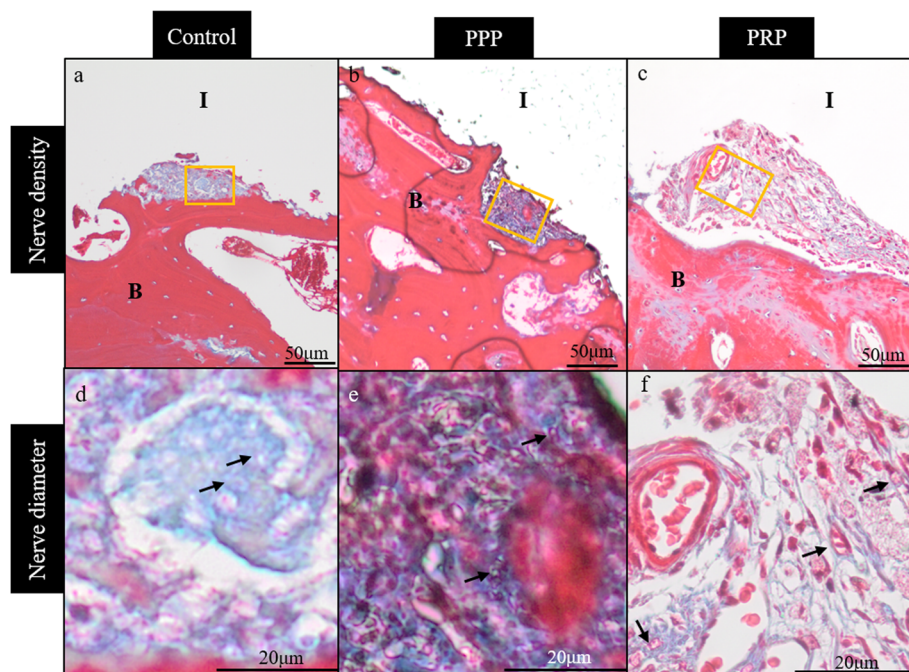


**Fig. 3** Histological sections stained with Masson's trichrome stain for control (a, d), platelet-poor plasma (b, e), platelet-rich plasma (c, f) group near the implant surface. No difference was observed in the myelinated nerve density between the three groups (upper row). The nerve fiber diameter in the PRP group was greater than in the control and PPP group (see arrows, bottom row). All sections derive from 6 months healing time and taken with a light microscope at  $\times 20$  (upper row) or  $\times 40$  magnification (bottom row). I, implant; B, bone

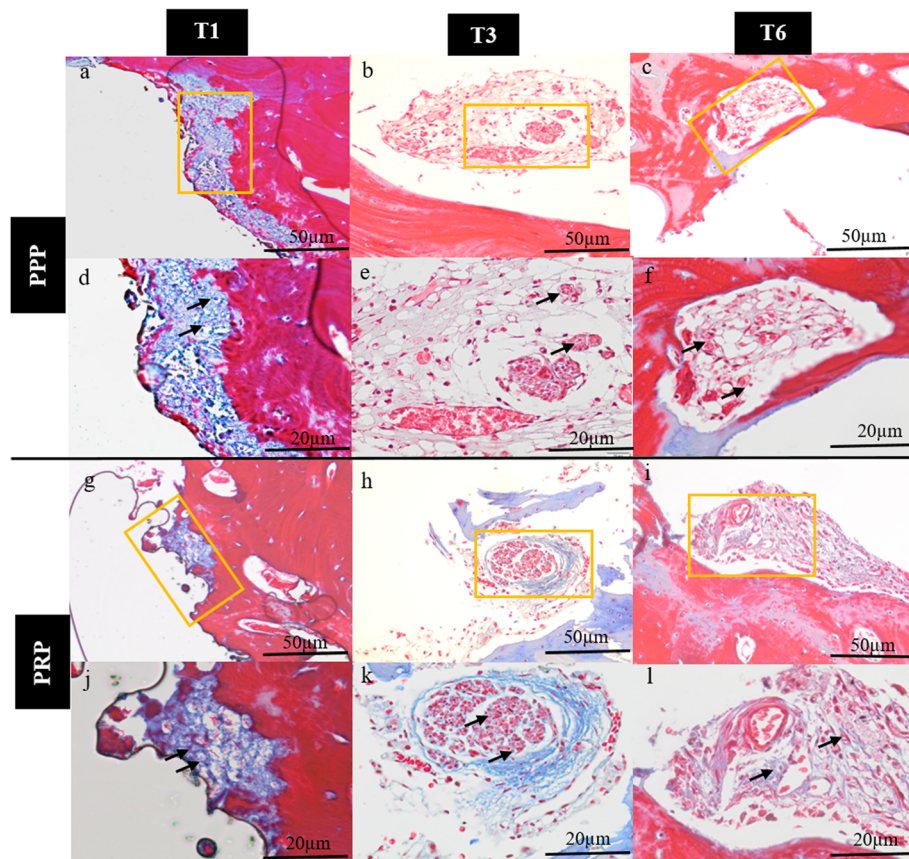


**Fig. 4** Histological sections stained with Masson's trichrome stain for platelet-poor and platelet-rich plasma after 1 (T1), 3 (T3), and 6 months (T6) healing time. The myelinated nerve fibers diameter (see arrows) increased with longer healing times for PPP (d–f) and PRP (j–l), but no effect was seen on nerve density (a–c and g–i). All sections were acquired with a light microscope at  $\times 20$  or  $\times 40$  magnification

concentration of PRP from the top layer and high concentration of PRP from the bottom layer into the implant bed.

In this study, the density and diameter of myelinated nerve fibers were examined in the region of 500  $\mu\text{m}$  away from implant because the mechanoreceptors in this zone are considered to be easily activated by the loading pressure [29]. For minimizing the potential bias between experimental animals, a split-mouth design was applied with identical implant placement and the platelet plasma treatment protocols. The results showed a significant increase in diameter of myelinated nerve fibers after 3 and 6 months healing time. Furthermore, PRP exhibited a significant effect on the diameter of the myelinated nerve fibers as compared to PPP, with bigger diameter fibers observed in the PRP group. Wada et al. [35] reported an increase in the number of neurofilament protein (NFP)-positive nerve fibers after 4 months loading time.

When comparing myelinated nerve density amongst all three groups, a tendency was observed that PPP or PRP might help to improve regeneration of nerve

fibers in peri-implant bone, more specifically 6 months after healing. Yet, this observation did not reach significance. This outcome could be explained based on short life of platelets (approximately 5–7 days) [36] and method of platelet plasma preparation and application. Literature reported that the concentration of PRP is dependent on its preparation process which can consecutively result in broad variability of growth factors [37, 38]. Graziani et. al reported that lower concentration of platelet plasma was better for enhancing cellular proliferation [38]. Cho et.al [39]. also found that PRPs' biological effect on nerve fibers was dependent on its frequency of application and concentration which was not considered in our study. For further experiments, it could be advised to optimize the animal model and application protocol for PRP and use a larger subject sample to verify the present results.

Various surgical options have been applied for repairing injured peripheral nerves [40–42]; however, these strategies fail to provide a suitable regenerative micro-environment at a cellular and molecular level.

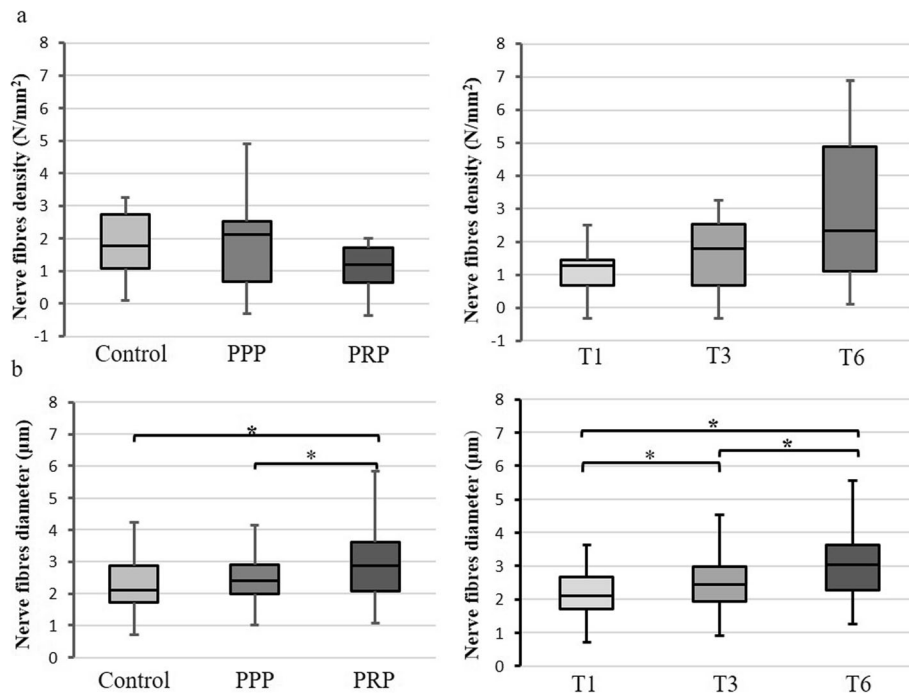


**Fig. 5** Box plots of nerve fiber density (a) and shortest diameter (b) for groups (control, platelet-poor, and platelet-rich plasma) and healing time (1, 3, and 6 months). The boundary the closest to 0 indicates the 25th percentile, a black line within the box marks the median, and the farthest from 0 indicates the 75th percentile. Whiskers above and below indicate the 10th and 90th percentile. No difference was observed in the myelinated nerve density, but a significant difference ( $p < 0.05$  indicated by an asterisk) was found for the shortest nerve diameter between groups and healing time

To overcome this limitation, PRP has been applied as an adjuvant therapeutic strategy for promoting nerve regeneration and repair [43]. Recent evidence suggests a desirable effect of PRP related to regeneration of injured peripheral nerves and it has been successfully applied clinically for sensory and motor fibers repair of neuromuscular units [44]. In the same instance, PRP-coated dental implants have also shown to promote bone regeneration and accelerate soft tissue healing [40]. However, there is lack of evidence demonstrating the effect of PRP using inferior alveolar nerve and lingual nerve models. Based on our findings, we believe that local application of PRP in cases of iatrogenic inferior alveolar and lingual nerve damage during routine implant surgery may provide accelerated healing and regeneration of nerve fibers, thereby improving neurosensory recovery.

Despite the current study limitations, the present report provides for the first time an animal model to evaluate regeneration of injured nerve fibers in the proximity of dental implants. It is considered a step forward in understanding PRPs' influence on implant rehabilitation surgery. Further studies should be performed to develop a standardized protocol for PRP preparation and application in the peri-implant region and assessing its effect on osseoperception.

## Conclusions

The present study showed that the healing time significantly influenced the diameter of the myelinated nerve fibers in the peri-implant bone. PRP exerted a significant effect on the diameter of the myelinated nerve fibers as compared to PPP. Large-scale animal studies and longer follow-up periods are needed to confirm these findings and to verify whether platelet plasma can facilitate nerve regeneration process.

## Acknowledgements

The authors are thankful to the laboratory technicians from the Research Base of West China Hospital, Sichuan University and Translational Cell and Tissue Research of University Hospitals Leuven, KU Leuven for their valuable help during this animal research, and to Xin Li (KU Leuven) for her help with the histological digitalization.

## Authors' contributions

HY, CP, and RJ designed this study. HY did the animal experiment. TV, KVE, IL, and TR helped with the histological staining. DS performed the measurements. JVD did the statistical analysis. SD wrote the first draft of the manuscript. SS, JVD, KO, and RJ corrected the manuscript. All authors have read and approved the final manuscript.

## Funding

This work was supported by a Sichuan Province Science and Technology Support Program (2016SZ0010). DS received fellowship support from the China Scholarship Council (201708210187). HY is a postdoctoral (11.N3.615N) and JVD is a predoctoral (11.ZU.117N) FWO-research fellow.

**Availability of data and materials**

The datasets used and/or analyzed during the current study are available from the corresponding author on reasonable request.

**Ethics approval and consent to participate**

This animal experiment was approved by the Bioethics Committee of Sichuan University (reference number: WCCSIRB-D-2014-010).

**Consent for publication**

Not applicable.

**Competing interests**

The authors declare that they have no competing interests.

**Author details**

<sup>1</sup>OMFS IMPATH Research Group, Department of Imaging and Pathology, Faculty of Medicine, KU Leuven and Oral and Maxillofacial Surgery, University Hospitals Leuven, Campus Sint-Rafaël, Kapucijnenvoer 33, BE-3000 Leuven, Belgium. <sup>2</sup>State Key Laboratory of Oral Diseases, West China College of Stomatology, Sichuan University, Chengdu, China. <sup>3</sup>Department of Dentomaxillofacial Radiology, Faculty of Dentistry, University of Ankara, Ankara, Turkey. <sup>4</sup>Group of Morphology, Biomedical Research Institute, Hasselt University, Diepenbeek, Belgium. <sup>5</sup>Translational Cell & Tissue Research, Department of Imaging & Pathology, KU Leuven, Leuven, Belgium. <sup>6</sup>Department of Dental Medicine, Karolinska Institute, Stockholm, Sweden.

Received: 16 May 2019 Accepted: 24 October 2019

Published online: 04 December 2019

**References**

- Gallucci GO, Hamilton A, Zhou W, Buser D, Chen S. Implant placement and loading protocols in partially edentulous patients: A systematic review. *Clin Oral Implants Res.* 2018;29:106–34.
- Pietrokovski J, Kaffe I, Arensburg B. Retromolar ridge in edentulous patients: clinical considerations. *J Prosthodont.* 2007;16(6):502–6.
- Hughes FJ. Chapter 34 - Periodontium and Periodontal Disease. In: Vishwakarma A, Sharpe P, Shi S, Ramalingam M, editors. *Stem Cell Biology and Tissue Engineering in Dental Sciences*. Boston: Academic Press; 2015. p. 433–44.
- Wadhwa S, Nanda R, Pilbeam C. Chapter 26-Mechanotransduction of Orthodontic Forces. In: Nanda R, Kapila S, editors. *Current Therapy in Orthodontics*. Saint Louis: Mosby; 2010. p. 339–52.
- Lambrichts I, Creemers J, van Steenberghe D. Morphology of neural endings in the human periodontal ligament: an electron microscopic study. *J Periodontol Res.* 1992;27(3):191–6.
- Jacobs R, van Steenberghe D. Role of periodontal ligament receptors in the tactile function of teeth: a review. *J Periodontol Res.* 1994;29(3):153–67.
- Mühlbradt L, Ulrich R, Möhlmann H, Schmid H. Mechanoperception of natural teeth versus endosseous implants revealed by magnitude estimation. *Int J Oral Maxillofac Implants.* 1989;4(2):125–30.
- Jacobs R, van Steenberghe D. Comparative evaluation of the oral tactile function by means of teeth or implant-supported prostheses. *Clin Oral Implants Res.* 1991;2(2):75–80.
- Jacobs R, van Steenberghe D. Comparison between implant-supported prostheses and teeth regarding passive threshold level. *Int J Oral Maxillofac Implants.* 1993;8(5):549–54.
- Hämmerle CH, Wagner D, Brägger U, Lussi A, Karayiannis A, Joss A, et al. Threshold of tactile sensitivity perceived with dental endosseous implants and natural teeth. *Clin Oral Implants Res.* 1995;6(2):83–90.
- van Steenberghe D. From osseointegration to osseoperception. *J Dent Res.* 2000;79(11):1833–7.
- Jacobs R, van Steenberghe D. From osseoperception to implant-mediated sensory-motor interactions and related clinical implications. *J Oral Rehabil.* 2006;33(4):282–92.
- Van Loven K, Jacobs R, Swinnen A, Van Huffel S, Van Hees J, Van Steenberghe D. Sensations and trigeminal somatosensory-evoked potentials elicited by electrical stimulation of endosseous oral implants in humans. *Arch Oral Biol.* 2000;45(12):1083–90.
- Wang Y-HKT, Ando H, Nakanishi E, Yoshizawa H, Zhang M, Fukuyama H, Wada S, Uchida Y. Nerve regeneration after implantation in peri-implant area. A histological study on different implant materials in dogs. Osseoperception. In: Jacobs R. (editor) *Osseoperception*. Leuven. 1998. p.3–11.
- Lambrichts I. Histological and ultrastructural aspects of bone innervation. In: Jacobs R. (editor) *Osseoperception*. Leuven. 1998. p.13–20
- Corpas LD, Lambrichts I, Quirynen M, Collaert B, Politis C, Vrielinck L, et al. Peri-implant bone innervation: Histological findings in humans. *Eur J Oral Implantol.* 2014;7(3):283–92.
- Choi B-H. Periodontal ligament formation around titanium implants using cultured periodontal ligament cells: a pilot study. *Int J of Oral Maxillofac Implants.* 2000;15(2).
- Yuan Q, Gong P, Tan Z. Schwann cell graft: a method to promote sensory responses of osseointegrated implants. *Med Hypotheses.* 2007;69(4):800–3.
- Ma L, Xiang L, Yao Y, Yuan Q, Li L, Gong P. CGRP-alpha application: a potential treatment to improve osseoperception of endosseous dental implants. *Med Hypotheses.* 2013;81(2):297–9.
- Huang Y, Jacobs R, Van Dessel J, Bornstein MM, Lambrichts I, Politis C. A systematic review on the innervation of peri-implant tissues with special emphasis on the influence of implant placement and loading protocols. *Clin Oral Implants Res.* 2015;26(7):737–46.
- Martínez CE, González SA, Palma V, Smith PC. Platelet-poor and platelet-rich plasma stimulate bone lineage differentiation in periodontal ligament stem cells. *J Periodontol.* 2016;87(2):e18–26.
- Shahidi M, Vatanmakanian M, Arami MK, Shirazi FS, Esmaeili N, Hydarporian S, et al. A comparative study between platelet-rich plasma and platelet-poor plasma effects on angiogenesis. *Med Mol Morphol.* 2018;51(1):21–31.
- Zheng C, Zhu Q, Liu X, Huang X, He C, Jiang L, et al. Improved peripheral nerve regeneration using acellular nerve allografts loaded with platelet-rich plasma. *Tissue Eng. Part A.* 2014;20(23-24):3228–40.
- Dhurat R, Suresh M. Principles and methods of preparation of platelet-rich plasma: a review and author's perspective. *J Cutan Aesthet Surg.* 2014;7(4): 189.
- Huang Y, van Dessel J, Martens W, Lambrichts I, Zhong WJ, Ma GW, et al. Sensory innervation around immediately vs. delayed loaded implants: a pilot study. *Int J Oral Sci.* 2015;7(1):49–55.
- Faul F, Erdfelder E, Lang A-G, Buchner A. G\* Power 3: A flexible statistical power analysis program for the social, behavioral, and biomedical sciences. *Behav Res Methods.* 2007;39(2):175–91.
- Lee JW, Kwon OH, Kim TK, Cho YK, Choi KY, Chung HY, et al. Platelet-rich plasma: quantitative assessment of growth factor levels and comparative analysis of activated and inactivated groups. *Arch Plast Surg.* 2013;40(5):530.
- Huang Y, Corpas LS, Martens W, Jacobs R, Lambrichts I. Histomorphological study of myelinated nerve fibres in the periodontal ligament of human canine. *Acta Odontol Scand.* 2011;69(5):279–86.
- Weiner S, Klein M, Doyle JL, Brunner M. Identification of axons in the peri-implant region by immunohistochemistry. *Int J of Oral Maxillofac Implants.* 1995;10(6):689–95.
- Linden R, Scott B. The effect of tooth extraction on periodontal ligament mechanoreceptors represented in the mesencephalic nucleus of the cat. *Arch Oral Biol.* 1989;34(12):937–41.
- Anjayani S, Wirohadidjojo YW, Adam AM, Suwandi D, Seweng A, Amiruddin MD. Sensory improvement of leprosy peripheral neuropathy in patients treated with perineural injection of platelet-rich plasma. *Int J Dermatol.* 2014;53(1):109–13.
- Khojasteh A, Hosseinpour S, Nazeman P, Dehghan M. The effect of a platelet-rich fibrin conduit on neurosensory recovery following inferior alveolar nerve lateralization: a preliminary clinical study. *Int J Oral Maxillofac Surg.* 2016;45(10):1303–8.
- Whitman DH, Berry RL, Green DM. Platelet gel: an autologous alternative to fibrin glue with applications in oral and maxillofacial surgery. *J of Oral Maxillofac Surg.* 1997;55(11):1294–9.
- Dolder JVD, Mooren R, Vloon AP, Stoeltinga PJ, Jansen JA. Platelet-rich plasma: quantification of growth factor levels and the effect on growth and differentiation of rat bone marrow cells. *Tissue Eng.* 2006;12(11):3067–73.
- Wada S, Kojo T, Wang YH, Ando H, Nakanishi E, Zhang M, et al. Effect of loading on the development of nerve fibers around oral implants in the dog mandible. *Clin Oral Implants Res.* 2001;12(3):219–24.
- Yamazaki T, Sabit H, Oya T, Ishii Y, Hamashima T, Tokunaga A, et al. Activation of MAP kinases, Akt and PDGF receptors in injured peripheral nerves. *J Peripher Nerv Syst.* 2009;14(3):165–76.
- Anitua E, Sánchez M, Orive G, Andia I. Delivering growth factors for therapeutics. *Trends Pharmacol Sci.* 2008;29(1):37–41.

38. Graziani F, Ivanovski S, Cei S, Ducci F, Tonetti M, Gabriele M. The in vitro effect of different PRP concentrations on osteoblasts and fibroblasts. *Clin Oral Implants Res.* 2006;17(2):212–9.
39. Cho HH, Jang S, Lee SC, Jeong HS, Park JS, Han JY, et al. Effect of neural-induced mesenchymal stem cells and platelet-rich plasma on facial nerve regeneration in an acute nerve injury model. *The Laryngoscope.* 2010; 120(5):907–13.
40. Albanese A, Licata ME, Polizzi B, Campisi G. Platelet-rich plasma (PRP) in dental and oral surgery: from the wound healing to bone regeneration. *Immun Ageing.* 2013;10(1):23.
41. Tabrizi R, Pourdanesh F, Jafari S, Behnia P. Can platelet-rich fibrin accelerate neurosensory recovery following sagittal split osteotomy? A double-blind, split-mouth, randomized clinical trial. *Int J Oral Surg.* 2018;47(8):1011–4.
42. Sánchez M, Anitua E, Delgado D, Sanchez P, Prado R, Orive G, et al. Platelet-rich plasma, a source of autologous growth factors and biomimetic scaffold for peripheral nerve regeneration. *Expert Opin Biol Ther.* 2017;17(2):197–212.
43. Sánchez M, Garate A, Bilbao AM, Oraa J, Yangüela F, Sánchez P, et al. Platelet-Rich Plasma for Injured Peripheral Nerves: Biological Repair Process and Clinical Application Guidelines. *IntechOpen: Neuropathies*; 2018.
44. Bastami F, Vares P, Khojasteh A. Healing Effects of Platelet-Rich Plasma on Peripheral Nerve Injuries. *J Craniofac Surg.* 2017;28(1):e49–57.

### Publisher's Note

Springer Nature remains neutral with regard to jurisdictional claims in published maps and institutional affiliations.

**Submit your manuscript to a SpringerOpen<sup>®</sup> journal and benefit from:**

- ▶ Convenient online submission
- ▶ Rigorous peer review
- ▶ Open access: articles freely available online
- ▶ High visibility within the field
- ▶ Retaining the copyright to your article

---

Submit your next manuscript at ▶ [springeropen.com](https://www.springeropen.com)

---

# CHAPTER 4

## **Effect of platelet-rich and platelet-poor plasma on 3D bone-to-implant contact: A preclinical micro-CT study**

Song D<sup>1</sup>

Shujaat S<sup>1</sup>

Huang Y<sup>1,2</sup>

Van Dessel J<sup>1</sup>

Politis C<sup>1</sup>

Lambrichts I<sup>3</sup>

Jacobs R<sup>1,4</sup>

<sup>1</sup>OMFS IMPATH research group, Department of Imaging & Pathology, Faculty of Medicine, KU Leuven, and Oral & maxillofacial Surgery, University Hospitals Leuven, Leuven, Belgium

<sup>2</sup>State Key Laboratory of Oral Diseases, West China College of Stomatology, Sichuan University, Chengdu, China

<sup>3</sup>Morphology Group, Biomedical Research Institute, Hasselt University, Diepenbeek, Belgium

<sup>4</sup>Department of Dental Medicine, Karolinska Institute, Stockholm, Sweden.

RESEARCH

Open Access



# Effect of platelet-rich and platelet-poor plasma on 3D bone-to-implant contact: a preclinical micro-CT study

Dandan Song<sup>1,2\*</sup> , Sohaib Shujaat<sup>1,2</sup>, Yan Huang<sup>1,2,3</sup>, Jeroen Van Dessel<sup>1,2</sup>, Constantinus Politis<sup>1,2</sup>, Ivo Lambrichts<sup>4</sup> and Reinhilde Jacobs<sup>1,2,5</sup>

## Abstract

**Background:** Bone-to-implant contact ratio (BIC%) plays a critical role in secondary stability of osseointegrated dental implants. The aim of this study was to identify the correlation of 2D/3D micro-CT images with histology as a gold standard for evaluating BIC% and to investigate the influence of the platelet-rich plasma (PRP) and platelet-poor plasma (PPP) on 3D BIC% following delayed implant placement with delayed loading (DIP+DL).

**Methods:** Nine beagle dogs were recruited. Following bilateral extraction of mandibular 3rd premolar, 4th premolar, and 1st molar, 54 screw-type titanium implants were inserted and randomly divided into one control and two test groups based on a split-mouth design. The control group involved DIP+DL ( $n = 18$ ) and both test groups included DIP+DL with local application of PRP ( $n = 18$ ) and PPP ( $n = 18$ ). A BIC analysis was performed utilizing 2D histomorphometry and 2D/3D micro-CT. Following identification of correlation between histology and 2D/3D micro-CT images, a 3D micro-CT assessment of the 3D BIC% at three follow-up time-points (1, 3, and 6 months) was carried out for observing the influence of PRP and PPP on BIC.

**Results:** The 2D micro-CT BIC% values revealed a strong positive correlation with histology ( $r = 0.98$ ,  $p < 0.001$ ) and a moderate correlation existed with 3D micro-CT ( $r = 0.67$ ,  $p = 0.005$ ). BIC levels at 1 month and combined influence of PPP and PRP irrespective of time-points revealed significantly higher 3D BIC% compared to the control. However, a reduction in 3D BIC% was observed at the 3rd and 6th month. No significant difference was observed between both PRP and PPP.

**Conclusions:** Both 2D and 3D micro-CT demonstrated a potential to be utilized as a complimentary method for assessing BIC compared to the histological gold standard. Overall, both PRP and PPP significantly facilitated bone healing and osseointegration with a higher 3D BIC at follow-up. However, their influence was reduced as the observation period was increased.

**Keywords:** Platelet-rich plasma, Osseointegration, Bone-implant interface, X-ray micro-CT, Dental implants

\* Correspondence: [dandansong9015@gmail.com](mailto:dandansong9015@gmail.com)

<sup>1</sup>OMFS IMPATH Research Group, Department of Imaging & Pathology, Faculty of Medicine, KU Leuven, Kapucijnenvoer 33, 3000 Leuven, Belgium  
<sup>2</sup>Oral and Maxillofacial Surgery, University Hospitals Leuven, Leuven, Belgium  
Full list of author information is available at the end of the article

## Background

Implant osseointegration has been described as the simultaneous contact and distant osteogenesis at the implant surface and osteotomy wall leading to new bone synthesis and a direct bone-to-implant contact (BIC) without intervening connective tissue [1]. The amount of BIC is an important determinant for achieving optimal secondary implant stability [2]. Amongst different methods proposed in literature for evaluating BIC, the BIC ratio (BIC%) is one of the most commonly utilized objective methods for quantifying the extent of osseointegration following implant placement [3]. It measures the bone in-growth in the transitional region and is defined as the percentage of the bone in contact with the implant surface. The success of implant is ensured when the BIC% is maintained at a minimum of 50–65% [4, 5]. Thereby, the fundamental goal of implant therapy is to obtain a favorable BIC to prevent implant micro-mobility and for maximizing the implant survival rate.

The two most commonly utilized imaging modalities for evaluating BIC% in animal models include histomorphometry and micro-computed tomography (micro-CT) [6, 7]. Although histomorphometry is a reliable method and has been utilized as a gold standard for measuring 2D BIC%, information acquired through two-dimensional (2D) slices is deemed insufficient for representing the three-dimensional (3D) bone structure [8]. To overcome the limitations associated with histomorphometry, micro-CT has been recommended for assessing BIC% based on its rapidity, reproducibility, and non-destructiveness [9]. Most of the evidence focusing on micro-CT assessment of BIC% are pseudo three-dimensional (3D) in nature, as instead of analyzing the true reconstructed 3D image, the measurements are performed on 2D cross-sectional images [10, 11]. Although, cross-sectional images are pseudo 3D, still they form a basis for validating the accuracy of micro-CT cross-sectional measurements compared to a histological reference.

In literature, various parameters have been reported to influence the BIC levels, such as, implant type and size [12, 13], implant surface treatment [14], bone quality and quantity [15], implant loading conditions [16, 17], and forces exerted on implant [18, 19]. Attempts have been made for enhancing the BIC values by modifying the roughness, composition, and surface treatment of the dental implants. Recently, multiple growth factors, most commonly, platelet-derived growth factors have been utilized for enhancing the BIC [20]. Some studies have shown improved implant stability and earlier osteogenesis with plasma containing higher concentration of platelets [21, 22]. However, there is lack of evidence related to the influence of different platelet-derived plasma concentrations on the 3D BIC at follow-up.

Therefore, the following animal study was conducted to address two aims. The first aim was to identify the correlation of 2D/3D micro-CT images with histology as a gold standard for evaluating BIC%. The second aim investigated the influence of the platelet-rich plasma (PRP) and platelet-poor plasma (PPP) on 3D BIC% following delayed implant placement with delayed loading (DIP+DL) utilizing micro-CT.

## Methods

### Animal model and sample size

The protocol for this study was approved by the Bioethics Committee of Sichuan University (reference No. WCCSIRB-D-2014-010) and complied with the ARRIVE guideline for preclinical studies [23]. Nine beagle dogs (weight 14–17 kg, age 12–14 months) were recruited. An identical housing and feeding condition were executed for all the animals at the Experimental Animal Center of Laboratory of Biotherapy. The sample size was in accordance with the previous studies [24–26] and also based on a priori power analysis in G\*power 3.1 at a power of 80% and 0.05 level of significance [27].

### PRP and PPP preparation

A volume of 5 ml venous blood was collected from the cephalic vein of one of the forelegs of each experimental dog. The samples were transferred into sterile tube containing 1 ml of sodium citrate which acted as an anticoagulant and placed into a centrifuge (Allegra X 30R centrifuge, CA, USA). A previously optimized double-centrifugation protocol was applied for the preparation of PRP and PPP [28]. The first centrifugation involved a relative centrifugal force (RCF) of 700 g for 8 min and a second one at a RCF of 1600 g for 8 min. Following separation, 1 ml of each PRP and PPP were extracted from the sample. Both PRP and PPP were stored at room temperature in a conventional shaker until use.

### Surgical procedure

Each dog was administered with a 1-week prophylactic antibiotic therapy (gentamycin sulphate 300 mg) both before and after surgery for preventing infection. All surgeries were performed under general (0.1 ml/kg xylazine hydrochloride) and local anesthesia (2–4 ml lidocaine 2% epinephrine). A bilateral extraction of mandibular 3rd premolar, 4th premolar, and 1st molar was performed. After 1-month healing time, 54 screw-type titanium dental implant with plasma-sprayed hydroxyapatite (HA) coating (3.3 mm  $\varnothing$   $\times$  8 mm, cylindrical, non-submerged healing, BLB, China) were inserted at the healed extraction sites ( $n = 6$  per dog). The implants were randomly divided into one control and two test groups ( $n = 18$  per group) based on a split-mouth design. The control group involved DIP+DL ( $n = 18$ ) and the two test groups

included DIP+DL with local application of PRP ( $n = 18$ ) and PPP ( $n = 18$ ). Each implant in the test groups was dipped in PPP or PRP solution prior to insertion in the alveolus. Implants were inserted with a controlled insertion torque ranging between 30 and 35 N cm. All surgical procedures were performed by an experienced oral and maxillofacial surgeon who was blinded to the allocation process. A resin crown was fabricated and placed onto each implant following 1 month of treatment with a resin cement (RelyX, Unicem, RX, 3 M ESPE, St. Paul, USA) under halogen light-curing unit for 20 s. Afterwards, an articulating paper (20- $\mu\text{m}$  thick, Accufilm II, RX, 3M ESPE, St. Paul, USA) was used to check the contacts and make occlusal adjustments of the prosthetic crown to prevent possible overloading with the opposing natural teeth.

**Three-dimensional micro-CT assessment**

A high-resolution micro-CT (Quantum FX Caliper, Life Sciences, Perkin Elmer) was utilized for acquiring radiographic images of the mandibular bone blocks with implants from each animal and analyzing BIC% follow-up changes at 1- (T1), 3- (T3), and 6-month (T6) time-points. The acquisition protocol included 20- $\mu\text{m}$  pixel size, 360° rotation, 90-kVp tube voltage, 160- $\mu\text{A}$  tube current, 180-s scanning time, and a 20- $\text{mm}^2$  field of view (FOV). All the images were manually reoriented along the long axis of the implant in axial, coronal, and sagittal plane utilizing Dataviewer software (Ver. 1.5.1.2; Bruker-

CT; Kontich, Belgium). Thereafter, image processing was performed with CT Analyser software (version 1.16.1.0, Skyscan1272, Bruker Microct, Kontich, Belgium). The whole implant body was included in the volume of interest (VOI).

The implant shoulder was set as the reference for the superior limit of the VOI and the apex of the implant as the inferior limit (Fig. 1). The height of all the VOIs were kept constant for standardizing its vertical limit. Following determination of a circular region of interest (ROI) and binarization, a segmentation algorithm with separate histogram thresholding was applied for creating a distinction between implant (minimum, 43; maximum, 100) and bone (minimum, 110; maximum, 255) and calculating 3D BIC [29]. The BIC at a distance of 5 pixels from the implant surface was selected and BIC% was automatically calculated and represented by the percent intersection surface (I.S/TS) (Fig. 1).

**Histological assessment**

Based on a random direct sampling technique, the dogs from each group were randomly euthanized at T1, T3, and T6 with an overdose of an intravenous injection of xylazine hydrochloride. Thereafter, bone blocks were prepared and decalcified with ethylenediaminetetraacetic acid (EDTA, 0.5 mol/L) and phosphate-buffered saline (pH 7.4) at 4 °C for 10 months. Care was taken to avoid damage to the samples while removing implants with surgical forceps. The bone blocks were dehydrated and

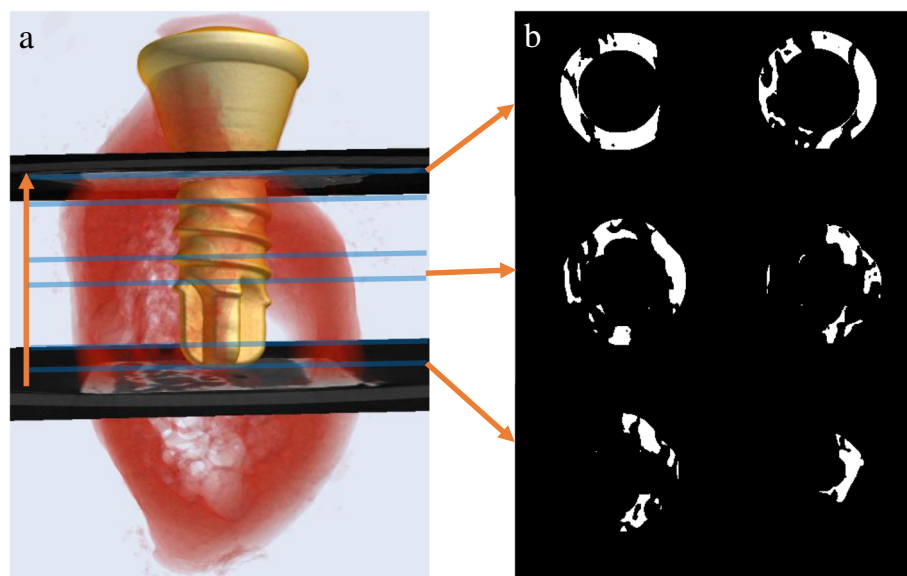


**Fig. 1** Automatic micro-CT-based evaluation of bone-to-implant contact (BIC) around the implant. **a** 3D surface reconstruction indicating the superior (implant shoulder) and inferior (implant apex) limit of volume of interest. **b** Binary images of BIC surface based on a custom processing with CTAn (version 1.16.1.0, Skyscan1272, Bruker Microct, Kontich, Belgium). Orange arrows indicate the series of slices from the implant apex to the shoulder level. Blue lines indicate the position of the images in **b** which show the amount of peri-implant bone descends from apex to coronal region

fully infiltrated with paraffin and sliced into thin serial sections (~6 μm) in a bucco-lingual direction. All slices were stained with Masson's trichrome stain. The BIC% was calculated based on a previously validated protocol [29].

Following selection of the matching histology slices and 2D micro-CT images, they were spatially aligned and registered for evaluating the same region as suggested by Soares et al. [30]. The BIC% was calculated by assessing the entire implant surface and contact areas between bone and implant using AxioVision software (Version 4.7.1; Carl Zeiss MicroImaging GmbH, Jena, Germany) (Fig. 2).

### Statistical analysis

The data analysis was performed using the SPSS software (Version 22, IBM, NY, USA). Normality of data distribution was assessed with the Shapiro-Wilk test. All the data showed normal distribution, thereby, parametric tests were utilized for assessing significance. The correlation between the 2D/3D micro-CT and histological BIC% was performed with the Pearson correlation coefficient. Afterwards, mean and standard deviation of the 3D micro-CT BIC% was calculated. Analysis of variance (ANOVA) and post hoc Bonferroni tests were employed for calculating the significance of difference between groups, different times points, and combined effect independent of time-points ( $\alpha = 0.05$ ).

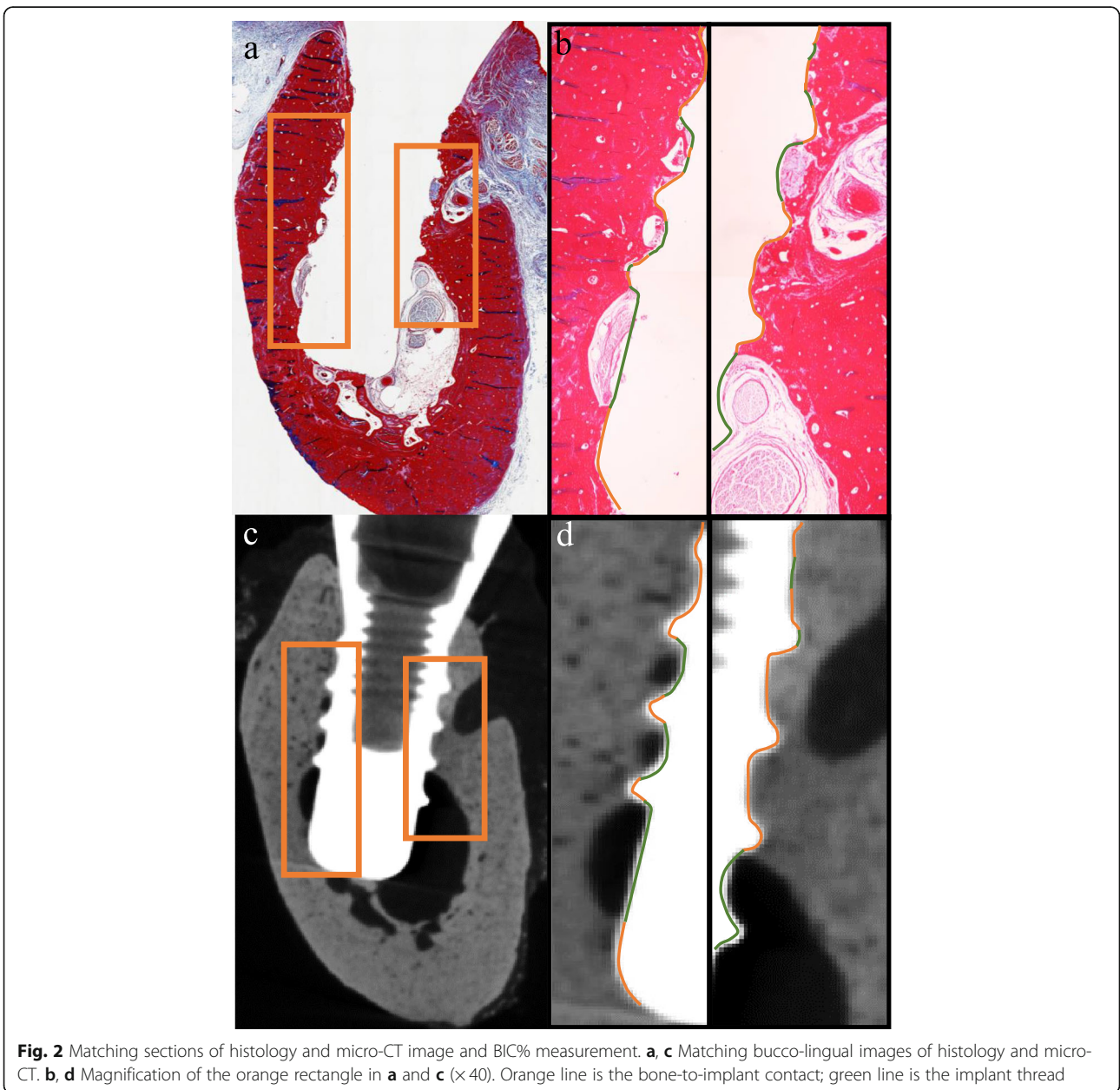


**Fig. 2** Matching sections of histology and micro-CT image and BIC% measurement. **a, c** Matching bucco-lingual images of histology and micro-CT. **b, d** Magnification of the orange rectangle in **a** and **c** (×40). Orange line is the bone-to-implant contact; green line is the implant thread

**Results**

All dogs remained in good health during the experiment. The implants in all groups were clinically stable till euthanasia with no sign of infection or any complication. The 2D BIC% values obtained from matching micro-CT and histology images revealed a strong positive significant correlation, regardless of the group or time-point ( $r = 0.98, p < 0.001$ ). However, a moderate correlation existed between 3D micro-CT and histology images ( $r = 0.67, p = 0.005$ ).

Table 1 describes the 3D BIC% of the control and test groups at the 1st, 3rd and 6th month observation time-points. At the 1st month of healing time, PPP ( $p = 0.09$ ) and PRP ( $p = 0.039$ ) test groups showed the highest 3D BIC% with a significant increase compared to the control group. However, no significant increase was observed at the 3rd and 6th month. Both test groups showed a decline in 3D BIC% at the 3rd and 6th month compared to the 1st month, and the 6th month time-point showed a further decrease in 3D BIC% compared to the 3rd month without any significant difference. At the 6th month time-point, the PPP test group showed higher 3D BIC% ( $55.3 \pm 8.7\%$ ) compared to PRP ( $52.9 \pm 7.5\%$ ) and the control group ( $51.5 \pm 4.7\%$ ) without any significant difference.

Overall, the 3D BIC% was found to be significantly high in PRP ( $63.8 \pm 4.4\%$ ,  $p = 0.024$ ) compared to the control ( $51.5 \pm 4.7\%$ ) irrespective of the time-point (Fig. 3), with PRP group showing the most increase in 3D BIC%. No significant difference was observed between PPP and PRP group.

**Discussion**

In our study, a strong correlation existed between 2D micro-CT and histology images, whereas with the utilization of 3D micro-CT, a moderate correlation was observed with a significant difference in BIC% of up to 4.9%. This minimal bias could be attributed to the absence of 3D BIC information in histology which varies depending on the implant surface being evaluated. Additionally, as the histological slices are taken at certain intervals at pre-selected locations which have a risk of misrepresenting, the entire osseous situation. Thereby, both 2D micro-CT and histological slices are unable to

represent the true 3D bone structure around the implant. Our findings were consistent with prior studies which also indicated a strong correlation between 2D micro-CT and histology and a moderate correlation between 3D micro-CT and histology [11, 31]. For overcoming the limitations of 2D histological and pseudo 3D micro-CT images, we utilized a high-resolution 3D micro-CT-based methodology for calculating the 3D BIC% by excluding four pixels closest to the implant. These steps ensured standardized BIC% assessment without under- and over-estimation and overcame the influence of partial volume effect around the trabecular edges and beam hardening near the implant surface.

The 3D BIC% was assessed at different follow-up time-points following application of PRP and PPP compared to the control group. Our findings suggested a significant increase in BIC% at the 1st month following both PRP and PPP application, thereafter a slight decrease was observed at follow-up. Studies have shown significantly higher BIC% at an early healing phase following PRP application, which was in accordance with our findings [32]. This might be explained based on the short life-span of platelets (approximately 5–10 days) [33]. A high concentration of platelet growth factors is initially secreted within the first 10 min following blood clotting and within the first hour, over 95% of the pre-synthesized growth factors contained in the alpha-granules complete their secretion [34]. Following initial burst release of PRP-derived growth factors, they continue to synthesize and secrete additional growth factors during their remaining life-span [35, 36]. These growth factors promote and accelerate tissue healing and regeneration [37, 38]. Additionally, the centrifugated platelets in the form of PRP also accelerate cell proliferation and bone healing. However, no studies were found assessing the influence of PPP which requires further investigations. The long-term influence of plasma leading to significant enhancement of bone formation in intra-bony periodontal defects and sinus augmentation has been well-documented [39–41]. However, it remains unclear and controversial whether long-term effect of PRP and PPP can be regarded as clinically favorable or not in implant therapy.

**Table 1** 3D bone-implant contact ratio of control (DIP+DL) and test groups (DIP+DL+PPP, and DIP+DL+PRP) at different follow-up time-points using micro-CT (\* $p < 0.05$ )

| Observation period | Group                                      | Bone-implant contact, mean $\pm$ SD (%)   | p value; (1) vs (2), (1) vs (3), (2)vs (3) |
|--------------------|--|---|--|
| 1 month            | (1) DIP+DL, (2) DIP+DL+PPP, (3) DIP+DL+PRP | 52.2 $\pm$ 3.2, <b>69.5 <math>\pm</math> 2.6*</b> , <b>73.4 <math>\pm</math> 5.6*</b> | <b>0.09*</b> , <b>0.039*</b> , 1           |
| 3 months           | (1) DIP+DL, (2) DIP+DL+PPP, (3) DIP+DL+PRP | 47.3 $\pm$ 11.2, 59.0 $\pm$ 2.7, 65.2 $\pm$ 4.0                                       | 1, 0.513, 0.819                            |
| 6 months           | (1) DIP+DL, (2) DIP+DL+PPP, (3) DIP+DL+PRP | 54.9 $\pm$ 7.7, 55.3 $\pm$ 9.1, 52.9 $\pm$ 7.1  | 1, 1, 1                                    |
| Overall            | (1) DIP+DL, (2) DIP+DL+PPP, (3) DIP+DL+PRP | 51.5 $\pm$ 4.7, 61.3 $\pm$ 4.8, <b>63.8 <math>\pm</math> 4.4*</b>                     | 0.078, <b>0.024*</b> , 1                   |

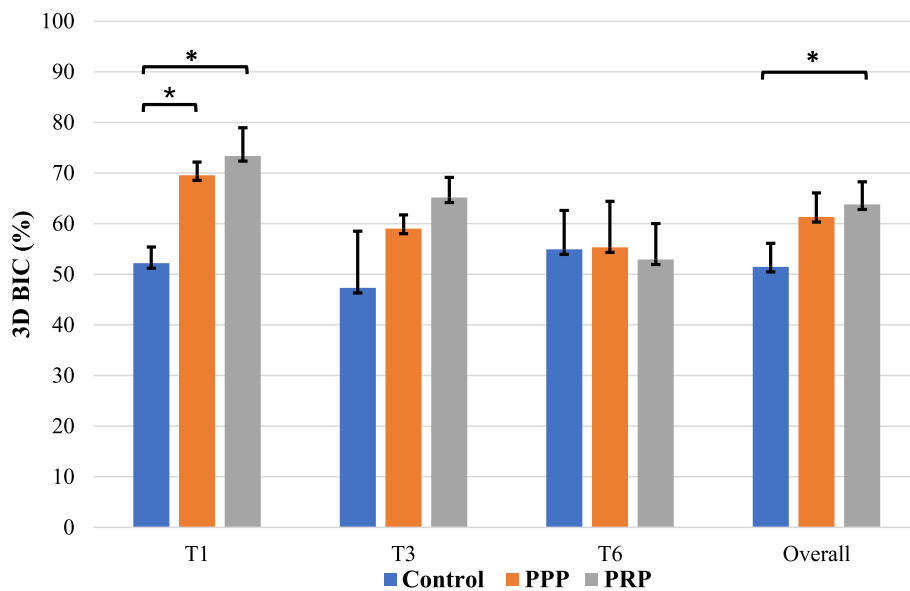


**Fig. 3** Impact of PRP and PPP on 3-dimension bone-implant-contact ratio (3D BIC%) at individual time-points and overall influence irrespective of time. PPP, platelet-poor plasma; PRP, platelet-rich plasma; T1, 1 month; T3, 3 months; T6, 6 months. \**p* < 0.05 statistically significant

When considering the overall combined impact of PPP and PRP irrespective of the time interval, an obvious increase in BIC% was observed with more than 60% in both test groups. Our findings were in an agreement with some studies [32, 42, 43]; at the same instance, inconsistencies were observed with other studies suggesting no influence of PPP or PRP on new bone formation [44–46]. The possible explanation for the inconsistent findings could be due to the different centrifugation techniques which can lead to substantial difference in platelet, leucocyte, and growth factors level. This requires further research to find an optimal standardized method for preparing plasma and later on studying which factors can lead to higher implant stability. The concentration of platelet in PRP ( $776.2 \pm 144.0 \times 10^9/L$ ) is almost 2000 times higher than that in PPP ( $4.8 \pm 1.8 \times 10^9/L$ ) [22]. However, in our study, both PRP and PPP have positive effect on promoting bone regeneration independent of the amount of platelet concentration. As the number of fibrin fibers is greater in PPP compared to PRP [47], which could explain the final biological bone healing effect of PPP during which lower platelet count is compensated by the fibrin fibers. The potential of these fibers acting to provide a scaffold for supporting cells and releasing growth factors should not be ignored. In some studies, PPP was discarded based on its low platelet nature [48, 49]. We believe, based on its potential in speeding up the bone regeneration regardless of the platelet concentration, future studies should also focus on the long-term impact of PPP on BIC.

The study had certain limitations. Firstly, primary implant stability was not evaluated. Secondly, the bone

blocks underwent decalcification prior to histological preparation which might have impacted the BIC calculation, yet researchers carefully removed the implant after decalcification ensuring no further harm to the peri-implant bony surface. Thirdly, the small sample size could have led to bias within our findings. Future pre-clinical studies with a larger sample size should focus on quantifying the combined impact of different plasma preparation techniques, implant treatment protocols, bone density, and other modified implant surfaces on long-term 3D BIC%. Additionally, further animal research should be carried out assessing the influence of PRP and PPP following implant placement in compromised bone defects. Later on, the results of this analysis could then be applied and tested in patients with poor wound healing.

### Conclusions

Both 2D and 3D micro-CT demonstrated a potential to be utilized as a complimentary method for assessing BIC compared to the histological gold standard. However, further studies should be considered for improving the correlation of 3D micro-CT with histological images. Overall, both PRP and PPP were able to contribute towards a significantly higher BIC following implant treatment. However, their influence was reduced as the observation period was increased, with BIC having the highest ratio at the 1st month and lowest at 6 months. It can be assumed that the plasma-fibrin may facilitate and speed up bone healing and osseointegration.

## Abbreviations

BIC%: Bone-to-implant contact ratio; 2D: Two-dimensional; 3D: Three-dimensional; PRP: Platelet-rich plasma; PPP: Platelet-poor plasma; DIP+DL: Delayed implant placement with delayed loading; micro-CT: Micro-computed tomography; RCF: Relative centrifugal force; FOV: Field of view; VOI: Volume of interest; ROI: Region of interest; HA: Hydroxyapatite

## Acknowledgements

The authors are thankful to the laboratory technicians from the Research Base of West China Hospital, Sichuan University, and Translational Cell and Tissue Research of University Hospitals Leuven, KU Leuven, for their valuable help during this animal research.

## Authors' contributions

All authors have read and approved the final manuscript. HY, CP, and RJ designed this study. HY did the animal experiment. IL helped with the histological staining. SD performed the measurements. JVD did the statistical analysis. SD and SS wrote the first draft of the manuscript. SS and RJ corrected the manuscript.

## Funding

This work was supported by a Sichuan Province Science and Technology Support Program (2016SZ0010). DS received fellowship support from China Scholarship Council (201708210187). HY is a postdoctoral (11.N3.615N) and JVD is a predoctoral (11.ZU.117N) FWO-research fellow.

## Availability of data and materials

The datasets used and/or analyzed during the current study are available from the corresponding author on reasonable request.

## Ethics approval and consent to participate

This animal experiment was approved by the Bioethics Committee of Sichuan University (reference number WCCSIRB-D-2014-010).

## Consent for publication

Not applicable.

## Competing interests

Dandan Song, Sohaib Shujaat, Yan Huang, Jeroen Van Dessel, Constantin Politis, Ivo Lambrechts, and Reinhilde Jacobs declare that they have no competing interests.

## Author details

<sup>1</sup>OMFS IMPATH Research Group, Department of Imaging & Pathology, Faculty of Medicine, KU Leuven, Kapucijnenvoer 33, 3000 Leuven, Belgium. <sup>2</sup>Oral and Maxillofacial Surgery, University Hospitals Leuven, Leuven, Belgium. <sup>3</sup>West China College of Stomatology, State Key Laboratory of Oral Disease & National Clinical Research Center for Oral Disease, Sichuan University, Chengdu, China. <sup>4</sup>Department of Morphology, Biomedical Research Institute, Hasselt University, Diepenbeek, Belgium. <sup>5</sup>Department of Dental Medicine, Karolinska Institute, Stockholm, Sweden.

Received: 8 August 2020 Accepted: 25 January 2021

Published online: 18 February 2021

## References

- Marco F, Milena F, Gianluca G, Vittoria O. Peri-implant osteogenesis in health and osteoporosis. *Micron* (Oxford, England : 1993). 2005;36:630–44.
- Sennerby L, Wennerberg A, Pasop F. A new microtomographic technique for non-invasive evaluation of the bone structure around implants. *Clin Oral Implants Res.* 2001;12:91–4.
- Roffi A, Filardo G, Kon E, Marcacci M. Does PRP enhance bone integration with grafts, graft substitutes, or implants? A systematic review. *BMC Musculoskelet Disord.* 2013;14:330.
- Albrektsson T, Sennerby L. Direct bone anchorage of oral implants: clinical and experimental considerations of the concept of osseointegration. *Int J Prosthodont.* 1990;3:30–41 PMID:2372366.
- De Smet E, Jaecques SV, Jansen JJ, Walboomers F, Vander Sloten J, Naert IE. Effect of constant strain rate, composed of varying amplitude and frequency, of early loading on peri-implant bone (re)modelling. *J Clin Periodontol.* 2007;34:618–24.
- Al Subaie AE, Eimar H, Abdallah MN, Durand R, Feine J, Tamimi F, et al. Anti-VEGFs hinder bone healing and implant osseointegration in rat tibiae. *J Clin Periodontol.* 2015;42:688–96.
- Bissinger O, Probst FA, Wolff KD, Jeschke A, Weitz J, Deppe H, et al. Comparative 3D micro-CT and 2D histomorphometry analysis of dental implant osseointegration in the maxilla of minipigs. *J Clin Periodontol.* 2017;44:418–27.
- Gao Y, Luo E, Hu J, Xue J, Zhu S, Li J. Effect of combined local treatment with zoledronic acid and basic fibroblast growth factor on implant fixation in ovariectomized rats. *Bone.* 2009;44:225–32.
- Feldkamp LA, Goldstein SA, Parfitt AM, Jesion G, Kleerekoper M. The direct examination of three-dimensional bone architecture in vitro by computed tomography. *J Bone Mineral Res.* 1989;4:3–11.
- Stoppie N, van der Waerden JP, Jansen JA, Duyck J, Wevers M, Naert IE. Validation of microfocus computed tomography in the evaluation of bone implant specimens. *Clin Implant Dent Relat Res.* 2005;7:87–94.
- Bernhardt R, Kuhlisch E, Schulz MC, Eckelt U, Stadlinger B. Comparison of bone-implant contact and bone-implant volume between 2D-histological sections and 3D-SRμCT slices. *Eur Cells Mater.* 2012;23:237–47.
- Akça K, Chang TL, Tekdemir I, Fanuscu MI. Biomechanical aspects of initial intraosseous stability and implant design: a quantitative micro-morphometric analysis. *Clin Oral Implants Res.* 2006;17:465–72.
- Bilhan H, Geckili O, Mumcu E, Bozdog E, Sünbuloğlu E, Kutay O. Influence of surgical technique, implant shape and diameter on the primary stability in cancellous bone. *J Oral Rehabil.* 2010;37:900–7.
- Germanier Y, Tosatti S, Broggin N, Textor M, Buser D. Enhanced bone apposition around biofunctionalized sandblasted and acid-etched titanium implant surfaces. A histomorphometric study in miniature pigs. *Clin Oral Implants Res.* 2006;17:251–7.
- Ruffoni D, Wirth AJ, Steiner JA, Parkinson IH, Müller R, van Lenthe GH. The different contributions of cortical and trabecular bone to implant anchorage in a human vertebra. *Bone.* 2012;50:733–8.
- Albrektsson T. Hard tissue implant interface. *Aust Dent J.* 2008;53(Suppl 1):S34–8.
- Romanos GE, Toh CG, Siar CH, Wicht H, Yacoub H, Nentwig GH. Bone-implant interface around titanium implants under different loading conditions: a histomorphometrical analysis in the Macaca fascicularis monkey. *J Periodontol.* 2003;74:1483–90.
- De Pauw GA, Dermout LR, Johansson CB, Martens G. A histomorphometric analysis of heavily loaded and non-loaded implants. *Int J Oral Maxillofac Implants.* 2002;17:405–12 PMID:12074457.
- Heitz-Mayfield LJ, Schmid B, Weigel C, Gerber S, Bosshardt DD, Jönsson J, et al. Does excessive occlusal load affect osseointegration? An experimental study in the dog. *Clin Oral Implants Res.* 2004;15:259–68.
- Kanno T, Takahashi T, Tsujisawa T, Ariyoshi W, Nishihara T. Platelet-rich plasma enhances human osteoblast-like cell proliferation and differentiation. *J Oral Maxillofac Surg.* 2005;63:362–9.
- Jiang N, Du P, Qu W, Li L, Liu Z, Zhu S. The synergistic effect of TiO<sub>2</sub> nanoporous modification and platelet-rich plasma treatment on titanium-implant stability in ovariectomized rats. *Int J Nanomedicine.* 2016;11:4719–33.
- Huang Y, Li Z, Van Dessel J, Salmon B, Huang B, Lambrechts I, et al. Effect of platelet-rich plasma on peri-implant trabecular bone volume and architecture: a preclinical micro-CT study in beagle dogs. *Clin Oral Implants Res.* 2019;30:1190–9.
- Kilkenny C, Browne WJ, Cuthill IC, Emerson M, Altman DG. Improving bioscience research reporting: the ARRIVE guidelines for reporting animal research. *PLoS Biol.* 2010;8:e1000412.
- Huang Y, Dessel JV, Depypere M, Elzideen M, Iliescu AA, Santos ED, et al. Validating cone-beam computed tomography for peri-implant bone morphometric analysis. *Bone Res.* 2014;2:14010.
- Huang Y, Van Dessel J, Liang X, Depypere M, Zhong W, Ma G, et al. Effects of immediate and delayed loading on peri-implant trabecular structures: a cone beam CT evaluation. *Clin Implant Dent Relat Res.* 2014;16:873–83.
- Pearce AJ, Richards RG, Milz S, Schneider E, Pearce SG. Animal models for implant biomaterial research in bone: a review. *Eur Cells Mater.* 2007;13:1–10.
- Faul F, Erdfelder E, Lang A-G, Buchner A. G\* Power 3: A flexible statistical power analysis program for the social, behavioral, and biomedical sciences. *Behav Res Methods.* 2007;39:175–91.
- Shin HS, Woo HM, Kang BJ. Optimisation of a double-centrifugation method for preparation of canine platelet-rich plasma. *BMC Veterinary Res.* 2017;13:198.

29. de Faria VK, dos Santos CL, da Silveira BM, Laperre K, Padovan LE, Jacobs R, et al. Micro CT assessment of bone microarchitecture in implant sites reconstructed with autogenous and xenogenous grafts: a pilot study. *Clin Oral Implants Res.* 2017;28:308–13.
30. Soares MQS, Van Dessel J, Jacobs R, da Silva Santos PS, Cestari TM, Garlet GP, et al. Zoledronic acid induces site-specific structural changes and decreases vascular area in the alveolar bone. *J Oral Maxillofac Surg.* 2018;76:1893–901.
31. Park YS, Yi KY, Lee IS, Jung YC. Correlation between microtomography and histomorphometry for assessment of implant osseointegration. *Clin Oral Implants Res.* 2005;16:156–60.
32. Zechner W, Tangl S, Tepper G, Fürst G, Bernhart T, Haas R, et al. Influence of platelet-rich plasma on osseous healing of dental implants: a histologic and histomorphometric study in minipigs. *Int J Oral Maxillofac Implants.* 2003;18:15–22 PMID:12608664.
33. Yamazaki T, Sabit H, Oya T, Ishii Y, Hamashima T, Tokunaga A, et al. Activation of MAP kinases, Akt and PDGF receptors in injured peripheral nerves. *J Peripheral Nervous Syst.* 2009;14:165–76.
34. Davis VL, Abukabda AB, Radio NM, Witt-Enderby PA, Clafshenkel WP, Cairone JV, et al. Platelet-rich preparations to improve healing. Part II: platelet activation and enrichment, leukocyte inclusion, and other selection criteria. *J Oral Implantol.* 2014;40:511–21.
35. Plachokova AS, van den Dolder J, van den Beucken JJ, Jansen JA. Bone regenerative properties of rat, goat and human platelet-rich plasma. *Int J Oral Maxillofac Surg.* 2009;38:861–9.
36. Cerciello S, Beitzel K, Howlett N, Russell RP, Apostolakos J, McCarthy MB, et al. The use of platelet-rich plasma preparations in the treatment of musculoskeletal injuries in orthopaedic sports medicine. *J Operative Techniques in Orthopaedics.* 2013;23:69–74.
37. Alsousou J, Thompson M, Hulley P, Noble A, Willett K. The biology of platelet-rich plasma and its application in trauma and orthopaedic surgery: a review of the literature. *J Bone Joint Surg Br.* 2009;91:987–96.
38. Davis VL, Abukabda AB, Radio NM, Witt-Enderby PA, Clafshenkel WP, Cairone JV, et al. Platelet-rich preparations to improve healing. Part I: workable options for every size practice. *J Oral Implantol.* 2014;40:500–10.
39. Peng W, Kim IK, Cho HY, Seo JH, Lee DH, Jang JM, et al. The healing effect of platelet-rich plasma on xenograft in peri-implant bone defects in rabbits. *Maxillofac Plast Reconstr Surg.* 2016;38:16.
40. Bae JH, Kim YK, Myung SK. Effects of platelet-rich plasma on sinus bone graft: meta-analysis. *J Periodontol.* 2011;82:660–7.
41. Ilgenli T, Dündar N, Kal BI. Demineralized freeze-dried bone allograft and platelet-rich plasma vs platelet-rich plasma alone in infrabony defects: a clinical and radiographic evaluation. *Clin Oral Investig.* 2007;11:51–9.
42. Albanese A, Licata ME, Polizzi B, Campisi G. Platelet-rich plasma (PRP) in dental and oral surgery: from the wound healing to bone regeneration. *J Immun Ageing.* 2013;10:23.
43. Marx RE, Carlson ER, Eichstaedt RM, Schimmele SR, Strauss JE, Georgeff KR. Platelet-rich plasma: growth factor enhancement for bone grafts. *Oral Surg Oral Med Oral Pathol Oral Radiol Endod.* 1998;85:638–46.
44. Wiltfang J, Kloss FR, Kessler P, Nkenke E, Schultze-Mosgau S, Zimmermann R, et al. Effects of platelet-rich plasma on bone healing in combination with autogenous bone and bone substitutes in critical-size defects. An animal experiment. *Clin Oral Implants Res.* 2004;15:187–93.
45. Choi BH, Im CJ, Huh JY, Suh JJ, Lee SH. Effect of platelet-rich plasma on bone regeneration in autogenous bone graft. *Int J Oral Maxillofac Surg.* 2004;33:56–9.
46. Raghoebar GM, Schortinghuis J, Liem RS, Ruben JL, van der Wal JE, Vissink A. Does platelet-rich plasma promote remodeling of autologous bone grafts used for augmentation of the maxillary sinus floor? *Clin Oral Implants Res.* 2005;16:349–56.
47. Hatakeyama I, Marukawa E, Takahashi Y, Omura K. Effects of platelet-poor plasma, platelet-rich plasma, and platelet-rich fibrin on healing of extraction sockets with buccal dehiscence in dogs. *Tissue Eng Part A.* 2014;20:874–82. <https://doi.org/10.1089/ten.TEA.2013.0058>.
48. Marx RE. Platelet-rich plasma: evidence to support its use. *J Oral Maxillofac Surg.* 2004;62:489–96.
49. Maghsoudi O, Shirazi SH, Abarkar M, Anvar SA. Standardization and modification techniques of platelet-rich plasma (PRP) preparation in rabbit. *Int Clin Pathol J.* 2015;1:5.

**Submit your manuscript to a SpringerOpen<sup>®</sup> journal and benefit from:**

- Convenient online submission
- Rigorous peer review
- Open access: articles freely available online
- High visibility within the field
- Retaining the copyright to your article

---

Submit your next manuscript at ► [springeropen.com](https://www.springeropen.com)

---



# CHAPTER 5

## Diagnostic accuracy of CBCT versus intraoral imaging for assessment of peri-implant bone defects

Song D<sup>1</sup>

Shujaat S<sup>1</sup>

De Faria Vasconcelos K<sup>1</sup>

Huang Y<sup>1,2</sup>

Politis C<sup>1</sup>

Lambrichts I<sup>3</sup>

Jacobs R<sup>1,4</sup>

<sup>1</sup>OMFS IMPATH research group, Department of Imaging & Pathology, Faculty of Medicine, KU Leuven, and Oral & maxillofacial Surgery, University Hospitals Leuven, Leuven, Belgium

<sup>2</sup>State Key Laboratory of Oral Diseases, West China College of Stomatology, Sichuan University, Chengdu, China

<sup>3</sup>Morphology Group, Biomedical Research Institute, Hasselt University, Diepenbeek, Belgium

<sup>4</sup>Department of Dental Medicine, Karolinska Institute, Stockholm, Sweden.

RESEARCH ARTICLE

Open Access



# Diagnostic accuracy of CBCT versus intraoral imaging for assessment of peri-implant bone defects

Dandan Song<sup>1\*</sup> , Sohaib Shujaat<sup>1</sup>, Karla de Faria Vasconcelos<sup>1</sup>, Yan Huang<sup>1,2</sup>, Constantinus Politis<sup>1</sup>, Ivo Lambrechts<sup>3</sup> and Reinhilde Jacobs<sup>1,4</sup>

## Abstract

**Background:** Early detection of marginal bone loss is vital for treatment planning and prognosis of teeth and implant. This study was conducted to assess diagnostic accuracy of CBCT compared to intra-oral (IO) radiography for detection, classification, and measurement of peri-implant bone defects in an animal model.

**Methods:** Fifty-four mandible blocks with implants were harvested from nine male health adult beagle dogs with acquisition of IO, CBCT and micro-CT images from all samples. Peri-implant bone defects from 16 samples were diagnosed using micro-CT and classified into 3 defect categories: dehiscence (n = 5), infrabony defect (n = 3) and crater-like defect (n = 8). Following training and calibration of the observers, they asked to detect location (mesial, distal, buccal, lingual) and shape of the defect (dehiscence, horizontal defect, vertical defect, crater-like defect) utilizing both IO and CBCT images. Both observers assessed defect depth and width on IO, CBCT and micro-CT images at each side of peri-implant bone defect via CT-analyzer software. Data were analyzed using SPSS software and a *p* value of < 0.05 was considered as statistically significant.

**Results:** Overall, there was a high diagnostic accuracy for detection of bone defects with CBCT images (sensitivity: 100%/100%), while IO images showed a reduction in accuracy (sensitivity: 69%/63%). Similarly, diagnostic accuracy for defect classification was significantly higher for CBCT, whereas IO images were unable to correctly identify vestibular dehiscence, with incorrect assessment of half of the infrabony defects. For accuracy of measuring defect depth and width, a higher correlation was observed between CBCT and gold standard micro-CT ( $r = 0.91$ , 95% CI 0.86–0.94), whereas a lower correlation was seen for IO images ( $r = 0.82$ , 95% CI 0.67–0.91).

**Conclusions:** The diagnostic accuracy and reliability of CBCT was found to be superior to IO imaging for the detection, classification, and measurement of peri-implant bone defects. The application of CBCT adds substantial information related to the peri-implant bone defect diagnosis and decision-making which cannot be achieved with conventional IO imaging.

**Keywords:** Alveolar bone loss, Peri-implantitis, CBCT, Dental radiography

## Background

Peri-implantitis is a pathological inflammatory reaction leading to progressive loss of the supporting bone which exceeds the physiological bone remodeling around an implant [1, 2]. To date, numerous studies have demonstrated the importance of radiographic imaging modalities for the diagnosis of bone

\*Correspondence: dandansong9015@gmail.com

<sup>1</sup> OMFS IMPATH Research Group, Department of Imaging and Pathology, Faculty of Medicine, KU Leuven and Oral and Maxillofacial Surgery, University Hospitals Leuven, Kapucijnenvoer 33, 3000 Leuven, Belgium  
Full list of author information is available at the end of the article



© The Author(s) 2021. **Open Access** This article is licensed under a Creative Commons Attribution 4.0 International License, which permits use, sharing, adaptation, distribution and reproduction in any medium or format, as long as you give appropriate credit to the original author(s) and the source, provide a link to the Creative Commons licence, and indicate if changes were made. The images or other third party material in this article are included in the article's Creative Commons licence, unless indicated otherwise in a credit line to the material. If material is not included in the article's Creative Commons licence and your intended use is not permitted by statutory regulation or exceeds the permitted use, you will need to obtain permission directly from the copyright holder. To view a copy of this licence, visit <http://creativecommons.org/licenses/by/4.0/>. The Creative Commons Public Domain Dedication waiver (<http://creativecommons.org/publicdomain/zero/1.0/>) applies to the data made available in this article, unless otherwise stated in a credit line to the data.

defects [3–5]. An accurate radiographic assessment of the morphology and size of the peri-implantitis bone defect is of vital clinical importance as it directly influences the implant survival and therapeutic outcome of both surgical and non-surgical defect treatment [6–8].

Two-dimensional (2D) imaging modalities such as intraoral (IO) and panoramic radiography are the most commonly utilized radiographic methods for defect detection in a clinical practice based on their low radiation exposure and cost-effectiveness [9–13]. However, they have certain limitations such as, 2D representation of three-dimensional (3D) anatomical structures, geometric distortion, lower spatial resolution, and image magnification which underestimates the defect [14–17]. Furthermore, their inability to diagnose and distinguish buccally and lingually located defects may lead to an inaccurate representation of the bone defect [18, 19]. To overcome the limitations associated with 2D radiography, cone beam computed tomography (CBCT) has been proposed and recommended by various studies as a modality of choice for assessment of periodontal bone defects [20–23]. Undoubtedly, CBCT offers higher accuracy compared to its 2D counterparts for an earlier bone defect detection, thereby allowing immediate application of interventions for controlling further bone loss. Nevertheless, only a few studies are available assessing the superiority of CBCT over 2D imaging for the assessment of peri-implant bone defects [23, 24].

Furthermore, micro-computed tomography (micro-CT), one of the most versatile non-invasive investigative techniques has been regarded as a standard tool for quantifying the density and architecture of bone in preclinical investigations. Micro-CT functions by illuminating a rotated object with x-rays and collects the magnified projection images via planar x-ray detector. Thereafter, multiple angular images are obtained and stacked together to form the 3D image. Henceforth, micro-CT not only has the ability of imaging the internal biological structures without the need for sample preparation but also provides with 3D representation of the anatomical structures. Previous studies have widely reported on the feasibility and reliability of using micro-CT to evaluate morphologic characteristics of cortical and trabecular bone in both animal and human models [25–28].

Therefore, the current study was conducted to assess the diagnostic accuracy of CBCT compared to IO radiography using the micro-CT as the standard for the detection, classification, and measurement of peri-implant bone defects in an animal model.

## Methods

Following ethical approval from the Bioethics Committee of Sichuan University (Reference No: WCCSIRB-D-2014-010), nine health male adult beagle dogs (weight 14–17 kg, age 12–14 months) with completely sound oral condition were recruited by following the ARRIVE guidelines [29] for preclinical animal studies (Supplementary file). All animals were provided by Laboratory Animal Center of Sichuan University. An identical housing and feeding condition was required for all the animals at the Experimental Animal Center of Laboratory of Biotherapy. With injecting general anesthesia with Sumianxin (0.1 ml/kg xylazine hydrochloride, Changchun Military Academy of Medical Sciences, Changchun, China) and local anesthesia (2–4 ml lidocaine 2% epinephrine, Tianjin Pharmaceutical Co. Ltd, Tianjin, China) at the surgical sites, a total of 54 screw-type titanium dental implants with plasma-sprayed hydroxyapatite (HA) coating (3.3 mm  $\varnothing$   $\times$  8 mm, cylindrical, non-submerged healing, BLB, China) were inserted in the mandibular region of each dog ( $n=6$  per dog). The sample size was calculated based on a prior power analysis in G\*power 3.1 at a power of 80% [30]. Following crown preparation and attachment, each implant was followed-up for a period of at least 1 months. The surgical procedure has been explained in a prior publication [31, 32]. Thereafter, all animals were euthanized using an overdose of xylazine hydrochloride (intravenous injection) and immediate perfusion of 4% paraformaldehyde and 0.0125% glutaraldehyde in 0.1 M phosphate buffer (pH 7.4). All dogs were healthy with clinically stable implants before sacrifice. The mandible blocks with implants were harvested and IO, CBCT and micro-CT images were acquired for each sample, where micro-CT acted as the gold standard. Table 1 describes the details of the acquisition devices and scanning parameters. Following image acquisition, 16 samples were found to have bone defects and were included in the study. The marginal bone level around the implant lower than the first screw loop of the implant from the top was judged as the bone defect; otherwise, the others were excluded. All the images were manually reoriented along with implants long axis with DataViewer (ver. 1.5.1.2, Bruker). Following orientation, three types of bone defects were recognized and diagnosed using micro-CT, which included dehiscence ( $n=5$ ), infrabony defect ( $n=3$ ) and crater-like defect ( $n=8$ ) (Fig. 1). The diagnosis was carried out by a consultant oral and maxillofacial radiologist with an experience of over 20 years. Later, two dentists were recruited as observers with an experience of at least 5 years in dental imaging. Following training and calibration of the observers, all the samples marked by the implant site were renumbered and randomized by the method of random sort in Excel. The

**Table 1** Details of the protocols for each acquisition device and scanning parameters

|                    | Intraoral radiography                           | Cone-beam computed tomography | Micro-CT                          |
|--------------------|---|-------------------------------|-----------------------------------|
| Product name       | Heliodent Plus                                  | 3D Accuitomo 170®             | Quantum FX                        |
| Company            | Sirona Dental Systems GmbH<br>Bensheim, Germany | J. Morita<br>Kyoto, Japan     | PerkinElmer, Inc.<br>Waltham, USA |
| Tube current (mA)  | 7   | 5                             | 0.16                              |
| Tube voltage (kV)  | 60  | 90                            | 90                                |
| Voxel size (mm)    | –   | 0.08                          | 0.02                              |
| Field of view (cm) | 3.3 × 4.3                                       | 10 × 5                        | 0.01 × 0.01                       |
| Exposure time (s)  | 0.12  | 17.5                          | 180                               |

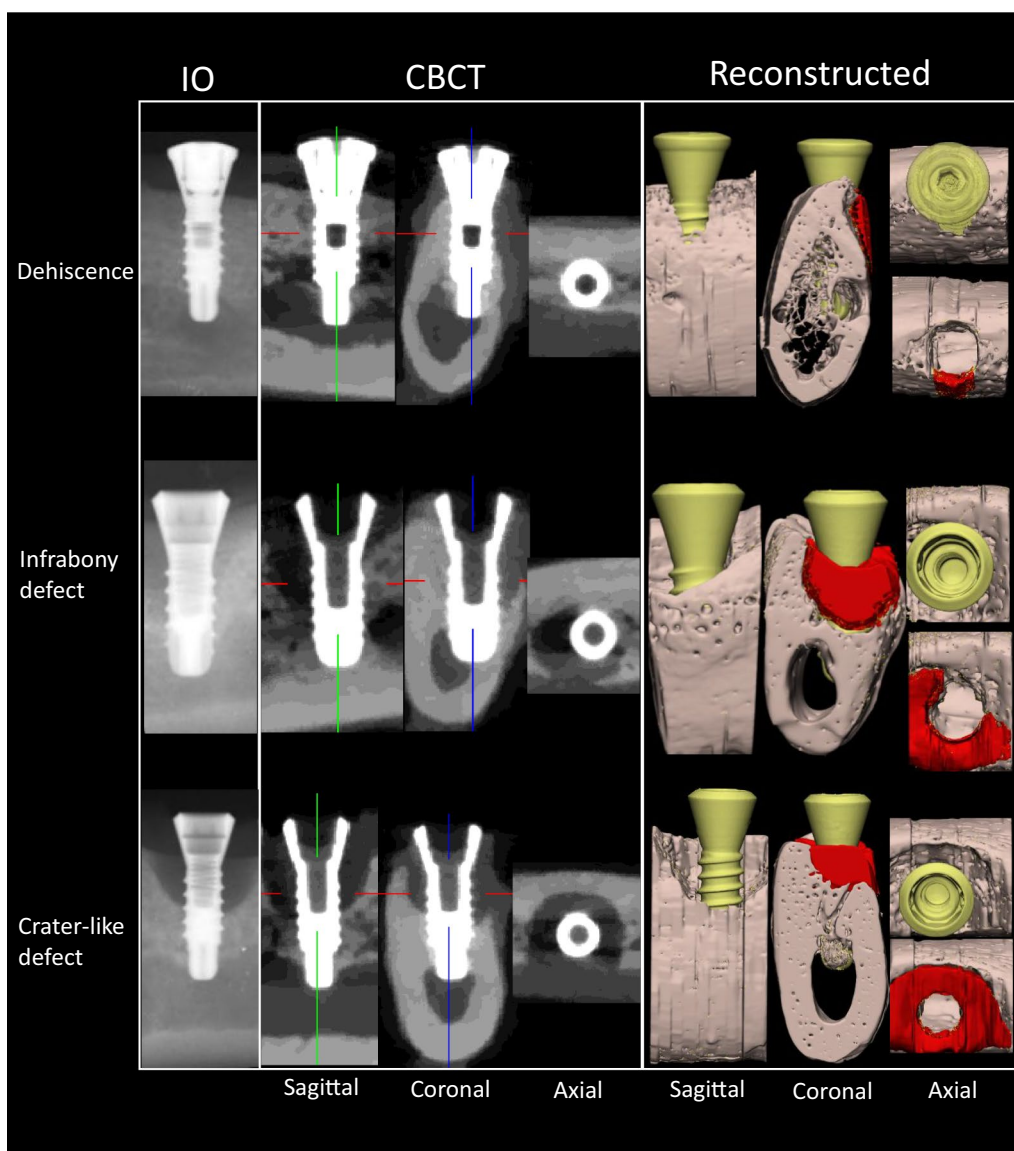


**Fig. 1** Shapes of peri-implant bone defects which were demonstrated in IO, CBCT and reconstructed imaging

observers were asked to detect the location of the defect (mesial, distal, buccal, lingual) and the shape of the defect (dehiscence, horizontal defect, vertical defect, crater-like defect). All evaluations were performed with both IO and CBCT images.

Following diagnosis, both observers measured the defect depth and width on IO, CBCT and micro-CT images at each side of peri-implant bone defect via CT-analyzer software (version 1.16.1.0, Skyscan1272, Bruker MicroCT, Kontich, Belgium). The slices in 3D images were standardized to that of 2D image. A mesio-distal and bucco-lingual slice was selected from the sagittal and coronal view individually on the 3D images and were oriented parallel to the long axis of implant. The width and depth of the defects were measured as shown in Fig. 2. The observers performed both diagnosis and measurement tasks at a two-week interval with randomization of the data for assessing the observer reliability.

**Statistical analysis**

Data were analyzed using SPSS software (Version 22, IBM, New York, USA). The diagnostic accuracy of IO and CBCT images for the defect detection and classification was assessed by calculating the sensitivity and intra- and inter-rater reliability (Cohen’s and Fleiss’s Kappa) of each method and observer. The interpretation of Kappa values was carried out as suggested by Landis and Koch [33]. Intra-class correlation coefficient (ICC) was utilized for calculating the absolute inter-protocol, intra-rater,

and inter-rater agreement for defects depth and width measurements. Kruskal-Wallis one-way ANOVA test was performed to compare the depth and width of the infrabony defect with that of the crater-like defect. A *p* value of < 0.05 was considered as statistically significant.

**Results**

Overall, a high agreement (Kappa: 0.92; 95% CI 0.88–0.96) and reliability (ICC: 0.97; 95% CI 0.96–0.97) was observed for the detection and classification of the defect on IO and CBCT images. Intra- and inter-rater agreement for the diagnosis with CBCT was found to be almost perfect for each observer. The reliability of CBCT images was also considerably high when compared with the micro-CT for the detection and classification of the bone defect (ICC: 0.93 and 0.96, 95% CI 0.9–0.95 & 0.95–0.98). Additionally, the intra-rater and inter-rater agreement between both observers was higher with CBCT compared to IO images (Table 2). Both observers showed a high diagnostic accuracy for detection of the bone defect with CBCT images (sensitivity: 100%/100%), whereas, IO images showed a reduction in the accuracy (sensitivity: 69%/63%). Similarly, the diagnostic accuracy for the classification of the defect was also higher for CBCT when compared with IO images (Table 3).

For the accuracy of measuring depth and width of the defect, the ICC and agreement with the gold-standard micro-CT was found to be approximately 1 (ICC: 0.99, 95% CI 0.996–0.998; Kappa: 0.91). A higher correlation

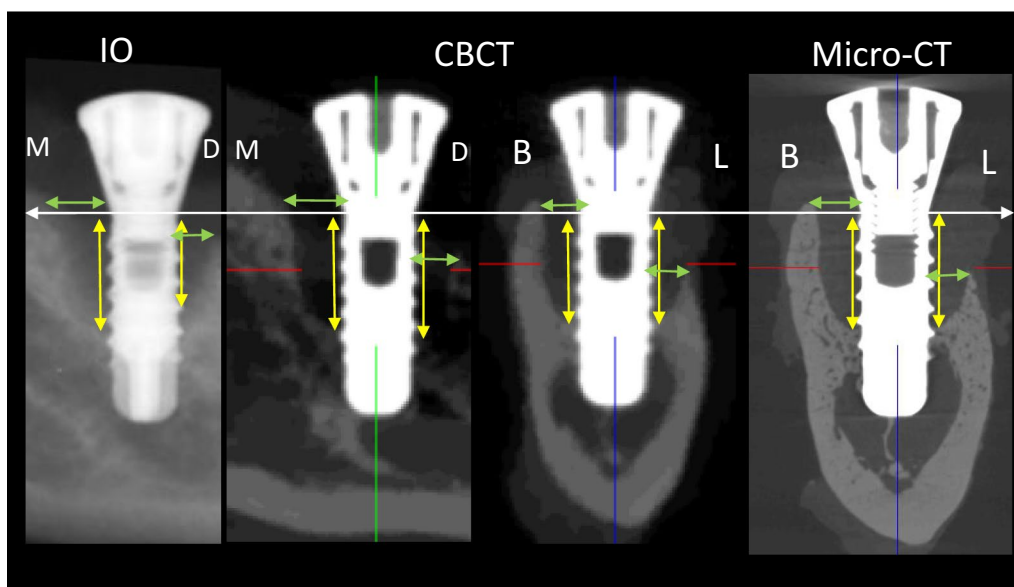


**Fig. 2** Method of depth and width measurement in intra-oral radiography (IO), cone-beam CT (CBCT) and micro-CT imaging. White arrow, implant shoulder as reference; Yellow arrow, depth of bone defect (from implant shoulder to the most apical of bone defect); Green arrow, width of bone defect (from implant shoulder to bone crest)

**Table 2 Reliability and agreement in detection of the bone lesion and morphology classification**

| Detection parameters | Methods | Observer effect |           |                |           |
|----------------------|---------|-----------------|-----------|----------------|-----------|
|                      |         | Reliability     |           | Agreement      |           |
|                      |         | ICC             | 95% CI    | Weighted Kappa | 95% CI    |
| Bone defect presence | IO      | 0.96            | 0.94–0.97 | 0.84           | 0.72–0.96 |
|                      | CBCT    | 0.97            | 0.96–0.98 | 0.87           | 0.74–0.99 |
|                      | Total   | 0.90            | 0.86–0.92 | 0.78           | 0.68–0.88 |
| Shape classification | IO      | 0.96            | 0.94–0.97 | 0.84           | 0.72–0.94 |
|                      | CBCT    | 1               | –         | 0.94           | 0.97–1    |
|                      | Total   | 0.92            | 0.90–0.94 | 0.82           | 0.74–0.90 |
| Total                |         | 0.97            | 0.96–0.97 | 0.92           | 0.88–0.96 |

Reliability, intra-class correlation coefficient; Agreement, inter-rater agreement; IO, intra-oral radiography; CBCT, cone beam computer tomography

**Table 3 Sensitivity of the diagnosis of bone defect presence and shape**

| Observers | Methods | Bone defect presence (%) | Bone defect shape |                      |                        |
|-----------|---------|--------------------------|-------------------|----------------------|------------------------|
|           |         |                          | Dehiscence        | Infrabony defect (%) | Crater-like defect (%) |
| 1         | IO      | 69                       | 0                 | 50                   | 78                     |
|           | CBCT    | 100                      | 100%              | 100                  | 90                     |
| 2         | IO      | 63                       | 0                 | 50                   | 78                     |
|           | CBCT    | 100                      | 100%              | 100                  | 89                     |

IO, intra-oral radiography, CBCT, cone beam computer tomography

was observed when CBCT was compared with micro-CT ( $r=0.91$ , 95% CI 0.86–0.94), whereas slightly lower correlation was seen with IO images ( $r=0.82$ , 95% CI 0.67–0.91).

The relationship between the bone defect morphology and size is demonstrated in Fig. 3. The depth for crater-like defect was larger than infrabony defect at all sides in both IO and CBCT images. The distal ( $p=0.003$ ) and buccal side ( $p=0.002$ ) showed a significantly larger depth in crater-like defects. Similarly, a larger defect width was observed for crater-like defects in both IO and CBCT images, except mesial side on CBCT images which showed a larger width in infrabony defect. Whereas, IO images showed a significantly larger width on the mesial side of the crater-like defect.

**Discussion**

Evidence suggests multiple studies underlining the importance of the accurate detection and classification of bone defect which can influence the treatment planning and prognosis of dental implant [34–36]. Therefore, the present study was conducted to assess the diagnostic accuracy of CBCT and IO imaging for the detection,

classification, and measurement of peri-implant bone defects.

Our findings suggested a higher reliability and diagnostic accuracy for the detection and classification of peri-implant defects with CBCT compared to IO images. Based on the 2D nature of IO radiographs, it only allowed accurate diagnosis of the horizontal and 1-wall vertical bone defects in a mesiodistal direction [5]. This could have led to a higher sensitivity of CBCT which offers 3D visualization of the bone. These findings were consistent with previous studies, which suggested CBCT to have a significantly higher diagnostic accuracy compared to digital periapical radiography for the detection of fenestration, dehiscence and three-walled periodontal defects [23, 24, 37]. In a study by Noujeim, et al. [22], a high sensitivity was recorded for the detection of large bone defects by both IO and CBCT imaging and they suggested CBCT imaging only for small bone defects of <1mm where IO radiography was considered insufficient for an accurate diagnosis. However, their study has limited clinical value as they observed defects only in the mesiodistal direction, and buccolingual aspect of the defect was not included in the evaluation. Whereas, in our study five bone defects were with dehiscence on the lingual side which could not be detected or classified accurately on IO radiographs, thereby leading to a further reduction in its diagnostic accuracy [5]. Similarly, inconsistency was observed with a study by Kühl, et al. [16], where authors found that IO radiography offered improved accuracy compared to CT-based images for the detection of peri-implant bone defect. The main reason for decreased accuracy of CT-based images in their study was based on the presence metal artefacts resulting in lower quality images. On the other hand, we acquired images with a high-resolution CBCT protocol and the CBCT device had an inbuilt metal artefact reduction algorithm resulting in high quality images.

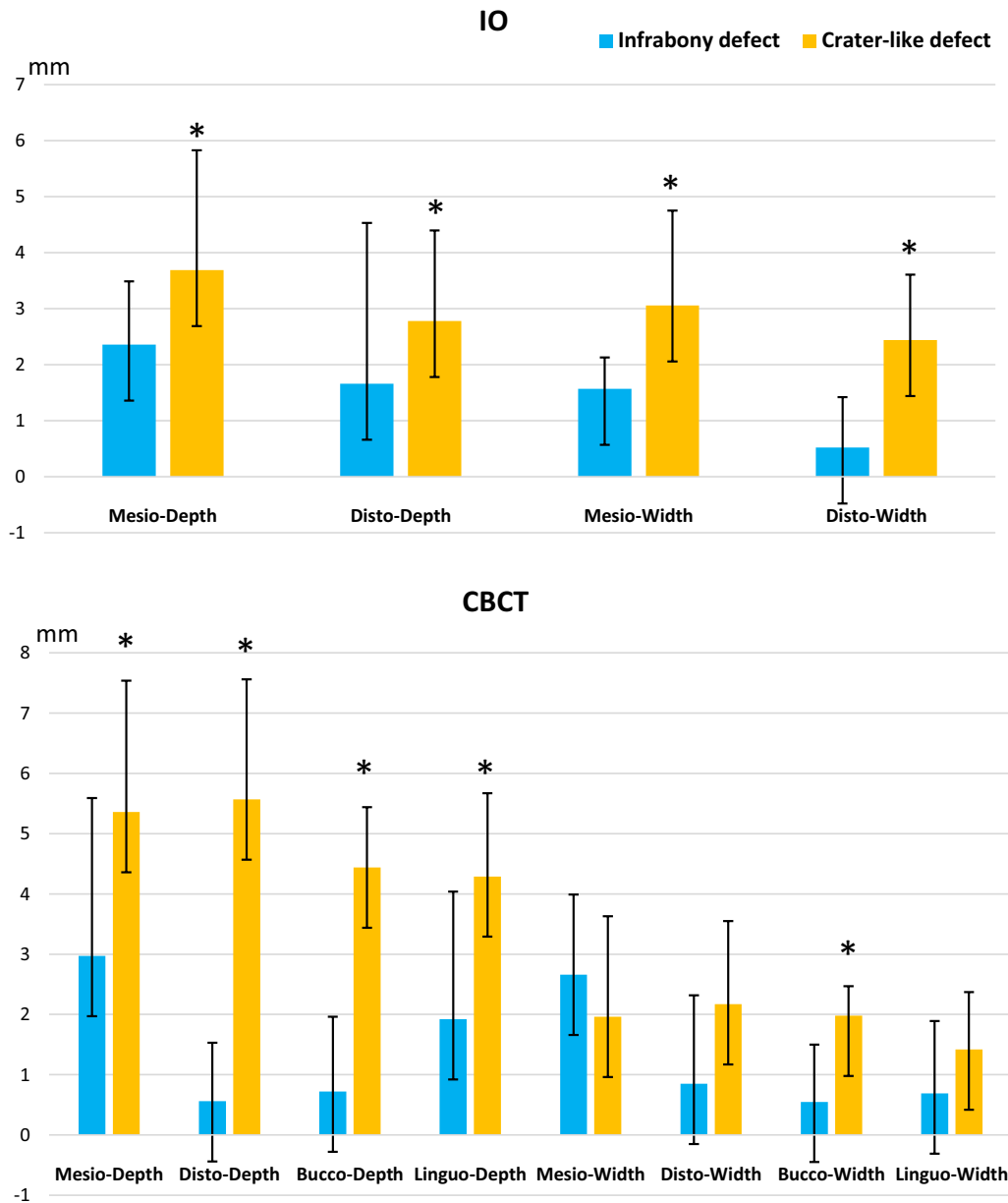


**Fig. 3** Graph of bone defect size (depth and width) for different shapes of peri-implant bone lesion in IO and CBCT imaging. \* $p < 0.05$ . IO: Intra-oral radiography; CBCT: cone beam computer tomography

In relation to the mesiodistal depth and width measurements of the bone defect, a high correlation was found for both IO ( $r=0.82$ ) and CBCT ( $r=0.92$ ) images when compared with the micro-CT. The slightly lower correlation value with IO could have resulted due to the overlapping effect and blurring of the peri-implant region. We found the size of defect to be significantly larger in crater-like defect compared to infrabony defect. A previous study observed peri-implant bone defects to be larger on buccal side compared to other walls in patients

with peri-implantitis [38]. In contrast, we found defects to be larger mesiodistally followed by lingual and buccal wall. The difference in study design where we utilized an animal model and location of the implant placement could have resulted in these inconsistent findings. The detection, classification and accurate measurements of the defect are all critical parameters as they might influence the success of an implant or regenerative therapy if required [39]. Although CBCT carries the risk of higher radiation dose compared to IO radiography, it can be

argued whether the benefit of an accurate diagnosis with CBCT outweighs the risks involved with a higher radiation dose. We believe that a clinician should not hesitate to order a CBCT for the diagnosis and follow-up of a peri-implant defect, as IO radiography is insufficient for an accurate diagnosis [40]. At the same instance, the scanning parameters should be optimized accordingly for reducing the radiation exposure to the patient.

Our study had certain limitations. Firstly, the sample size was not sufficient for drawing a meaningful conclusion related to the relationship between the bone defect type and size. Secondly, the setup for the high resolution CBCT was obviously diverting from that of a normal patient acquisition. We realise that this may cause some deviation when transferring the present imaging data and outcome to the clinic situation. However, the high-dose allowed accurate investigation of infra-bony defects which might get impeded due to the presence of implant-related artefacts if a lower dose is applied. Further studies are required to assess the diagnostic accuracy of low-dose CBCT protocols in patients for detecting and classifying peri-implant bone defects. In the midst of these limitations, we provided evidence related to the detection of bone defects which might not be visible on IO radiographs, thereby leading to an inaccurate diagnosis and treatment planning. Although IO radiography is considered as a clinical standard for assessing peri-implant bone defects [41], the importance of CBCT imaging for diagnosis and follow-up should not be ignored for employing timely management of the defect [42, 43]. Further studies should be carried out with patient specific low-dose CBCT protocols to assess their accuracy for peri-implant bone defect diagnosis. Also, future studies should pay attention to the implant blooming artefacts that are impacting peri-implant visibility and are influenced by CBCT device and protocol characteristics as well as by implant material and design [44, 45].

## Conclusions

The diagnostic accuracy and reliability of CBCT was found to be superior to IO imaging for the detection, classification, and measurement of peri-implant bone defects. The application of CBCT adds substantial information related to the peri-implant bone defect diagnosis and decision-making which cannot be achieved with conventional IO imaging. However, benefit-risk ratio should be kept in mind and CBCT should be acquired for cases where a peri-implant bone defect might influence the implant survival rate.

## Abbreviations

CBCT: Cone beam computed tomography; Micro-CT: Micro-computed tomography; IO: Intraoral radiography; 2D: Two-dimensional; 3D:

Three-dimensional; HA: Plasma-sprayed hydroxyapatite; ICC: Intra-class correlation coefficient.

## Acknowledgements

The authors are thankful to the laboratory technicians from the Research Base of West China Hospital, Sichuan University and Translational Cell and Tissue Research of University Hospital Leuven, KU Leuven for their valuable help during this animal study.

## Authors' contribution

CP, IL, and RJ designed this study. HY did the animal experiment. DS and KFV performed the measurements. DS and SS wrote the first draft of the manuscript. SS and RJ corrected the manuscript. All authors have read and approved the final manuscript.

## Funding

DS received fellowship support from China Scholarship Council. (201708210187). The funding plays no role in the design of the study and collection, analysis, and interpretation of data and in writing the manuscript.

## Availability of data and materials

The datasets used and/or analyzed during the current study are available from the corresponding author on reasonable request.

## Ethics approval and consent to participate

This animal experiment was approved by the Bioethics Committee of Sichuan University (reference number: WCCSIRB-D-2014-010).

## Consent for publication

Not applicable.

## Competing interests

The authors declare that they have no competing interests.

## Author details

<sup>1</sup> OMFS IMPATH Research Group, Department of Imaging and Pathology, Faculty of Medicine, KU Leuven and Oral and Maxillofacial Surgery, University Hospitals Leuven, Kapucijnenvoer 33, 3000 Leuven, Belgium. <sup>2</sup> West China College of Stomatology, State Key Laboratory of Oral Disease & National Clinical Research Center for Oral Disease, Sichuan University, Chengdu, China. <sup>3</sup> Department of Morphology, Biomedical Research Institute, Hasselt University, Diepenbeek, Belgium. <sup>4</sup> Department of Dental Medicine, Karolinska Institute, Stockholm, Sweden.

Received: 13 January 2021 Accepted: 1 February 2021

Published online: 10 February 2021

## References

- Zitzmann NU, Berglundh T. Definition and prevalence of peri-implant diseases. *J Clin Periodontol*. 2008;35(Suppl 8):286–91.
- Berglundh T, Zitzmann NU, Donati M. Are peri-implantitis lesions different from periodontitis lesions? *J Clin Periodontol*. 2011;38(Suppl 11):188–202.
- Schwarz F, Herten M, Sager M, Bieling K, Sculean A, Becker J. Comparison of naturally occurring and ligature-induced peri-implantitis bone defects in humans and dogs. *Clin Oral Implants Res*. 2007;18:161–70.
- Harris D, Horner K, Gröndahl K, Jacobs R, Helmrot E, Benic GI, et al. E.A.O. guidelines for the use of diagnostic imaging in implant dentistry 2011. A consensus workshop organized by the European Association for Osseointegration at the Medical University of Warsaw. *Clin Oral Implants Res*. 2012;23:1243–53.
- Hilgenfeld T, Juerchott A, Deisenhofer UK, Krisam J, Rammelsberg P, Heiland S, et al. Accuracy of cone-beam computed tomography, dental magnetic resonance imaging, and intraoral radiography for detecting peri-implant bone defects at single zirconia implants—an in vitro study. *Clin Oral Implants Res*. 2018;29:922–30.
- Tözüm TF, Turkyilmaz I, Yamalik N, Karabulut E, Turkyilmaz AS, Eratalay K. Analysis of the possibility of the relationship between various implant-related measures: an 18-month follow-up study. *J Oral Rehabil*. 2008;35:95–104.

7. Merheb J, Coucke W, Jacobs R, Naert I, Quirynen M. Influence of bony defects on implant stability. *Clin Oral Implants Res.* 2010;21:919–23.
8. Tsitoura E, Tucker R, Suvan J, Laurell L, Cortellini P, Tonetti M. Baseline radiographic defect angle of the intrabony defect as a prognostic indicator in regenerative periodontal surgery with enamel matrix derivative. *J Clin Periodontol.* 2004;31:643–7.
9. Papananou PN, Tonetti MS. Diagnosis and epidemiology of periodontal osseous lesions. *Periodontology* 2000. 2000;22:8–21.
10. Tugnait A, Clerehugh V, Hirschmann PN. The usefulness of radiographs in diagnosis and management of periodontal diseases: a review. *J Dent.* 2000;28:219–26.
11. Tugnait A, Clerehugh V, Hirschmann PN. Use of the basic periodontal examination and radiographs in the assessment of periodontal diseases in general dental practice. *J Dent.* 2004;32:17–25.
12. Esmaeli F, Shirmohammadi A, Faramarzie M, Abolfazli N, Rasouli H, Fallahi S. Determination of vertical interproximal bone loss topography: correlation between indirect digital radiographic measurement and clinical measurement. *Iran J Radiol.* 2012;9:83–7.
13. De Bruyn H, Vandeweghe S, Ruyffelaert C, Cosyn J, Sennerby L. Radiographic evaluation of modern oral implants with emphasis on crestal bone level and relevance to peri-implant health. *Periodontology* 2000. 2013;62:256–70.
14. Jeffcoat MK, Wang IC, Reddy MS. Radiographic diagnosis in periodontics. *J Periodontol.* 1995;7:54–68.
15. Eickholz P, Kim T, Benn D, Staehle H. Accuracy of radiographic assessments of interproximal bone loss. *Oral Surg Oral Med Oral Pathol Oral Radiol Oral Endod.* 1998;85:99–106.
16. Kühn S, Zürcher S, Zitzmann NU, Filippi A, Payer M, Dagassan-Berndt D. Detection of peri-implant bone defects with different radiographic techniques—a human cadaver study. *Clin Oral Implants Res.* 2016;27:529–34.
17. Ritter L, Elger MC, Rothamel D, Fienitz T, Zinser M, Schwarz F, et al. Accuracy of peri-implant bone evaluation using cone beam CT, digital intra-oral radiographs and histology. *Dentomaxillofac Radiol.* 2014;43:20130088.
18. Rees TD, Biggs NL, Collings CK. Radiographic interpretation of periodontal osseous lesions. *Oral Surg Oral Med Oral Pathol.* 1971;32:141–53.
19. Schwarz F, Sahm N, Schwarz K, Becker J. Impact of defect configuration on the clinical outcome following surgical regenerative therapy of peri-implantitis. *J Clin Periodontol.* 2010;37:449–55.
20. Vandenberghe B, Jacobs R, Yang J. Diagnostic validity (or acuity) of 2D CCD versus 3D CBCT-images for assessing periodontal breakdown. *Oral Surg Oral Med Oral Pathol Oral Radiol Endod.* 2007;104:395–401.
21. Braun X, Ritter L, Jervøe-Storm PM, Frentzen M. Diagnostic accuracy of CBCT for periodontal lesions. *Clin Oral Investig.* 2014;18:1229–36.
22. Noujeim M, Prihoda T, Langlais R, Nummikoski P. Evaluation of high-resolution cone beam computed tomography in the detection of simulated interradicular bone lesions. *Dentomaxillofac Radiol.* 2009;38:156–62.
23. Bayat S, Talaeipour AR, Sarlati F. Detection of simulated periodontal defects using cone-beam CT and digital intraoral radiography. *Dentomaxillofac Radiol.* 2016;45:20160030.
24. Christiaens V, De Bruyn H, De Vree H, Lamoral S, Jacobs R, Cosyn J. A controlled study on the accuracy and precision of intraoral radiography in assessing interproximal bone defect morphology around teeth and implants. *Eur J Oral Implantol.* 2018;11:361–7.
25. Bonnet N, Laroche N, Vico L, Dolleans E, Courteix D, Benhamou CL. Assessment of trabecular bone microarchitecture by two different x-ray microcomputed tomographs: a comparative study of the rat distal tibia using Skyscan and Scanco devices. *Med Phys.* 2009;36:1286–97.
26. Bouxsein ML, Boyd SK, Christiansen BA, Guldberg RE, Jepsen KJ, Müller R. Guidelines for assessment of bone microstructure in rodents using micro-computed tomography. *J Bone Miner Res.* 2010;25(7):1468–86.
27. Arvidsson A, Sarve H, Johansson CB. Comparing and visualizing titanium implant integration in rat bone using 2D and 3D techniques. *J Biomed Mater Res Part B.* 2015;103:12–20.
28. Van Dessel J, Nicolielo LF, Huang Y, Slagmolen P, Politis C, Lambrichts I, et al. Quantification of bone quality using different cone beam computed tomography devices: accuracy assessment for edentulous human mandibles. *Eur J Oral Implantol.* 2016;9:411–24.
29. Percie du Sert N, Hurst V, Ahluwalia A, Alam S, Avey MT, Baker M, et al. The ARRIVE guidelines 2.0: updated guidelines for reporting animal research. *BMC Vet Res.* 2020;16:242.
30. Faul F, Erdfelder E, Lang A-G, Buchner A. G\* Power 3: a flexible statistical power analysis program for the social, behavioral, and biomedical sciences. *Behav Res Methods.* 2007;39:175–91.
31. Song D, Huang Y, Van Dessel J, Shujaat S, Orhan K, Vanganswinkel T, et al. Effect of platelet-rich and platelet-poor plasma on peri-implant innervation in dog mandibles. *Int J Implant Dent.* 2019;5:40.
32. Huang Y, Li Z, Van Dessel J, Salmon B, Huang B, Lambrichts I, et al. Effect of platelet-rich plasma on peri-implant trabecular bone volume and architecture: a preclinical micro-CT study in beagle dogs. *Clin Oral Implants Res.* 2019;30:1190–9.
33. Landis JR, Koch GG. An application of hierarchical kappa-type statistics in the assessment of majority agreement among multiple observers. *Biometrics.* 1977;33:363–74.
34. Oliveira Costa F, Cota LO, Costa JE, Pordeus IA. Periodontal disease progression among young subjects with no preventive dental care: a 52-month follow-up study. *J Periodontol.* 2007;78:198–203.
35. Cortellini P, Prato GP, Tonetti MS. Periodontal regeneration of human infrabony defects. I. Clinical measures. *J Periodontol.* 1993;64:254–60.
36. Tonetti MS, Prato GP, Williams RC, Cortellini P. Periodontal regeneration of human infrabony defects. III. Diagnostic strategies to detect bone gain. *J Periodontol.* 1993;64(4):269–77.
37. Vandenberghe B, Jacobs R, Yang J. Detection of periodontal bone loss using digital intraoral and cone beam computed tomography images: an in vitro assessment of bony and/or infrabony defects. *Dentomaxillofac Radiol.* 2008;37:252–60.
38. Monje A, Insua A, Rakic M, Nart J, Moyano-Cuevas JL, Wang HL. Estimation of the diagnostic accuracy of clinical parameters for monitoring peri-implantitis progression: an experimental canine study. *J Periodontol.* 2018;89:1442–51.
39. Bender P, Salvi GE, Buser D, Sculean A, Bornstein MM. Correlation of three-dimensional radiologic data with subsequent treatment approach in patients with peri-implantitis: a retrospective analysis. *Int J Periodontics Restor Dent.* 2017;37:481–9.
40. Eickholz P, Hausmann E. Accuracy of radiographic assessment of interproximal bone loss in intrabony defects using linear measurements. *Eur J Oral Sci.* 2000;108:70–3.
41. Pepelassi EA, Tsiklakis K, Diamanti-Kipiotti A. Radiographic detection and assessment of the periodontal endosseous defects. *J Clin Periodontol.* 2000;27:224–30.
42. Guerrero ME, Jacobs R, Loubele M, Schutyser F, Suetens P, van Steenberghe D. State-of-the-art on cone beam CT imaging for preoperative planning of implant placement. *Clin Oral Investig.* 2006;10:1–7.
43. Maki K, Inou N, Takanishi A, Miller AJ. Computer-assisted simulations in orthodontic diagnosis and the application of a new cone beam X-ray computed tomography. *Orthodont Craniofac Res.* 2003;6(Suppl 1):95–101. discussion 79–82.
44. Codari M, de Faria Vasconcelos K, Ferreira Pinheiro Nicolielo L, Haiter Neto F, Jacobs R. Quantitative evaluation of metal artifacts using different CBCT devices, high-density materials and field of views. *Clin Oral Implants Res.* 2017;28:1509–14.
45. Vanderstuyft T, Tarce M, Sanaan B, Jacobs R, de Faria Vasconcelos K, Quirynen M. Inaccuracy of buccal bone thickness estimation on cone-beam CT due to implant blooming: An ex-vivo study. *J Clin Periodontol.* 2019;46:1134–43.



# CHAPTER 6

## **In vivo quantification of mandibular bone remodeling and vascular changes in a Wistar rat model: a novel HR-MRI and micro-CT fusion technique**

Song D<sup>1</sup>

Shujaat S<sup>1</sup>

Zhao RT<sup>1</sup>

Huang Y<sup>1,2</sup>

Shaheen E<sup>1</sup>

Van Dessel J<sup>1</sup>

Orhan K<sup>1,3</sup>

Vande Velde G<sup>3</sup>

Coropciuc R<sup>1</sup>

Pauwels R<sup>1,4,5</sup>

Politis C<sup>1</sup>

Jacobs R<sup>1,6</sup>

<sup>1</sup>OMFS IMPATH research group, Department of Imaging & Pathology, Faculty of Medicine, KU Leuven, and Oral & maxillofacial Surgery, University Hospitals Leuven, Leuven, Belgium

<sup>2</sup>State Key Laboratory of Oral Diseases, West China College of Stomatology, Sichuan University, Chengdu, China

<sup>3</sup>Morphology Group, Biomedical Research Institute, Hasselt University, Diepenbeek, Belgium

<sup>4</sup>Department of Dental Medicine, Karolinska Institute, Stockholm, Sweden.

# In vivo quantification of mandibular bone remodeling and vascular changes in a Wistar rat model: A novel HR-MRI and micro-CT fusion technique

Dandan Song<sup>1</sup>, Sohaib Shujaat<sup>1</sup>, Ruiting Zhao<sup>1</sup>, Yan Huang<sup>1</sup>, Eman Shaheen<sup>1</sup>,  
Jeroen Van Dessel<sup>1</sup>, Kaan Orhan<sup>1,2</sup>, Greetje Vande Velde<sup>3</sup>, Ruxandra Coropciuc<sup>1</sup>,  
Ruben Pauwels<sup>1,4,5</sup>, Constantinus Politis<sup>1</sup>, Reinhilde Jacobs<sup>1,6,\*</sup>

<sup>1</sup>OMFS IMPATH Research Group, Department of Imaging and Pathology, Faculty of Medicine, KU Leuven and Oral and Maxillofacial Surgery, University Hospitals Leuven, Leuven, Belgium

<sup>2</sup>Department of Dentomaxillofacial Radiology, Faculty of Dentistry, University of Ankara, Ankara, Turkey

<sup>3</sup>Biomedical MRI, Department of Imaging and Pathology, Faculty of Medicine, KU Leuven, Leuven, Belgium

<sup>4</sup>Department of Radiology, Faculty of Dentistry, Chulalongkorn University, Bangkok, Thailand

<sup>5</sup>Aarhus Institute of Advanced Studies, Aarhus University, Aarhus, Denmark

<sup>6</sup>Department of Dental Medicine, Karolinska Institute, Stockholm, Sweden

## ABSTRACT

**Purpose:** This study was performed to introduce an *in vivo* hybrid multimodality technique involving the co-registration of micro-computed tomography (micro-CT) and high-resolution magnetic resonance imaging (HR-MRI) to concomitantly visualize and quantify mineralization and vascularization at follow-up in a rat model.

**Materials and Methods:** Three adult female rats were randomly assigned as test subjects, with 1 rat serving as a control subject. For 20 weeks, the test rats received a weekly intravenous injection of 30 µg/kg zoledronic acid, and the control rat was administered a similar dose of normal saline. Bilateral extraction of the lower first and second molars was performed after 10 weeks. All rats were scanned once every 4 weeks with both micro-CT and HR-MRI. Micro-CT and HR-MRI images were registered and fused in the same 3-dimensional region to quantify blood flow velocity and trabecular bone thickness at T0 (baseline), T4 (4 weeks), T8 (8 weeks), T12 (12 weeks), T16 (16 weeks), and T20 (20 weeks). Histological assessment was the gold standard with which the findings were compared.

**Results:** The histomorphometric images at T20 aligned with the HR-MRI findings, with both test and control rats demonstrating reduced trabecular bone vasculature and blood vessel density. The micro-CT findings were also consistent with the histomorphometric changes, which revealed that the test rats had thicker trabecular bone and smaller marrow spaces than the control rat.

**Conclusion:** The combination of micro-CT and HR-MRI may be considered a powerful non-invasive novel technique for the longitudinal quantification of localized mineralization and vascularization. (*Imaging Sci Dent* 2020; 50: 199-208)

**KEY WORDS:** Vascular Remodeling; Radiology; Jaw; Rats

## Introduction

Bone is a highly vascularized feedback-controlled composite organ that fulfills several interconnected functions, including locomotion, phosphate and calcium metabolism, the synthesis of endocrine molecules, and hematopoiesis.<sup>1-3</sup> It is a dynamic tissue that is continuously being modeled and remodeled to maintain the integrity of skeletal

The project was supported by the China Scholarship Council (No. 201708210187). Ruben Pauwels is supported by the European Union Horizon 2020 Research and Innovation Programme under the Marie Skłodowska-Curie grant agreement number 754513 and by the Aarhus University Research Foundation (AIAS-COFUND). Received March 2, 2020; Revised June 7, 2020; Accepted June 25, 2020  
\*Correspondence to : Prof. Reinhilde Jacobs  
OMFS IMPATH Research Group, Department of Imaging and Pathology, Katholieke University Leuven, Campus Sint-Rafaël, Kapucijnenvoer 33, 3000 Leuven, Belgium  
Tel) 32-16332452, E-mail) reinhilde.jacobs@kuleuven.be

structure via the regulated activity of osteoblast and osteoclast cells.<sup>4,6</sup>

The preferred method for assessment of bone and vascular microstructure includes 2-dimensional histological sections,<sup>7</sup> micro-computed tomography (micro-CT) imaging with or without contrast agents, and laser Doppler flowmetry.<sup>8-10</sup> Histomorphology has been considered as a gold standard for identifying and visualizing the microstructure of bone and blood vessels; however, it is an invasive and time-consuming procedure and is associated with random sampling errors.<sup>11</sup> Similarly, micro-CT with or without contrast agents is a powerful non-invasive technique for the visualization of bone and vascular microstructure in 3 dimensions, but it cannot be used for hemodynamic analysis.<sup>12,13</sup> Jia et al.<sup>14</sup> and Roche et al.<sup>15</sup> have suggested the application of micro-CT with a barium sulfate contrast agent to characterize and quantify bone remodeling and blood vessel structure. However, this technique can only be used to easily view large vascular structures and cannot visualize vascularity within trabecular bone.<sup>16,17</sup> Recently, high-resolution magnetic resonance imaging (HR-MRI) has been proposed for the quantification of vascularity at the micro-anatomical level, but this technique cannot be used to quantify the bone microstructure.<sup>18,19</sup>

To overcome the aforementioned limitations of individual imaging modalities, various co-registered hybrid multimodal imaging techniques have been suggested to offer more accurate and detailed insight into the physiology of bone and its associated vasculature compared to the assessment of separate images. Methods such as the co-registration of micro-CT/micro-positron emission tomography,<sup>20,21</sup> micro-CT/single-photon emission computed tomography,<sup>22</sup> micro-CT/MRI,<sup>23</sup> CT/MRI,<sup>24</sup> dynamic contrast-enhanced CT/MRI,<sup>25</sup> and micro-digital subtraction angiography/MRI<sup>26</sup> have been proposed to offer better insight into the physiological processes of bone remodeling, angiogenesis, and blood flow. However, the potential of co-registered intermodal imaging for the assessment of bone structure and microvascularization at follow-up remains unclear, and few studies have been conducted on bone remodeling and blood flow velocity (BFV) at follow-up. Although histomorphometric analysis is usually considered the gold standard, it cannot be used to assess the evolution of bone changes over time unless a multifold sample of animals is utilized. We hypothesized that a combination of micro-CT and HR-MRI could provide a better understanding of the follow-up interaction between angiogenic and osteogenic pathways within a region of interest. As such, the purpose

of this study was to introduce an *in vivo* hybrid multimodal technique with co-registered micro-CT/HR-MRI data to concomitantly visualize and quantify bone remodeling and vascularization at follow-up in a rat model.

## Materials and Methods

The experimental protocol was approved by the Ethical Committee for Animal Experimentation of KU Leuven in Leuven, Belgium (reference no. P264/2015) and was carried out in accordance with the UK Animals (Scientific Procedures) Act of 1986 and the EU Directive 2010/63/EU for animal experiments.

A sample of 4 female Wistar rats (200-250 g; aged 12 weeks) was obtained. Three adult female rats were randomly assigned as test subjects, and 1 rat was assigned as a control subject. For 20 weeks, the test rats received an intravenous injection of zoledronic acid (ZA; 30 µg/kg per week), while the control rat was intravenously administered normal saline (30 µg/kg per week). At the end of the 10th week, bilateral extraction of the lower first and second molars was performed in each rat under general anesthesia (1.5%-2% isoflurane in 100% oxygen) to simulate a bisphosphonate-related osteonecrosis of the jaw (BRONJ)-associated bone defect.<sup>27,28</sup> Based on the genetic differences between humans and rodents, a 10-week ZA delivery period with the mentioned dosage frequency along with tooth extraction is known to be capable of effectively replicating a BRONJ-associated bone defect.<sup>29</sup> ZA was delivered for an additional 10 weeks after tooth extraction so that follow-up changes in the region of the bone defect could be observed.

### Micro-CT acquisition

The rats were anesthetized by placing them in an anesthesia induction chamber, to which isoflurane inhalation anesthesia was delivered at a rate of 5 cc/minute for 3-5 minutes. Following anesthesia, each rat was scanned by placing it on a stable platform with a gas mask on its nose to avoid movement, and a cylindrical plastic holder was applied to immobilize the head. The trabecular bone changes were observed by scanning all rats once every 4 weeks (T0: baseline, T4: 4 weeks, T8: 8 weeks, T12: 12 weeks, T16: 16 weeks, T20: 20 weeks) with a dedicated *in vivo* micro-CT scanner (SkyScan 1076; Bruker microCT, Kontich, Belgium), operating at 80 kV and 120 µA with a 1-mm aluminum filter and a scanning time of approximately 11 minutes. Furthermore, an averaging frame of 6° was

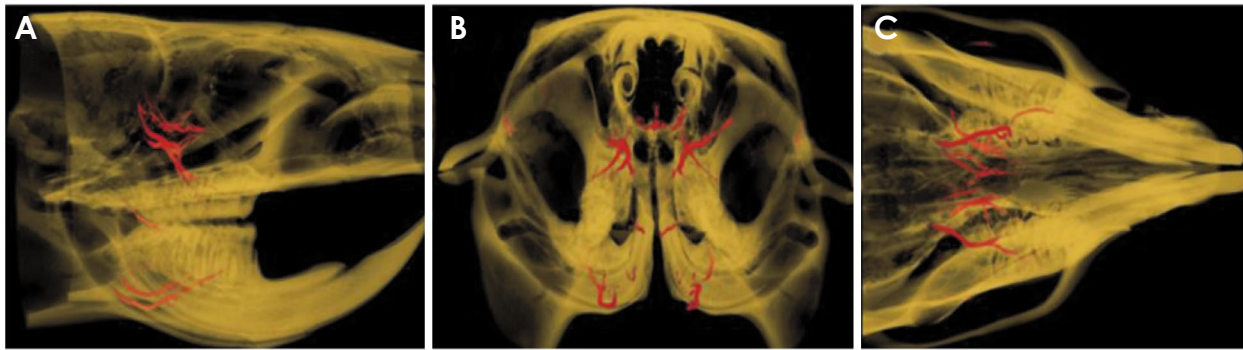


**Fig. 1.** Registered high-resolution magnetic resonance images and micro-computed tomography images allowing accurate projection of the available blood vessels onto the jaw bone. A. Longitudinal view. B. Coronal view. C. Inferior view.

applied along with a  $220^\circ$  arc of rotation around the vertical axis with a rotation step of  $0.8^\circ$ . With the same settings, bone mineral density phantoms of  $0.25 \text{ g/cm}^3$  and  $0.75 \text{ g/cm}^3$  were scanned to perform bone mineral density calibration with respect to the attenuation values. The rats were scanned once every 4 weeks to keep the scanning protocol timing consistent and to minimize the impact of radiation on the bone tissue microstructure. Additionally, scanning was carried out 2 weeks after tooth extraction rather than immediately to allow for soft tissue healing over the simulated defect. Following image acquisition, 3-dimensional (3D) datasets with an isotropic voxel size of  $35 \mu\text{m}^3$  were reconstructed without smoothing and were processed using NRecon software (version 1.6.10.4; Bruker microCT). A beam hardening correction of 30% was applied for image conversion.

#### HR-MRI acquisition

HR-MRI scanning was performed at the same time points as micro-CT imaging and under a similar anesthetic protocol. To observe the vascular changes, T2-weighted HR-MRI images were acquired utilizing a Biospec 9.4-T small-animal MRI scanner with high resolution ( $59 \times 59 \times 59 \mu\text{m}$ ; HR-MRI) (Bruker Biospin, Ettlingen, Germany) with a 20-cm horizontal bore and an actively shielded gradient insert. A cross-coil setup was applied, consisting of a horizontal radio-frequency coil (transmit/receive coil, 7.2-cm diameter; Bruker Biospin) and a rat head surface receiving coil (Rapid Biomedical, Rimpfar, Germany). Magnetic resonance angiography (MRA) was performed with a time-of-flight (TOF) 2-dimensional sequence (echo time: 3.5 ms, repetition time: 18 ms, slice thickness: 1 mm, matrix size:  $256 \times 256$ , slices: 60, and FOV:  $40 \times 26 \text{ mm}$ ), resulting in in-plane resolution 3D T2-weighted anatomical MRI and MRA.

#### Registration of HR-MRI and micro-CT images

The HR-MRI 3D reconstructed images were spatially aligned with the micro-CT images in the same 3D space using Amira software (version 6.3.0; Thermo Fisher Scientific, Merignac, France). Manual registration was applied to visualize the vascular and skeletal structures in longitudinal (Fig. 1A), coronal (Fig. 1B), and inferior (Fig. 1C) 3D views. Thereafter, the micro-CT and HR-MR images were fused in Synapse 3D<sup>®</sup> software (Fujifilm Medical, Tokyo, Japan) (Fig. 2) for quantification of rat jawbone remodeling and vascularization. For fusion, a suitable region of interest (ROI) was defined to enable the calculation of vascularity as close as possible to the affected bone. Fusion was carried out separately for each rat at each time point.

#### Bone morphometric analysis

Following fusion, the micro-CT images were transformed using CT-Analyzer<sup>®</sup> software (Bruker microCT) for the calculation of morphometric parameters at all-time points. No blurring of the images due to breathing were observed. A volume of interest (VOI) was manually selected to include mandibular alveolar bone bilaterally at the apical region of the first and second molar of each rat while excluding the root surface and mandibular canal (Figs. 3A and B). Later, segmentation within the selected VOI was performed using a global automatic threshold algorithm. The trabecular thickness (Tb.Th; mm) was semi-automatically calculated at all time points before (Figs. 3C and D) and after (Figs. 3E and F) extraction.

#### BFV analysis

For the quantification of vascular changes, fused micro-CT images and TOF-MRA were used to estimate the relative BFV in the rat mandible as suggested by Huang et al.<sup>30</sup> The closest artery and its branch connected to the

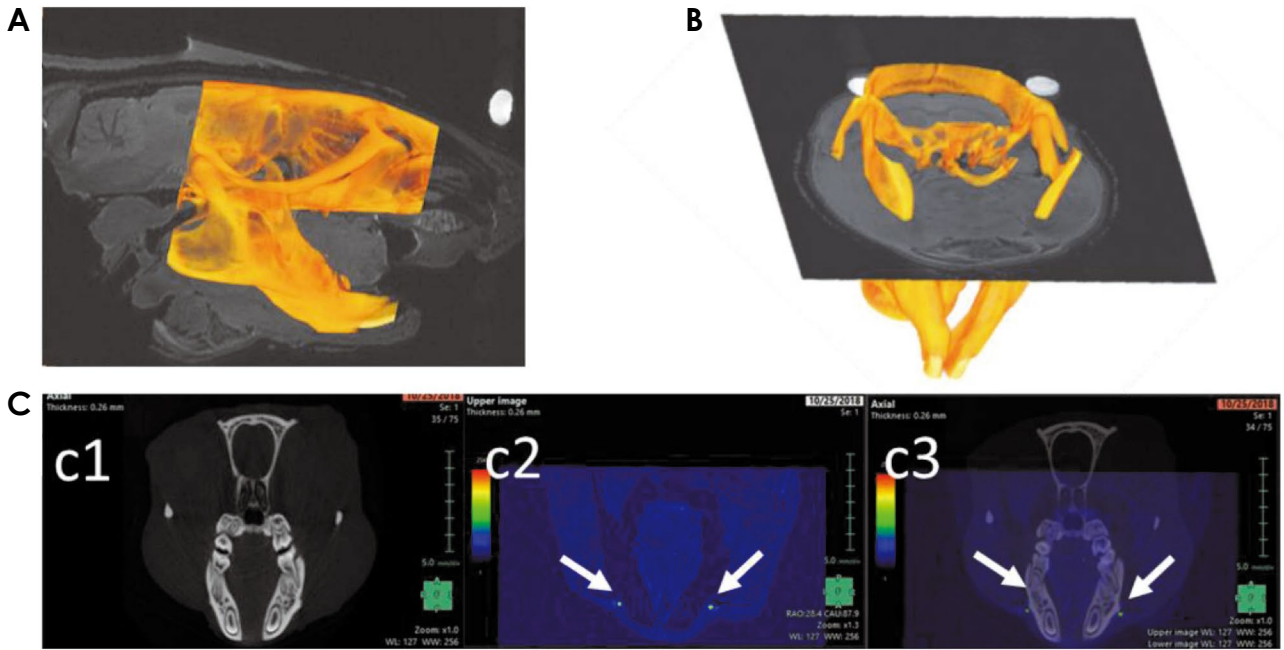


**Fig. 2.** Combination of micro-computed tomography and high-resolution magnetic resonance imaging (HR-MRI) scans. A. Three-dimensional (3D) sagittal view. B. 3D coronal view (posterior). C. Sample of imaging fusion (c1) hard tissue from micro-CT imaging and (c2) soft tissue from HR-MRI. (c3) Imaging fusion of c1 and c2.

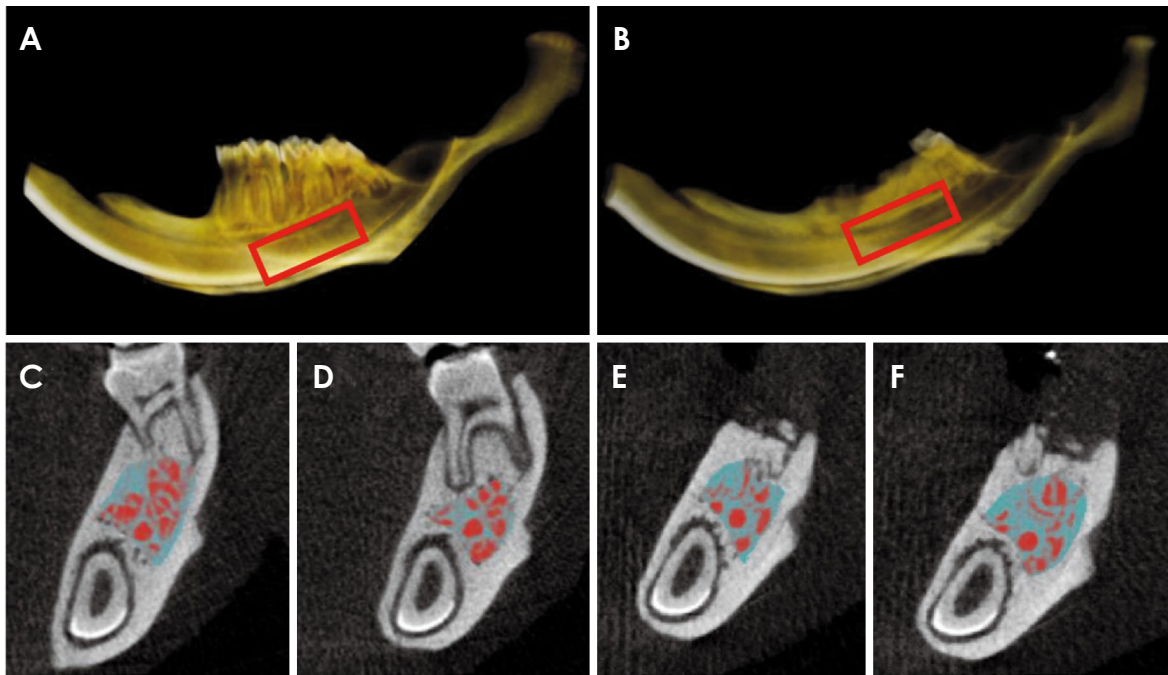


**Fig. 3.** Example of trabecular bone thickness changes in a test rat. A. Volume of interest (VOI) at the periapical region of the first and second molar. B. VOI following tooth extraction. C, D. Trabecular bone changes before tooth extraction (at 4 weeks). E, F. Trabecular bone changes after tooth extraction (at 12 weeks). Bone is shown in light blue, while bone space is shown in red in B, C, E, and F.

extraction site were selected, and the BFV was measured using the MRA images in 3D Synapse software (Figs. 4A-C). BFV estimation was attained by calculating the dis-

placement of blood between 2 consecutive images and determining the blood velocity using the fused images. An ROI consisting of the closest artery and its branch connect-

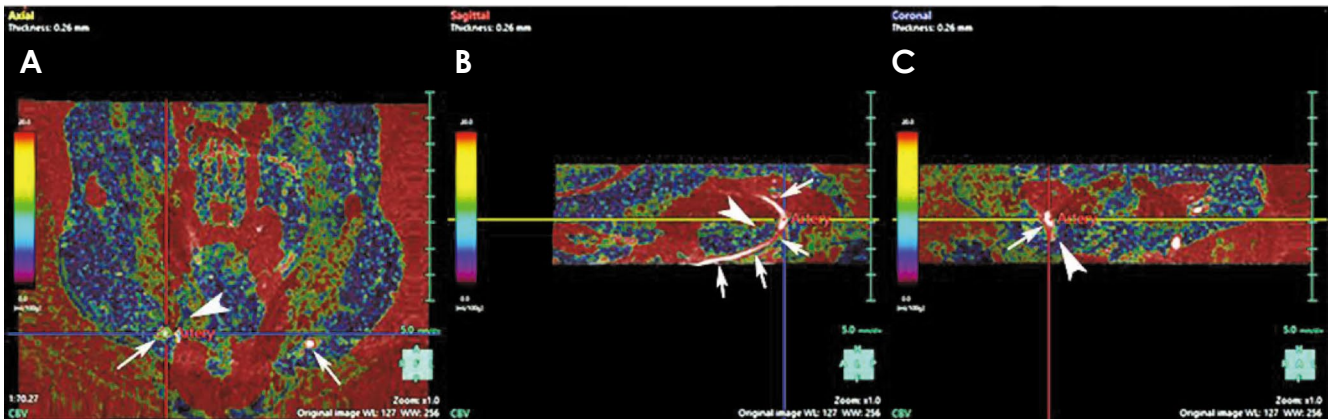


**Fig. 4.** Calculation of relative blood flow velocity using dedicated 3-dimensional software. A. Superimposed time-of-flight magnetic resonance angiography (TOF-MRA) and micro-computed tomography (micro-CT) images. The base image is a micro-CT scan, and the fused image is a TOF-MRA scan. B, C. The arrows denote the artery and its part connected to the tooth extraction site, while arrowheads denote the mandibular trabecular bone, coded in blue.

ed to the extraction site with dimensions of  $1 \times 1$  pixels was selected to calculate the average velocity in the sagittal and coronal sections. The gray-level image intensity values of the artery's interior, acquired from the TOF-MRA ROIs, were used to estimate the relative BFV. The relative velocity values were then linearly fitted to the reference values. All measurements were converted to pixels/s. A single experienced observer performed the image registration and evaluation at all time points (from T0 to T20). The calculated BFV distribution was visualized using color-coding on the fused images.

#### Histological analysis

Histological assessment was the gold standard with which the findings were compared. All rats were sacrificed immediately after the T20 micro-CT and HR-MRI scans. Following euthanasia of all rats with an overdose of general anesthesia (1.5%-2% isoflurane in 100% oxygen), the mandibles were harvested, fixed in buffered formalin (pH 7.4), and embedded in paraffin blocks. The bone samples were decalcified under controlled slow oscillations in a 1:1 solution of 4% formic acid and 10% neutral buffered formaldehyde at a pH of 7.4 for 4 days; following demineralization, the samples were rinsed with distilled water. A single 6- $\mu$ m section of each sample parallel to the mandibular body (Fig. 5A) was stained with hematoxylin solution (Gill III; Leica Microsystems, Diegem, Belgium) and 1% aqueous eosin solution (Leica Microsystems). The histological sections were manually registered and spatially aligned with the corresponding reconstructed micro-CT and HR-MRI images for evaluation of the same region of interest.<sup>28</sup> Thereafter, histological assessment of blood vessels was

performed using a light microscope (Axio Imager M2; Carl Zeiss Microscopy, Jena, Germany).

The data obtained in this study were analyzed with IBM SPSS Statistics version 22 (IBM Corp., Armonk, NY, USA). The Mann-Whitney *U* test was applied to compare the control and test rats, as the data were not normally distributed. When interpreting the results, 0.05 was utilized as the level of significance.

## Results

The rats in the study demonstrated good hemostasis following surgery and a normal recovery from anesthesia. In all cases, micro-CT revealed broken apical root remnants after extraction due to the presence of divergence and broadening in the apical root portion. However, complete and normal mucosal healing was observed at approximately 2 weeks in all rats without any visible infection.

The micro-CT component of the registered micro-CT/HR-MRI data showed an increase in Tb.Th from baseline to T20 in both the test and control rats (Fig. 5B). However, this difference lacked significance at all time points ( $P > 0.05$ ). The micro-CT findings were consistent with the histomorphometric analysis at T20, which revealed thicker trabecular bone and smaller marrow spaces in the test rats than in the control rat (Figs. 5C and D). Additionally, the registered HR-MRI component and 3D reconstruction of blood vessels showed a reduction in test-rat BFV (Fig. 5E) and bone vascularity (Figs. 5F and G) at the same region of interest relative to the control rat at follow-up. Although an increase in BFV was observed before tooth extraction, both control and test rats showed a decrease in BFV at

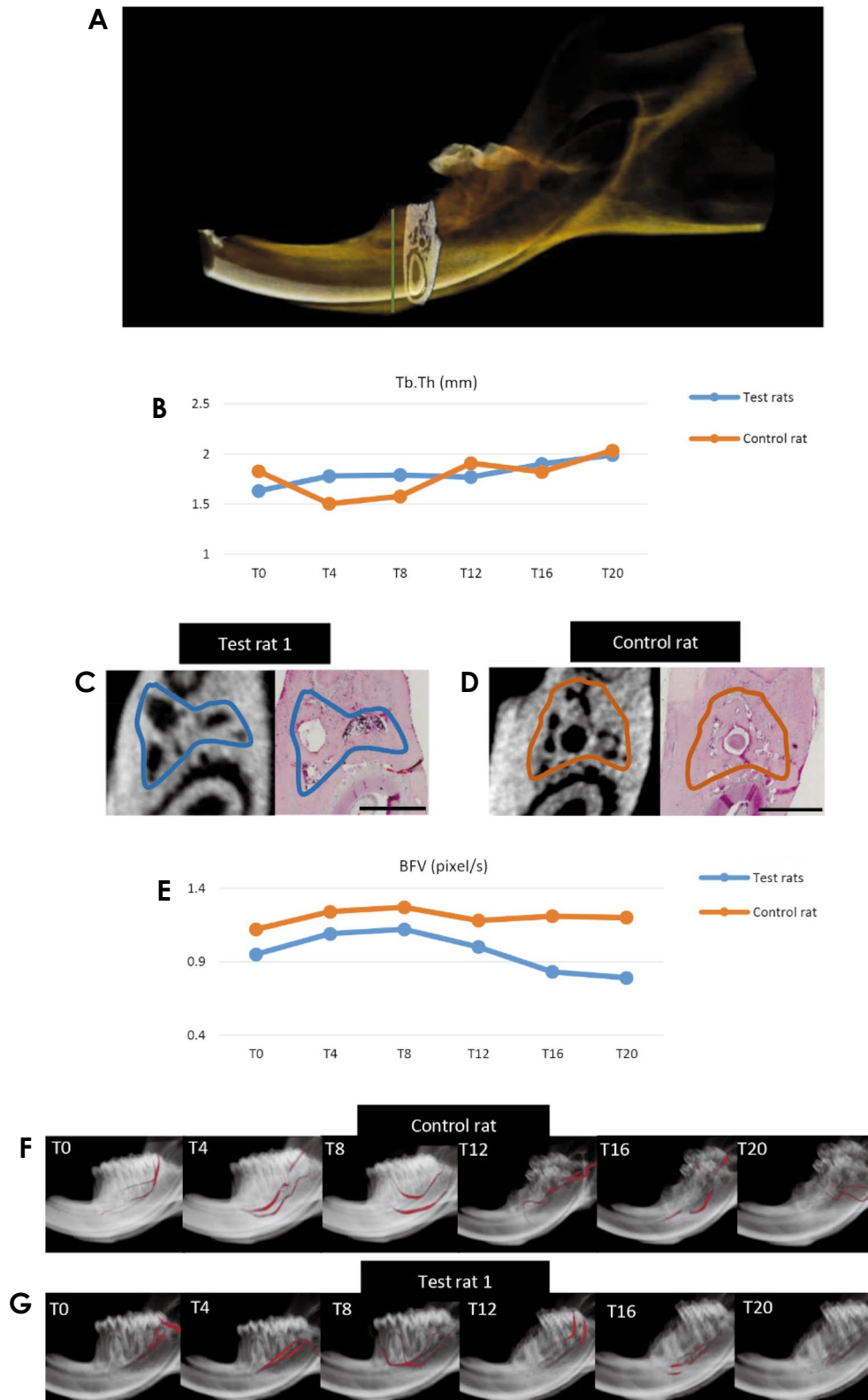


**Fig. 5.** Vascular and trabecular changes. A. Three-dimensional (3D) representation of the cutting direction for histological sectioning (green line: cutting plane). B. Graphical representation of changes in trabecular bone thickness in the test rats and control rat. C, D. Thicker trabecular bone and smaller marrow spaces in the micro-CT scan and histological section in a test rat compared to the control rat at T20. E. Graphical representation of BFV changes in control and test rats. F. 3D vascular changes in the control rat. G. 3D vascular changes in a test rat. BFV: blood flow velocity, Tb.Th: trabecular bone thickness, T0: baseline, T4: (4 weeks), T8: 8 weeks, T12: 12 weeks, T16: 16 weeks, and T20: 20 weeks. Bar: 1000  $\mu$ m.

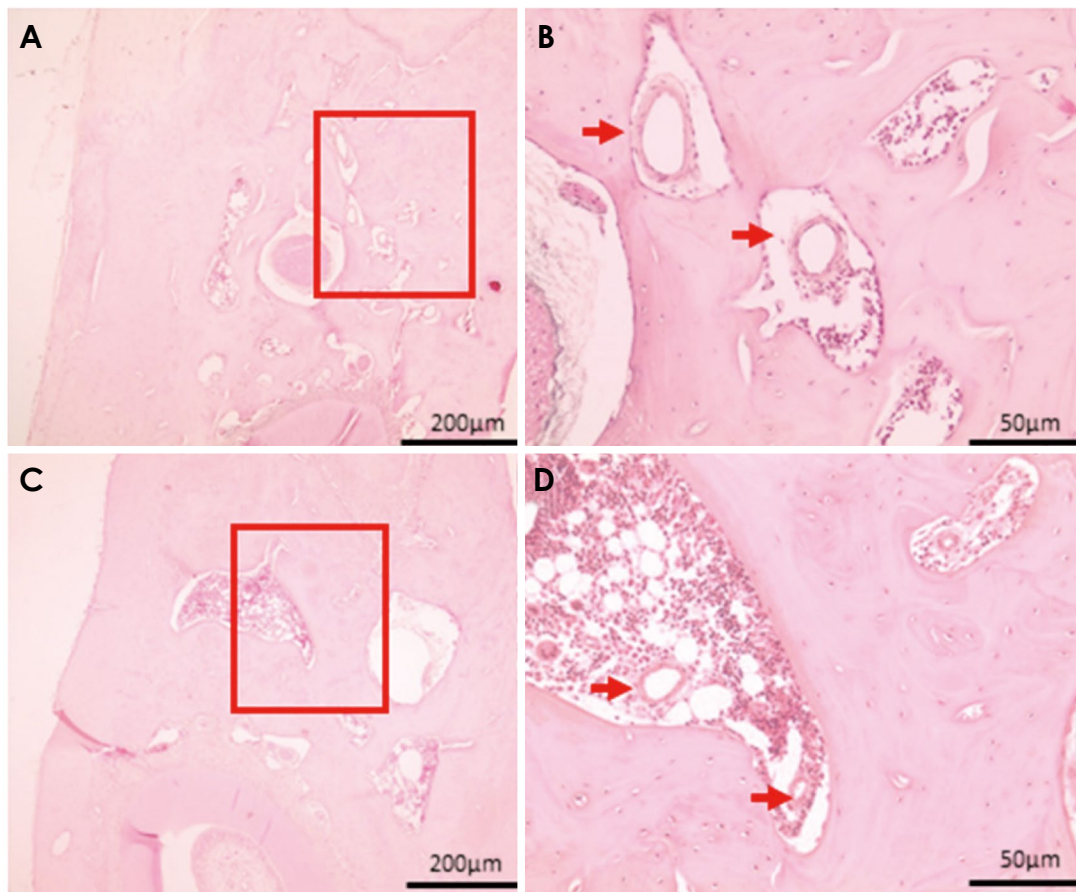


**Fig. 6.** Histomorphometric analysis of the blood vessels in the region of interest. A. Normal blood vessels observed in the control rat. B. Magnification of the red square in A. C. Inflamed and defective blood vessel revealed in the test rat. D. Magnification of the red square in C. Red arrow: blood vessel.

follow-up. The difference between the left and right mandibular BFV values in each rat was insignificant at all time points ( $P > 0.05$ ). The histomorphometric images at T20 were also in accordance with the HR-MRI findings, as they demonstrated reduced trabecular bone vasculature and blood vessel density in both test and control rats and thereby confirmed the reduction in BFV. Histomorphometric analysis further revealed the presence of normal and healthy blood vessels in the control rat (Figs. 6A and B), whereas inflamed and smaller blood vessels were observed in the test rats (Figs. 6C and D). These findings were also consistent with the HR-MRI images, which revealed a greater reduction in BFV in the test rats than in the control rat based on the presence of less dense blood vessels.

### Discussion

The high mineralization of human jaw bone is linked to its local vascularity.<sup>31</sup> Furthermore, the skeletal vascula-

ture plays an important role in providing nutrients to bone, and any alteration in vascularization can directly influence skeletal metabolic activity and remodeling.<sup>32</sup> Bone disorders such as osteoporosis, rheumatoid arthritis, BRONJ, and other skeletal disorders are known to create imbalance in the remodeling process, thereby influencing the structural and functional integrity of bone and blood vessels<sup>33</sup>. Therefore, in the present study, a multimodal imaging technique involving a combination of micro-CT and HR-MRI was utilized for the 3D visualization, quantification, and longitudinal monitoring of bone remodeling and BFV in a BRONJ-like defect. To the best of our knowledge, a multimodal technique that can effectively and concomitantly assess bone remodeling and vascularity at follow-up has not yet been reported.

Previous studies have demonstrated the estimation of vascularization via perfusion imaging involving HR-MRI and dynamic contrast imaging techniques.<sup>34-36</sup> However, the disadvantages of perfusion imaging include the confu-

sion or omission of microstructure resulting from low spatial resolution. Additionally, numerous micro-CT protocols involving vascular contrast agents have also been applied to assess blood vessels, but they cannot be used to accurately assess the microvasculature.<sup>14,28</sup> Therefore, in this study, we utilized HR-MRI, which allows assessment of vascular structures and BFV at the microscopic level without the need for histological sectioning and staining.<sup>37</sup> As part of this technique, we evaluated the vascularity changes utilizing TOF-MRA, which is a common method for clinical blood vessel examination and blood flow imaging. The utilization of HR-MRI for the microanatomical and neurovascular assessment of the mandibular incisive canal,<sup>38</sup> nasopalatine canal, and superior and inferior genial spinal foramina<sup>39,40</sup> has been extensively reported. The combination of HR-MRI with micro-CT as a gold standard for bone morphometry allowed for the accurate determination of trabecular structural changes and BFV in the same region of interest.

Batise et al.<sup>41</sup> co-registered HR-MRI and micro-CT datasets in an *ex vivo* rabbit anterior cruciate ligament transection model and confirmed the successful application of this method in accurately quantifying the localized changes in both soft and hard tissue. However, the authors failed to quantify changes at follow-up. Other studies have involved the co-registration of micro-CT and MRI datasets for the assessment of bone and vascular changes; however, the application of MRI is limited based on low spatial resolution and the inability to provide detailed information related to microvascular structures in animal studies.<sup>23,24</sup> In contrast, our methodology allowed accurate quantification of both bone microstructure and blood vessels in the test and control rats at follow-up, suggesting that a combination of HR-MRI and micro-CT may provide a reasonable means to monitor the localized progression of ONJ in a preclinical rat model.

The combination of different imaging modalities provided localization and distinction of mineralization and vascularization in the mandible. The changes in trabecular bone and vascularity were assessed in the same ROI, and our findings associated with bone remodeling were consistent with the results of the histomorphometric analysis. We observed localized mineralization and a reduction in vascularization with smaller marrow spaces and narrow canals, which were in accordance with the previous findings.<sup>28,42,43</sup>

It should be mentioned that based on the small sample size, significant evidence regarding the interaction of bone vascularization and remodeling could not be found. Further

prospective studies utilizing a similar methodology should thus be carried out with a larger sample size to confirm our findings. It is also recommended to explore the potential of adding a contrast medium, so as to focus on possible beneficial effects for co-registered imaging of vascularization and bone remodeling.

In conclusion, the combination of micro-CT and HR-MRI may be considered a powerful non-invasive tool for the longitudinal concomitant quantification of bone remodeling and vascularization. The present protocol should be further applied and validated with an integrated animal experimental design.

**Conflicts of Interest:** None

## References

1. Maes C. Role and regulation of vascularization processes in endochondral bones. *Calcif Tissue Int* 2013; 92: 307-23.
2. Driessens M. Circulatory aspects of reflex sympathetic dystrophy. In: Schoutens A, Gardeniers JW, Hughes SP. Bone circulation and vascularization in normal and pathological conditions. New York: Springer; 1993. p. 217-31.
3. Boerckel JD, Uhrig BA, Willett NJ, Huebsch N, Guldberg RE. Mechanical regulation of vascular growth and tissue regeneration in vivo. *Proc Natl Acad Sci U S A* 2011; 108: E674-80.
4. Eghbali-Fatourehchi GZ, Mödder UI, Charatcharoenwitthaya N, Sanyal A, Undale AH, Clowes JA, et al. Characterization of circulating osteoblast lineage cells in humans. *Bone* 2007; 40: 1370-7.
5. Ishii M, Egen JG, Klauschen F, Meier-Schellersheim M, Saeki Y, Vacher J, et al. Sphingosine-1-phosphate mobilizes osteoclast precursors and regulates bone homeostasis. *Nature* 2009; 458: 524-8.
6. Thompson B, Towler DA. Arterial calcification and bone physiology: role of the bone-vascular axis. *Nat Rev Endocrinol* 2012; 8: 529-43.
7. Mark H, Penington A, Nannmark U, Morrison W, Messina A. Microvascular invasion during endochondral ossification in experimental fractures in rats. *Bone* 2004; 35: 535-42.
8. Deshpande SS, Donneys A, Farberg AS, Tchanque-Fossuo CN, Felice PA, Buchman SR. Quantification and characterization of radiation-induced changes to mandibular vascularity using micro-computed tomography. *Ann Plast Surg* 2014; 72: 100-3.
9. Prajapati SI, Keller C. Contrast enhanced vessel imaging using microCT. *J Vis Exp* 2011; 47: 2377.
10. Abma E, Stock E, De Spiegelaere W, Van Brantegem L, Vanderperren K, Ni Y, et al. Power Doppler ultrasound and contrast-enhanced ultrasound demonstrate non-invasive tumour vascular response to anti-vascular therapy in canine cancer patients. *Sci Rep* 2019; 9: 9262.
11. Hillier ML, Bell LS. Differentiating human bone from animal bone: a review of histological methods. *J Forensic Sci* 2007;

- 52: 249-63.
12. Jorgensen SM, Demirkaya O, Ritman EL. Three-dimensional imaging of vasculature and parenchyma in intact rodent organs with X-ray micro-CT. *Am J Physiol* 1998; 275: H1103-14.
  13. Yang J, Pham SM, Crabbe DL. High-resolution micro-CT evaluation of mid-to long-term effects of estrogen deficiency on rat trabecular bone. *Acad Radiol* 2003; 10: 1153-8.
  14. Fei J, Peyrin F, Malaval L, Vico L, Lafage-Proust MH. Imaging and quantitative assessment of long bone vascularization in the adult rat using microcomputed tomography. *Anat Rec (Hoboken)* 2010; 293: 215-24.
  15. Roche B, David V, Vanden-Bossche A, Peyrin F, Malaval L, Vico L, et al. Structure and quantification of microvascularisation within mouse long bones: what and how should we measure? *Bone* 2012; 50: 390-9.
  16. Weinstein RS, Wan C, Liu Q, Wang Y, Almeida M, O'Brien CA, et al. Endogenous glucocorticoids decrease skeletal angiogenesis, vascularity, hydration, and strength in aged mice. *Aging Cell* 2010; 9: 147-61.
  17. Ding WG, Wei ZX, Liu JB. Reduced local blood supply to the tibial metaphysis is associated with ovariectomy-induced osteoporosis in mice. *Connect Tissue Res* 2011; 52: 25-9.
  18. Barentsz JO, Engelbrecht M, Jager GJ, Witjes JA, de LaRoette J, van der Sanden BP, et al. Fast dynamic gadolinium-enhanced MR imaging of urinary bladder and prostate cancer. *J Magn Reson Imaging* 1999; 10: 295-304.
  19. Benjaminsen IC, Graff BA, Brurberg KG, Rofstad EK. Assessment of tumor blood perfusion by high-resolution dynamic contrast-enhanced MRI: a preclinical study of human melanoma xenografts. *Magn Reson Med* 2004; 52: 269-76.
  20. Zagorchev L, Oses P, Zhuang ZW, Moodie K, Mulligan-Kehoe MJ, Simons M, et al. Micro computed tomography for vascular exploration. *J Angiogenesis Res* 2010; 2: 7.
  21. Liang H, Yang Y, Yang K, Wu Y, Boone JM, Cherry SR. A microPET/CT system for in vivo small animal imaging. *Phys Med Biol* 2007; 52: 3881-94.
  22. Bernsen MR, Vaissier PE, Van Holen R, Booij J, Beekman FJ, de Jong M. The role of preclinical SPECT in oncological and neurological research in combination with either CT or MRI. *Eur J Nucl Med Mol Imaging* 2014; 41 Suppl 1: S36-49.
  23. Kłodowski K, Kamiński J, Nowicka K, Tarasiuk J, Wroński S, Swiętek M, et al. Micro-imaging of implanted scaffolds using combined MRI and micro-CT. *Comput Med Imaging Graph* 2014; 38: 458-68.
  24. Basha MA, AlAzzazy MZ, Ahmed AF, Yousef HY, Shehata SM, El Sammak DA, et al. Does a combined CT and MRI protocol enhance the diagnostic efficacy of LI-RADS in the categorization of hepatic observations? A prospective comparative study. *Eur Radiol* 2018; 28: 2592-603.
  25. Lin MT, Wang CC, Cheng YF, Eng HL, Yen YH, Tsai MC, et al. Comprehensive comparison of multiple-detector computed tomography and dynamic magnetic resonance imaging in the diagnosis of hepatocellular carcinoma with varying degrees of fibrosis. *PLoS One* 2016; 11: e0166157.
  26. Badea CT, Hedlund LW, De Lin M, Boslego Mackel JF, Johnson GA. Tumor imaging in small animals with a combined micro-CT/micro-DSA system using iodinated conventional and blood pool contrast agents. *Contrast Media Mol Imaging* 2006; 1: 153-64.
  27. Longo AB, Sacco SM, Ward WE. Proper positioning and restraint of a rat hind limb for focused high resolution imaging of bone micro-architecture using in vivo micro-computed tomography. *J Vis Exp* 2017; 129: 56346.
  28. Soares MQ, Van Dessel J, Jacobs R, da Silva Santos PS, Cestari TM, Garlet GP, et al. Zoledronic acid induces site-specific structural changes and decreases vascular area in the alveolar bone. *J Oral Maxillofac Surg* 2018; 76: 1893-901.
  29. Sharma D, Hamlet S, Petcu E, Ivanovski S. Animal models for bisphosphonate-related-osteonecrosis of the jaws - an appraisal. *Oral Dis* 2013; 19: 747-54.
  30. Huang TC, Chang CK, Liao CH, Ho YJ. Quantification of blood flow in internal cerebral artery by optical flow method on digital subtraction angiography in comparison with time-of-flight magnetic resonance angiography. *PLoS One* 2013; 8: e54678.
  31. Faot F, Chatterjee M, de Camargos G, Duyck J, Vandamme K. Micro-CT analysis of the rodent jaw bone micro-architecture: a systematic review. *Bone Rep* 2015; 2: 14-24.
  32. Siddiqui JA, Partridge NC. Physiological bone remodeling: systemic regulation and growth factor involvement. *Physiology (Bethesda)* 2016; 31: 233-45.
  33. Bamias A, Kastritis E, Bamia C, Mouloupoulos LA, Melakopoulos I, Bozas G. Osteonecrosis of the jaw in cancer after treatment with bisphosphonates: incidence and risk factors. *J Clin Oncol* 2005; 23: 8580-7.
  34. Principi M, Italiani M, Guiducci A, Aprile I, Muti M, Giulianelli G, et al. Perfusion MRI in the evaluation of the relationship between tumour growth, necrosis and angiogenesis in glioblastomas and grade I meningiomas. *Neuroradiology* 2003; 45: 205-11.
  35. Law M, Cha S, Knopp EA, Johnson G, Arnett J, Litt AW. High-grade gliomas and solitary metastases: differentiation by using perfusion and proton spectroscopic MR imaging. *Radiology* 2002; 222: 715-21.
  36. Lee SJ, Kim JH, Kim YM, Lee GK, Lee EJ, Park IS, et al. Perfusion MR imaging in gliomas: comparison with histologic tumor grade. *Korean J Radiol* 2001; 2: 1-7.
  37. Vandersteen M, Beuls E, Gelan J, Adriaensens P, Vanormelingen L, Palmers Y, et al. High field magnetic resonance imaging of normal and pathologic human medulla oblongata. *Anat Rec* 1994; 238: 277-86.
  38. Jacobs R, Lambrechts I, Liang X, Martens W, Mraiwa N, Adriaensens P, et al. Neurovascularization of the anterior jaw bones revisited using high-resolution magnetic resonance imaging. *Oral Surg Oral Med Oral Pathol Oral Radiol Endod* 2007; 103: 683-93.
  39. Kress B, Gottschalk A, Anders L, Stippich C, Palm F, Bähren W, et al. High-resolution dental magnetic resonance imaging of inferior alveolar nerve responses to the extraction of third molars. *Eur Radiol* 2004; 14: 1416-20.
  40. Du Tolt DF, Nortjé C. The maxillae: integrated and applied anatomy relevant to dentistry. *SADJ* 2003; 58: 325-30.
  41. Batiste DL, Kirkley A, Lavery S, Thain LM, Spouge AR,

- Gati JS, et al. High-resolution MRI and micro-CT in an ex vivo rabbit anterior cruciate ligament transection model of osteoarthritis. *Osteoarthritis Cartilage* 2004; 12: 614-26.
42. Kün-Darbois JD, Libouban H, Mabilieu G, Pascaretti-Grizon F, Chappard D. Bone mineralization and vascularization in bisphosphonate-related osteonecrosis of the jaw: an experimental study in the rat. *Clin Oral Investig* 2018; 22: 2997-3006.
43. Bi Y, Gao Y, Ehrchiou D, Cao C, Kikuri T, Le A, et al. Bisphosphonates cause osteonecrosis of the jaw-like disease in mice. *Am J Pathol* 2010; 177: 280-90.



# CHAPTER 7

**General Discussion**

**Conclusions and Future perspectives**

## 7.1 General discussion

Dental implant treatment has become a routine treatment option for prosthetic replacement of missing teeth<sup>1</sup>. Yet and unfortunately, extraction of teeth will impact sensory-motor function considering the loss of sensory feedback deriving from damage to the periodontal ligament. Indeed periodontal mechanoreceptors are responsible for transmission of loading information and send to the neurosensory pathway feedback within cerebral cortex<sup>2,3</sup>. After tooth removal, periodontal nerves endings have been stimulated successfully in the healed extracted sockets with proven recovery of innervation in the peri-implant bone within 2 weeks after implant placement<sup>4,5</sup>. Some psychophysical and neurophysiological evidences suggested that part of the sensory stability restored in the edentulous patients after wearing the prostheses supported by osseointegrated implants<sup>6-10</sup>. A small number of nerve fibres in the peri-implant bone region has been detected in some preclinical studies<sup>11-13</sup>. The initial purpose of this doctoral thesis was to elaborate the effect of immediate and delayed implant placement and loading protocols, local application of platelet-rich plasma (PRP) and platelet-poor plasma (PPP) on the neural and bony changes following the dental implant placement. Therefore, two split-mouth dog models were developed to study the myelinated nerve fibres in the peri-implant bone in **Chapters 2 & 3** of this thesis.

In this general discussion, an extensive summary is given to each chapter in this thesis. The hypotheses proposed in the **General Introduction (Chapter 1)** were then discussed. Then, the impact of the current results on the nerve fibres and bone-to-implant interface followed by different implant protocols and local application of PRP and PPP were described. Finally, the validation of the radiographic assessment including their primary limitations were clarified.

**Chapter 2** investigated the recovery pattern and the morphological characteristics of myelinated nerve fibres around dental implant used in immediate vs delayed implant placement and followed by immediate, delayed, and unloaded protocols based on an animal model. To ensure each treatment protocol was applied in all the positions in the arch, a split-mouth design was used and at least four samples for each implant treatment protocol were inserted on the 2<sup>nd</sup> premolar to the 1<sup>st</sup> molar in the lower jaws. Since the density of nerve fibres varies among anterior and posterior teeth, this design can help to remove the vast amounts of inter-individual variability from the estimates of treatment effect. Quantification of peri-implant myelinated nerve fibre was addressed and characterized histomorphologically.

The main findings in this study as a significantly higher nerve density around implants of the

immediately placed and loaded group, which supported the hypothesis that early loading promotes more favourable peri-implant innervation recovery. Although it should be noted that a specific function of these regenerated nerve fibres could not be confirmed, it can be assumed that immediate implant placement after extraction brings the nerves in place with activation of peripheral regrowth signals preventing degeneration<sup>14</sup>. Loading might lead to activation of peri-implant nerve signals and promote further peri-implant nerve regeneration. We also found that the density of nerve fibres increased slightly following the loaded implant at a longer follow-up period. The nerve fibres were a bit densely innervated at 6-month follow-up than that at 3-month follow-up. Another result found that the distribution of nerve fibres in the apical region were obviously dense compared with the cervical region and middle region, which also revealed that high stimuli could help with the improvement of the nerve restoration or regeneration. Thus, it is reasonable to assume that the innervation pattern in the peri-implant bone is not only affected by external loading protocol, but also depended on the location and distribution of loadings. And this reinnervation after 3 months tended to be stable. Although the investigation of the functional role of nerve fibres was not verified in this study due to the limitation of the animal model study, the psychophysical and neurophysiological evidences of osseoperception following dental implant treatment has been fully documented in **Chapter 1**.

The study described in **Chapter 3** was designed to evaluate the effect of local application of PRP and PPP on the myelinated nerve fibres in the peri-implant bone region. Autologous plasma fractions have been applied for stimulating new bone formation<sup>15-17</sup>, angiogenesis<sup>18-20</sup>, and peripheral nerve regeneration<sup>21,22</sup>. The growth factors contained in the platelet including transforming growth factor- $\beta$  (TGF- $\beta$ ) and platelet-derived growth factor (PDGF) are responsible for the proliferation of fibroblasts and smooth muscles cells, neovascularization, and collagen synthesis<sup>23-25</sup>. Application of PRP has been demonstrated and proven to be beneficial for repairing damaged nerve trucks and receptors<sup>21,26,27</sup>. All implants underwent delayed implant placement and delayed loading (DIP + DL) protocol and some implants were dipped in the PRP or PPP which were regarded as the test groups. It has been confirmed that placing the implant and loaded followed by a healing period in the preclinical study could increase the implant initial stability<sup>28,29</sup>. The myelinated nerve fibres in the region of 500  $\mu$ m away from implant were involved in the quantification because the mechanoreceptors in this zone are easily activated by the loading pressure<sup>30</sup>. The main finding in this study showed that the myelinated nerve fibres in the peri-implant bone region were more mature in the group using PRP treatment than using PPP treatment. The implant sites with PRP treatment were

innervated with larger diameter nerve fibres. The diameter of the myelinated nerve fibres was significantly larger at 3-month and 6-month follow-up period. Due to some limitations of small sample size of animal study, there was no powerful evidence showing the impact of the PRP and PPP on density of the myelinated nerve fibres.

Based on the same animal model in **Chapter 3**, **Chapter 4** was designed to study the bony changes using the radiographic imaging. In the **Chapter 4**, we hypothesize that high concentration of platelet can facilitate bone formation surrounding the implant. The amount of bone-to-implant contact (BIC), as one indicator for quantifying the osseointegration, is an important determinant for achieving optimal secondary implant stability<sup>31</sup>. In the prior study, histomorphometry and micro-computed tomography (micro-CT) were mostly utilized in measurement of BIC ratio<sup>32,33</sup>. Histomorphometry has been considered as a gold standard for the microstructure analysis for decades, but preparation procedure is not only a time-consuming process, but it can also destroy the tissue structure<sup>34,35</sup>. Besides, it should not be ignored that only 2-dimensional bone structure around the implant were measured by histomorphometry. Even though it is a reliable method for elaborating BIC%, the bone information acquired through the 2D slices is deemed insufficient for representing the three-dimensional (3D) bone structure<sup>36</sup>. Thus recently, micro-CT as a non-destructive and reproducible radiographic technique has been explored in pre-clinical research for assessment of bone architecture<sup>37</sup>. A lot of publications have reported high correlations in evaluating the BIC ratio on 2D cross-sectional images using micro-CT and histology<sup>38,39</sup>. However, like the histomorphometry, 2D BIC ratio is not sufficient for referring the condition of 3D bone structure around the implant. The entire bone structure around the implant is manually selected and 3D BIC was measured in binary images automatically using CT-analyzer software. Although it cannot be denied that the cross-sectional images applied in this assessment are pseudo 3D, still they form the basis of valuing the BIC more comprehensively than 2D slices of histomorphometry.

As a gold standard, the histology was employed to validate the accuracy of micro-CT in measuring 2D BIC%. High correlation( $r = 0.98$ ) was found for both measurements on 2D BIC%, while only moderate correlation ( $r = 0.67$ ) for measuring 3D BIC% and 2D BIC%. The findings in this study showed that compared to the control group, the 3D BIC% was significantly higher in the PPP ( $p = 0.09$ ) and PRP group ( $p = 0.039$ ) at 1-month follow-up period. The 3D BIC% also slightly reduced at the 3-month follow-up and 6-month follow-up. The results help us confirmed the hypothesis that PRP is useful for improvement of the bone formation following implant placement. Besides, PPP application was also showed a positive

effect on the bone formation during the early healing time. Although, the concentration of platelet in PRP ( $776.2 \pm 144.0 \times 10^9/L$ ) is almost 160-fold higher than in PPP ( $4.8 \pm 1.8 \times 10^9/L$ ) in our study, high concentrate of fibrin fibres in PPP might compensate the lower platelet and provide a scaffold for supporting cells and releasing growth factors. It has been well documented that the application of PRP has outstanding effect on the improvement of the bone healing and angiogenesis. The growth factors released from the PRP along with the blood clots also played a critical role in the early stage of bone regeneration<sup>40,41</sup>. The life of platelet is only about 5-10 days, which might be one reason for the capability of PRP in promotion of bone repair only in the early stage<sup>42</sup>. The mechanism of PPP in bone healing, however, remains unclear due to the relative rare research. The limitation of animal model lies in the small sample size and complex condition in the post-operation management, which might lead to bias within the findings.

The purpose of the study in **Chapter 5** is to validate the diagnostic accuracy of CBCT versus IO in detection, classification, and quantification of the peri-implant bone defect. Through high-resolution micro-CT, 16 samples out of 54 were confirmed the presence of bone defect, and the shapes of the defect were reconstructed using micro-CT, which included dehiscence (n = 5), infrabony defect (n = 3) and crater-like defect (n = 8). This evaluation was performed by two experienced radiologists using the same images from CBCT and IO. Owing to the low-dose and low-cost, IO is widely accepted by patients in the regular examination following the dental disease treatment, and even in the implantology, IO is also the initial choice for the long-term follow-up after dental implant treatment<sup>43,44</sup>. However, the limitation of 2D imaging representing the 3D structure would thus be the failure of bucco-lingual defect detection, and the low-resolution and geometric distortion would also lead to the underestimation of bone defect<sup>45,46</sup>. To overcome the limitations, CBCT was strongly recommended as the alternative method in the regular examination following the dental implant treatment and other bone disease.

High reliability (ICC: 0.97) and agreement (Kappa: 0.92) were acquired between the observers. The findings in this study showed high sensitivity of CBCT in detecting and classifying the peri-implant bone defect. The outcomes in previous study regarding the superiority of the CBCT over 2D imaging remain in debate<sup>47-50</sup>. In general, CBCT may have a higher diagnostic accuracy in detection of fenestration, dehiscence, and three-walled periodontal defects due to the 3D bone visualization<sup>48,49,51</sup>, yet once dealing with implants, CT-based imaging might hamper peri-implant bone defect detection because the presence of metal artifacts<sup>52</sup>. However,

with imaging advances, inbuilt metal artefact reduction algorithms and high quality CBCT images may help to overcome this limitation in future clinic practice.

**Chapter 6** is a pilot study in which only four rats were included. The objective of this pilot study is to develop a new method for elaboration of local bone remodeling and vascular changes longitudinally combining the micro-CT and high-resolution magnetic resonance imaging (HR-MRI). In this study, weekly injection of zoledronic acid (ZA) for 20 weeks and tooth extraction were performed on three rats to develop an animal model with bisphosphonate-related osteonecrosis of the jaw (BRONJ)<sup>53,54</sup>. And one rat acting as control was administrated with normal saline solution. All animals were scanned by micro-CT and HR-MRI every four weeks for 20 weeks. As is in **Chapter 4** and **Chapter 5**, micro-CT is one of the most versatile non-invasive investigative techniques and has been regarded as a standard tool for quantifying the density and architecture of bone in preclinical investigations. Previous studies have widely reported on the feasibility and reliability of using micro-CT to evaluate morphologic characteristics of cortical and trabecular bone in both animal and human models<sup>55,56</sup>. HR-MRI technique has been advocated recently for quantifying vascularity at a micro-anatomical level<sup>57,58</sup>. Therefore, we speculated that a combination of micro-CT and HR-MRI could provide a better understanding of follow-up interaction between angiogenic and osteogenic pathways at the same region of interest. The micro-CT findings in this study were consistent with histomorphometric changes at 20-week which revealed thicker trabecular bone and smaller marrow spaces in the test rats compared to the control. The registered HR-MRI component and three-dimensional reconstruction of blood vessels showed a reduction in test rats blood flow velocity (BFV) and bone vascularity in the same region of interest compared to the control rat at various follow-up time points. Although, an increase in BFV was observed before tooth extraction, both control and test rats showed a decrease in BFV following tooth extraction. The histomorphometric images at 20-week were in accordance with the HR-MRI findings demonstrating a reduced trabecular bone vasculature and blood vessels density in both test and control rats, thereby confirming the reduction in BFV. Furthermore, combination of HR-MRI with micro-CT as a gold standard for bone morphometry allowed accurate determination of trabecular bone changes and BFV in the same region of interest. The approach of combining different imaging modalities provided a predictable result of locally mineralization and vascularization in the bone. The changes in trabecular bone pattern and vascularity were assessed in the same ROI and our findings associated with bone remodelling were consistent with that of histomorphometric analysis. However, a limitation of this study is that the

technique of the combination of micro-CT and HR-MRI can only be applied in the pre-clinical small animal model.

The studies presented in this doctoral thesis were able to assess the efficacy of different implant placement protocols and autologous plasma on the peri-implant innervation and bone remodelling. In relation to the implant placement protocols, the immediate implant placement and immediate loading protocol maintained the integrity of the extraction socket with an optimal soft tissue contour compared to the delayed implant placement and delayed loading protocol<sup>59-61</sup>. The early loading has the ability to transmit the mechanical stimuli to the peri-implant bone more effectively with an increased production of the nerve fibres at the bone-to-implant interface, thereby offering a higher degree of osseoperception<sup>62</sup>. These findings confirmed the general hypothesis that the different implant placement protocols offered variability in relation to osseoperception. PRP is widely applied in nerve restoration and bone formation owing to its high content of growth factors<sup>23</sup>. Furthermore, the outcomes of the thesis also suggested an improved bone-to-implant contact following the application of both platelet-rich plasma and platelet-poor plasma compared to the control group. These findings confirmed our hypothesis that the application of autologous plasma is beneficial for bone formation.

## **7.2 Conclusions**

From the studies mentioned in the previous chapters, the following conclusions can be drawn:

The presence of the neural structures within a range of 300-500 µm in the peri-implant bone region are confirmed in an histomorphometric analysis. And they are concentrated in the screw thread, bone marrow, and haversian canals (**Chapter 2 and Chapter 3**). Myelinated nerve fibres densely populated peri-implant apical bone region. In comparison with the unloaded implant, the loaded implant showed higher innervation in the peri-implant bone region and the immediate loaded group has contributed more to the density of myelinated nerve fibres in **Chapter 2**. The nerve density and diameter also proved to be increasing along with the longer follow-up healing time. Local application of PRP might have thereby enhanced the growth of the nerve fibres while PPP had no effect (**Chapter 3**). However, no convincing impact of PRP and PPP on the density of myelinated nerve fibres was shown. Large scale animal studies and longer follow-up periods are needed to confirm these findings and to verify whether platelet plasma can facilitate the nerve regeneration process. Besides, further functional measures on the peri-implant nerve fibres are still required.

**Chapter 4** recommended that local application of PRP and PPP have a positive effect on the 3D BIC ratio following implant treatment. Their influence was reduced as the observation period was increased, with BIC having the highest ratio at 1 month and lowest at 6 months. It can be assumed that the plasma-fibrin may facilitate and speed up bone healing and osseointegration.

Furthermore, **Chapter 5** confirmed high-resolution CBCT is superior to IO in diagnostic accuracy and reliability in detection, classification, and measurement of per-implant bone defect. The application of CBCT adds substantial information related to the peri-implant bone defect diagnosis and decision-making which cannot be achieved with conventional intra-oral imaging. However, benefit-risk ratio should be kept in mind and CBCT should be acquired for cases where a peri-implant bone defect might influence implant survival rate.

Finally, the combination of micro-CT and HR-MRI might be considered as a powerful non-invasive tool for longitudinal concomitant quantification of bone remodeling and vascularization (**Chapter 6**).

### **7.3 Future perspectives**

This thesis reported the impact of various implant placement and loading protocols, as well as local application PRP and PPP, on the innervation in the peri-implant bone region in split-mouth designed animal models, followed by detection of bone formation after dental implant treatment with utilities of PRP and PPP. The main purposes of this project were to provide randomized controlled evidence for the development of peri-implant nerve fibres and bone formation in the jaw bones, and to radiographic assessment on bony and vascular changes.

The findings in this thesis provide solid evidence at a microscopic level for understanding mechanisms of innervation recovery in the peri-implant bone under various implant placement and loading protocols, and extra treatment of PRP and PPP, along with some limitations in the implementation of the animal experiments. Specific interesting and valuable prospects for future researches which could be addressed are:

Considering the psychophysical and neurophysiological evidences, it would be of interest to clarify whether those differences we found in morphometric parameters can lead to the restoration of neurosensory pathway feedback with clinical significance. It might be possible to further explore osseoperception at a clinical level by collecting data or samples from patients who can offer retrieved implants, to confirm the function and origin of the nerve fibres in the

peri-implant bone, and even to reveal the potential factors for the improvement of osseoperception.

In addition, well-designed randomized control trials (RCTs) and large sample size animal model with strictly control on biological, psychological, and methodological factors, including additional physiological testing to standardize the frequency and direction of loading, are required to predict and investigate more potential controllable positive factors contributing to improve the tactile sensibility and innervation pattern surrounding endosseous implants.

The morphological findings in this doctoral thesis promote related studies on peripheral mechanisms and new hypotheses, such as PRP and PPP to improve the growth of peripheral nerve fibers regeneration and bone formation following dental implant placement. Further study should expand the sample size of the animal models to reveal the effect of PRP and PPP on nerve fibres regeneration and to determine what platelet growth factors are responsible for this positive function. Furthermore, the standardized protocol for centrifugation of whole blood is needed to acquire more effective PRP.

To validate the CBCT technique as a clinical imaging modality in detecting peri-implant bone defect, more research is needed to fully standardize imaging process, optimize reconstruction and exposure factors, and minimize metal artefacts on detecting and classifying the bone defect which could be applied in clinical practice. Given the rapid advances in CBCT, it might be very helpful to further exam the influence of varying types of CBCT systems, different acquisition protocols in comparison to micro-CT systems, before applying our observation as an accurate clinical reference.

Lastly, the findings of this doctoral thesis might contribute to our understanding on peri-implant nerve tissue healing mechanisms. We hope that the currently gathered knowledge, may broaden our understanding of the osseoperception mechanism, thereby allowing to continue striving towards global physiological integration of a dental implant in both bone and body.

## 7.4 References

1. Warreth A, Ibiyou N, O'Leary RB, Cremonese M, Abdulrahim M. Dental implants: An overview. *Dent Update*. 2017;44(7):596-620.
2. Jacobs R, van Steenberghe D. Comparative evaluation of the oral tactile function by means of teeth or implant-supported prostheses. *Clin Oral Implants Res*. 1991;2(2):75-80.
3. Piacino MG, Isola G, Cannavale R, et al. From periodontal mechanoreceptors to chewing motor control: A systematic review. *Arch Oral Biol*. 2017;78:109-121.
4. Linden R, Scott B. The effect of tooth extraction on periodontal ligament mechanoreceptors represented in the mesencephalic nucleus of the cat. *Arch Oral Biol*. 1989;34(12):937-941.
5. Wang YJO. Nerve regeneration after implantation in peri-implant area. A histological study on different implant materials in dogs. In: Jacobs R, ed. *Osseoperception*. Leuven: Catholic University Leuven. 1998:3-11.
6. Van Steenberghe D, Jacobs R. Jaw motor inputs originating from osseointegrated oral implants. *J Oral Rehabil*. 2006;33(4):274-281.
7. Jacobs R, van Steenberghe D. From osseoperception to implant-mediated sensory-motor interactions and related clinical implications. *J Oral Rehabil*. 2006;33(4):282-292.
8. Habre-Hallage P, Abboud-Naman NB, Reyhler H, van Steenberghe D, Jacobs R. Assessment of changes in the oral tactile function of the soft tissues by implant placement in the anterior maxilla: A prospective study. *Clin Oral Invest*. 2010;14(2):161-168.
9. Habre-Hallage P, Dricot L, Jacobs R, van Steenberghe D, Reyhler H, Grandin CB. Brain plasticity and cortical correlates of osseoperception revealed by punctate mechanical stimulation of osseointegrated oral implants during fMRI. *Eur J Oral Implant*. 2012;5(2):175-190.
10. Habre-Hallage P, Abboud-Naaman NB, Reyhler H, van Steenberghe D, Jacobs R. Perceptual changes in the peri-implant soft tissues assessed by directional cutaneous kinaesthesia and graphaesthesia: A prospective study. *Clin Implant Dent Relat Res*. 2011;13(4):296-304.
11. Wada S, Kojo T, Wang YH, et al. Effect of loading on the development of nerve fibers around oral implants in the dog mandible. *Clin Implant Dent Relat Res*.

- 2001;12(3):219-224.
12. Corpas Ldos S, Lambrichts I, Quirynen M, et al. Peri-implant bone innervation: histological findings in humans. *Eur J Oral Implant.* 2014;7(3):283-292.
  13. Huang Y, van Dessel J, Martens W, et al. Sensory innervation around immediately vs. delayed loaded implants: a pilot study. *Int J Oral Sci.* 2015;7(1):49-55.
  14. Del Fabbro M, Boggian C, Taschieri S. Immediate implant placement into fresh extraction sites with chronic periapical pathologic features combined with plasma rich in growth factors: preliminary results of single-cohort study. *J Oral Maxillofac Surg.* 2009;67(11):2476-2484.
  15. Martínez CE, González SA, Palma V, Smith PC. Platelet-Poor and Platelet-Rich Plasma Stimulate Bone Lineage Differentiation in Periodontal Ligament Stem Cells. *J Periodontol.* 2016;87(2):e18-e26.
  16. Civinini R, Macera A, Nistri L, Redl B, Innocenti M. The use of autologous blood-derived growth factors in bone regeneration. *Clin Cases Miner Bone Metabol.* 2011;8(1):25-31.
  17. Xie H, Cao L, Ye L, et al. Autogenous bone particles combined with platelet-rich plasma can stimulate bone regeneration in rabbits. *Exp Ther Med.* 2020;20(6):279.
  18. Martínez CE, Smith PC, Palma Alvarado VA. The influence of platelet-derived products on angiogenesis and tissue repair: a concise update. *Front Physiol.* 2015;6:290.
  19. Shahidi M, Vatanmakanian M, Arami MK, et al. A comparative study between platelet-rich plasma and platelet-poor plasma effects on angiogenesis. *Med Mol Morphol.* 2018;51(1):21-31.
  20. Berndt S, Carpentier G, Turzi A, Borlat F, Cuendet M, Modarressi A. Angiogenesis Is Differentially Modulated by Platelet-Derived Products. *Biomed.* 2021;9(3).
  21. Zheng C, Zhu Q, Liu X, et al. Improved peripheral nerve regeneration using acellular nerve allografts loaded with platelet-rich plasma. *Tissue Eng Part A.* 2014;20(23-24):3228-3240.
  22. Sánchez M, Anitua E, Delgado D, et al. Platelet-rich plasma, a source of autologous growth factors and biomimetic scaffold for peripheral nerve regeneration. *Expert Opinion Biol Therapy.* 2017;17(2):197-212.
  23. Pavlovic V, Ciric M, Jovanovic V, Stojanovic P. Platelet Rich Plasma: a short overview

- of certain bioactive components. *Open Med.* 2016;11(1):242-247.
24. Lubkowska A, Dolegowska B, Banfi G. Growth factor content in PRP and their applicability in medicine. *J Biol Regul Homeost Agents.* 2012;26(2 Suppl 1):3s-22s.
  25. Jungbluth P, Grassmann JP, Thelen S, et al. Concentration of platelets and growth factors in platelet-rich plasma from Goettingen minipigs. *GMS Interdiscip Plastic Reconstr Surg DGPW.* 2014;3:Doc11.
  26. Anjayani S, Wirohadidjojo YW, Adam AM, Suwandi D, Seweng A, Amiruddin MD. Sensory improvement of leprosy peripheral neuropathy in patients treated with perineural injection of platelet-rich plasma. *Int J Dermat.* 2014;53(1):109-113.
  27. Khojasteh A, Hosseinpour S, Nazeman P, Dehghan MM. The effect of a platelet-rich fibrin conduit on neurosensory recovery following inferior alveolar nerve lateralization: a preliminary clinical study. *Int J Oral Maxillofac Surg.* 2016;45(10):1303-1308.
  28. Albrektsson T, Zarb G, Worthington P, Eriksson AR. The long-term efficacy of currently used dental implants: a review and proposed criteria of success. *Int J Oral Maxillofac Implants.* 1986;1(1):11-25.
  29. Adell R, Lekholm U, Rockler B, Brånemark PI. A 15-year study of osseointegrated implants in the treatment of the edentulous jaw. *Int J Oral Surg.* 1981;10(6):387-416.
  30. Weiner S, Klein M, Doyle JL, Brunner M. Identification of axons in the peri-implant region by immunohistochemistry. *Int J Oral Maxillofac Implants.* 1995;10(6):689-695.
  31. Sennerby L, Wennerberg A, Pasop F. A new microtomographic technique for non-invasive evaluation of the bone structure around implants. *Clin Oral Implants Res.* 2001;12(1):91-94.
  32. Al Subaie AE, Eimar H, Abdallah MN, et al. Anti-VEGFs hinder bone healing and implant osseointegration in rat tibiae. *J Clin Periodontol.* 2015;42(7):688-696.
  33. Bissinger O, Probst FA, Wolff KD, et al. Comparative 3D micro-CT and 2D histomorphometry analysis of dental implant osseointegration in the maxilla of minipigs. *J Clin Periodontol.* 2017;44(4):418-427.
  34. Kulak CA, Dempster DW. Bone histomorphometry: a concise review for endocrinologists and clinicians. *Arq Bras Endocrinol Metabol.* 2010;54(2):87-98.
  35. Malhan D, Muelke M, Rosch S, et al. An Optimized Approach to Perform Bone Histomorphometry. *Front Endocrinol.* 2018;9:666.
  36. Gao Y, Luo E, Hu J, Xue J, Zhu S, Li JJB. Effect of combined local treatment with zoledronic acid and basic fibroblast growth factor on implant fixation in ovariectomized

- rats. *Bone*. 2009;44(2):225-232.
37. Feldkamp LA, Goldstein SA, Parfitt AM, Jesion G, Kleerekoper M. The direct examination of three-dimensional bone architecture in vitro by computed tomography. *J Bone Miner Res*.1989;4(1):3-11.
  38. Park YS, Yi KY, Lee IS, Jung YC. Correlation between microtomography and histomorphometry for assessment of implant osseointegration. *Clin Oral Implants Res*. 2005;16(2):156-160.
  39. Bernhardt R, Kuhlisch E, Schulz MC, Eckelt U, Stadlinger B. Comparison of bone-implant contact and bone-implant volume between 2D-histological sections and 3D-SRmicroCT slices. *Eur Cells Mater*. 2012;23:237-247; discussion 247-238.
  40. Rodriguez IA, Growney Kalaf EA, Bowlin GL, Sell SA. Platelet-rich plasma in bone regeneration: engineering the delivery for improved clinical efficacy. *Biomed Res Int*. 2014;2014:392398.
  41. Okada H, Takahashi K, Ogura N, Tomoki R, Ito K, Kondoh T. Plasma rich in growth factors stimulates proliferation, migration, and gene expression associated with bone formation in human dental follicle cells. *J Dent Sci*. 2016;11(3):245-252.
  42. Zechner W, Tangl S, Tepper G, et al. Influence of platelet-rich plasma on osseous healing of dental implants: a histologic and histomorphometric study in minipigs. *Int J Oral Maxillofac Implants*. 2003;18(1):15-22.
  43. Papapanou PN, Tonetti MS. Diagnosis and epidemiology of periodontal osseous lesions. *Periodontol 2000*. 2000;22:8-21.
  44. Tugnait A, Clerehugh V, Hirschmann PN. Use of the basic periodontal examination and radiographs in the assessment of periodontal diseases in general dental practice. *J Dent*. 2004;32(1):17-25.
  45. Eickholz P, Hausmann E. Accuracy of radiographic assessment of interproximal bone loss in intrabony defects using linear measurements. *Eur J Oral Sci*. 2000;108(1):70-73.
  46. Eickholz P, Kim T, Benn D, Staehle H. Accuracy of radiographic assessments of interproximal bone loss. *Oral Surg Oral Med Oral Pathol Oral Radiol Oral Endod*.1998;85:99-106.
  47. Arvidsson A, Sarve H, Johansson CB. Comparing and visualizing titanium implant integration in rat bone using 2D and 3D techniques. *J Biomed Mater Res Part B*. 2015;103(1):12-20.

48. Bayat S, Talaeipour AR, Sarlati F. Detection of simulated periodontal defects using cone-beam CT and digital intraoral radiography. *Dentomaxillofac Radiol.* 2016;45(6):20160030.
49. Christiaens V, De Bruyn H, De Vree H, Lamoral S, Jacobs R, Cosyn J. A controlled study on the accuracy and precision of intraoral radiography in assessing interproximal bone defect morphology around teeth and implants. *Eur J Oral Implantol.* 2018;11(3):361-367.
50. Hilgenfeld T, Juerchott A, Deisenhofer UK, et al. Accuracy of cone-beam computed tomography, dental magnetic resonance imaging, and intraoral radiography for detecting peri-implant bone defects at single zirconia implants-An in vitro study. *Clin Oral Implants Res.* 2018;29(9):922-930.
51. Vandenberghe B, Jacobs R, Yang J. Detection of periodontal bone loss using digital intraoral and cone beam computed tomography images: an in vitro assessment of bony and/or infrabony defects. *Dentomaxillofac Radiol.* 2008;37(5):252-260.
52. Kühl S, Zürcher S, Zitzmann NU, Filippi A, Payer M, Dagassan-Berndt D. Detection of peri-implant bone defects with different radiographic techniques - a human cadaver study. *Clin Oral Implants Res.* 2016;27(5):529-534.
53. Longo AB, Sacco SM, Ward WE. Proper Positioning and Restraint of a Rat Hind Limb for Focused High Resolution Imaging of Bone Micro-architecture Using In Vivo Micro-computed Tomography. *JoVE.* 2017(129):e56346.
54. Soares MQS, Van Dessel J, Jacobs R, et al. Zoledronic acid induces site-specific structural changes and decreases vascular area in the alveolar bone. *J Oral Maxillofac Surg.* 2018;76(9):1893-1901.
55. Bonnet N, Laroche N, Vico L, Dolleans E, Courteix D, Benhamou CL. Assessment of trabecular bone microarchitecture by two different x-ray microcomputed tomographs: a comparative study of the rat distal tibia using Skyscan and Scanco devices. *Med Phys.* 2009;36(4):1286-1297.
56. Bouxsein ML, Boyd SK, Christiansen BA, Guldborg RE, Jepsen KJ, Müller R. Guidelines for assessment of bone microstructure in rodents using micro-computed tomography. *J Bone Miner Res.* 2010;25(7):1468-1486.
57. Barentsz JO, Engelbrecht M, Jager GJ, et al. Fast dynamic gadolinium-enhanced MR imaging of urinary bladder and prostate cancer. *J Magnetic Res Imaging.* 1999;10(3):295-304.

58. Benjaminsen IC, Graff BA, Brurberg KG, Rofstad EK. Assessment of tumor blood perfusion by high-resolution dynamic contrast-enhanced MRI: A preclinical study of human melanoma xenografts. *Mag Res Med.* 2004;52(2):269-276.
59. Lazzara RJ. Immediate implant placement into extraction sites: surgical and restorative advantages. *Int J Periodontics Restorative Dent.* 1989;9(5):332-343.
60. Denissen HW, Kalk W, Veldhuis HA, van Waas MA. Anatomic consideration for preventive implantation. *Int J Oral Maxillofac Implants.* 1993;8(2):191-196.
61. Watzek G, Haider R, Mensdorff-Pouilly N, Haas R. Immediate and delayed implantation for complete restoration of the jaw following extraction of all residual teeth: a retrospective study comparing different types of serial immediate implantation. *Int J Oral Maxillofac Implants.* 1995;10(5):561-567.
62. Leucht P, Kim JB, Wazen R, et al. Effect of mechanical stimuli on skeletal regeneration around implants. *Bone.* 2007;40(4):919-930.

## SUMMARY

Since the introduction of osseoperception, the assessment methodologies including psychophysics, neurophysiology, and histology have been employed to unravel this phenomenon by qualifying and quantifying tactile sensibility, activated cortex areas, and mechanoreceptors in the peri-implant tissue. However, histomorphometric evidence on peri-implant mechanoreceptors is still insufficient and the impact on promoting recovery of the sensory sensibility remains unclear. Therefore, the initial purpose of this doctoral thesis was to explore the innervation in the peri-implant bone in two split designed animal studies, with a special focus on the effects of various implant placement and loading protocols and potential impacts of utility of platelet-rich plasma (PRP) and platelet-poor plasma (PPP). Subsequently, the effects of the PRP and PPP on the bone-to-implant contact using micro-CT. Then, based on the same animal model, the accuracy and applicability of CBCT for the detection and classification of the bone defect around the implant were evaluated by comparing intraoral imaging. Finally, the combined effect of micro-CT and high resolution of MRI were studied to measure the longitudinal mineralization and vascularization.

The thesis started with a general understanding of osseoperception from three prospects, histological findings, psychophysical findings, and neurophysiological findings in **Chapter 1**. Next, the overall aim and hypotheses of the whole thesis were presented.

In **Chapter 2**, a split-mouth designed animal study was performed to provide comprehensive histomorphometric evidence of osseoperception at the site of implant placement subjected to different implant placement and loading protocols, as well as the information of the distribution of the peri-implant innervation in the osseous. Myelinated nerve fibres were mostly found in peri-implant apical regions. The results also suggested that immediate implant placement and immediate loading was preferred to allow optimized peri-implant reinnervation. This exploration could add evidence to the understanding of the osseoperception mechanism and, as a result, improve the success rate of global physiological integration next to osseointegration in the human body.

Same as the **Chapter 2**, the goal of **Chapter 3** was to quantify the myelinated nerve fibres in the peri-implant bone region following dental implant treatment with local application of PRP and PPP. The results found that PRP had a positive effect on nerve fibre maturation, with the diameter of the nerve fibres in the PRP group being significantly larger compared to that in PPP group. Longer healing time seemed to benefit the growth of the nerve fibres. However,

due to the limitation of the animal model, this finding failed to reveal the effect PRP and PPP on the innervation pattern in the peri-implant bone.

In **Chapter 4**, we turned to examine the impact of PRP and PPP on the bone-to-implant contact (BIC). The amount of BIC is a determinant of the secondary stability of osseointegrated implant. It is interesting to find that both PRP and PPP showed positive effect on the BIC at the first month after implant loading, while there was a slight reduction at third month and sixth month. Further study with a large sample size of animal models and more RCTs should be carried out to discover the different impact of the PRP and PPP on the bone formation.

**Chapter 5** aimed to validate the diagnostic accuracy of CBCT versus intraoral imaging in detection, classification, and measurement of the peri-implant bone defect. This exploration suggested that the CBCT had superiority over 2D imaging in detecting the bone defect in the buccal-lingual sides, as well as the small defect. However, a proper acquisition protocol of CBCT should be further developed for converting this finding to clinic practice.

A pilot study in **Chapter 6** initially investigated the combined effect of micro-CT and HR MRI in the assessment of the long-term bone and vascular changes in the jawbone based on a pre-clinical study. The registration of micro-CT and MRI could provide the information of both hard and soft tissue in the localization region. Owing to the limitation of this pilot study, the results could only report that the vascular changes had the consistent tendency in MRI and histomorphometry, and the concomitant bone changes showed by the micro-CT as well. This exploration helped to develop a novel invasive radiographic technique to perform long-term follow-up of bone (re)modelling and vascularization in the pre-clinical research by combining the micro-CT and MRI.

Finally, the general discussion and conclusion of the above-mentioned studies and recommendation for future research were presented in **Chapter 7**. To further uncover the osseoperception phenomenon, this doctoral thesis was in an endeavour to elaborate the effects of delayed and immediate implant placement and loading protocols, as well as the application of PRP and PPP on the healing of nerve fibres and bone formation around oral implants. Eventually, the current results broaden our knowledge on the neural and bony changes following dental implant placement.

# SAMENVATTING

Sinds de introductie van osseoperceptie zijn diverse evaluatiemethodologieën met inbegrip van psychofysica, neurofysiologie en histologie aangewend om dit fenomeen te ontrafelen door het kwalificeren en kwantificeren van tactiele sensibiliteit, geactiveerde cortexgebieden en mechanoreceptoren in het peri-implantaire weefsel. Histomorfometrisch bewijs van peri-implantaire mechanoreceptoren is echter nog onvoldoende en de impact op het bevorderen van het herstel van de zintuiglijke gevoeligheid blijft onduidelijk. Daarom was het initiële doel van deze doctoraatsthesis het onderzoeken van de innervatie in het peri-implantaire bot in twee *split-mouth* dierstudies, met speciale aandacht voor de effecten van verschillende implantaatplaatsings- en belastingsprotocollen en mogelijke effecten van het gebruik van bloedplaatjesrijk plasma (PRP) en bloedplaatjes-arm plasma (PPP). Vervolgens werden de effecten van PRP en PPP op het bot-op-implantaatcontact onderzocht met behulp van micro-CT. Daarna werden, op basis van hetzelfde diermodel, de nauwkeurigheid en toepasbaarheid van CBCT voor de detectie en classificatie van het botdefect rond het implantaat geëvalueerd door intraorale beeldvorming te vergelijken. Tenslotte werd het gecombineerde effect van micro-CT en hoge resolutie van MRI bestudeerd om de longitudinale mineralisatie en vascularisatie te meten.

Het proefschrift startte met een algemeen inleiding van osseoperceptie vanuit drie perspectieven, histologische bevindingen, psychofysische bevindingen, en neurofysiologische bevindingen in **Hoofdstuk 1** Vervolgens werden het algemene doel en de hypothesen van het gehele proefschrift gepresenteerd.

In **hoofdstuk 2** werd een *split-mouth* dierstudie uitgevoerd om uitgebreid histomorfometrisch bewijs te verkrijgen van de osseoperceptie op de plaats van implantaat plaatsing, onderworpen aan verschillende implantatie- en belastingsprotocollen, evenals informatie over de distributie van peri-implantaire innervatie in het bot. Gemyeliniseerde zenuwvezels werden vooral aangetroffen in de apicale regio's van het peri-implantaat. De resultaten suggereerden ook dat onmiddellijke plaatsing van het implantaat en onmiddellijke belasting de voorkeur verdienden om een optimale peri-implantaire reinnervatie mogelijk te maken. Dit onderzoek kan bijdragen aan het begrip van het osseoperceptiemechanisme en, als gevolg daarvan, het succespercentage verbeteren van globale fysiologische integratie naast osseointegratie in het menselijk lichaam. Net als in hoofdstuk 2, was het doel van **hoofdstuk 3** het kwantificeren van de gemyeliniseerde zenuwvezels in de peri-implantaire botregio na behandeling van dentale implantaten met lokale toepassing van PRP en PPP. De resultaten toonden aan dat PRP een positief effect had op de maturatie van de zenuwvezels, waarbij de diameter van de zenuwvezels in de PRP groep

significant groter was, vergeleken met die in de PPP groep. Een langere genezingstijd leek de groei van de zenuwvezels ten goede te komen. Echter, vanwege de beperking van het diermodel, kon deze bevinding het effect van PRP en PPP op het innervatiepatroon in het peri-implantaire bot niet aantonen.

In **hoofdstuk 4** onderzochten we de invloed van PRP en PPP op het bot-implantaat contact (BIC). De hoeveelheid BIC is een bepalende factor voor de secundaire stabiliteit van het osseogeïntegreerde implantaat. Het is interessant om vast te stellen dat zowel PRP als PPP een positief effect hadden op de BIC tijdens de eerste maand na het plaatsen van het implantaat, terwijl er een lichte vermindering was tijdens de derde en zesde maand. Verder onderzoek met een grote steekproefgrootte van diermodellen en meer RCT's moeten worden uitgevoerd om de verschillende effecten van PRP en PPP op de botvorming te ontdekken.

**Hoofdstuk 5** richtte zich op het valideren van de diagnostische nauwkeurigheid van CBCT versus intraorale beeldvorming in detectie, classificatie en meting van het peri-implantaire botdefect. Dit onderzoek suggereerde dat de CBCT superieur was aan 2D beeldvorming in het detecteren van het botdefect in de buccaal-linguale zijden, evenals het kleine defect. Echter, een goed protocol voor het verkrijgen van CBCT beelden moet verder worden ontwikkeld om deze bevinding om te zetten naar de klinische praktijk.

Een piloot studie in **Hoofdstuk 6** onderzocht in eerste instantie het gecombineerde effect van micro-CT en HR MRI bij de beoordeling van de lange termijn bot en vasculaire veranderingen in het kaakbot op basis van een preklinische studie. De registratie van micro-CT en MRI kon de informatie van zowel hard als zacht weefsel in het lokalisatiegebied verschaffen. Door de beperking van deze pilootstudie, konden de resultaten enkel melden dat de vasculaire veranderingen een consistente tendens vertoonden in MRI en histomorfometrie, en dat de gelijktijdige botveranderingen ook door de micro-CT werden aangetoond. Dit onderzoek heeft bijgedragen tot de ontwikkeling van een nieuwe invasieve radiografische techniek voor de langetermijnopvolging van bot(re)modellering en vascularisatie in het preklinisch onderzoek door de combinatie van micro-CT en MRI.

Tenslotte werden de algemene discussie en conclusie van de bovengenoemde studies en aanbevelingen voor toekomstig onderzoek gepresenteerd in **Hoofdstuk 7**. Om het osseoperceptie fenomeen verder bloot te leggen, werd in dit doctoraal proefschrift getracht de effecten van vertraagde en onmiddellijke implantatie en belastingprotocols, alsook de toepassing van PRP en PPP op de genezing van zenuwvezels en botvorming rond orale implantaten uit te werken. Uiteindelijk verbreden de huidige resultaten onze kennis over de neurale en benige veranderingen na het plaatsen van orale implantaten.

## SCIENTIFIC ACKNOWLEDGEMENTS

The author of this thesis was supported by China Scholarship Council (No. 201708210187). The projects in this thesis National were supported by Nature Science Foundation of China (No. 81370026) and Sichuan Province Science and Technology Support Program (2016SZ0010). Dr. Yan Huang was a postdoctoral (11.N3.615N) and JVD is a predoctoral (11.ZU.117N) FWO-research fellow. Meanwhile, this work could not have been brought to a successful conclusion without the help of many people, whom I would like to gratefully acknowledge for their contributions.

### Chapter 2:

Dandan Song: Conducting the animal experiment, data collection and analysis, drafting manuscripts, critical revision and approval of manuscript;

Prof. Xin Liang and Prof. GuoWu Ma: Designing this study;

Prof. Weijian Zhong, Hui Zheng and Ying Zhai: Conducting animal experiment;

Sohaib Shujaat, Prof. Ivo Lambrichts, And Prof. Reinhilde Jacobs: Critical revision and approval of manuscript;

Jeroen Van Dessel: Critical revision and statistics.

Further acknowledgement: To laboratory technicians from Dalian Medical of University and Translational Cell and Tissue Research unit of KU Leuven for their valuable help during this animal research.

### Chapter 3:

Dandan Song: Data collection and analysis, drafting manuscripts, critical revision and approval of manuscript;

Yan Huang: Conducting animal experiment, data collection, critical revision and approval of manuscript;

Prof. Constantinus Politis, Prof. Reinhilde Jacobs: Study design;

Tim Vangansewinkel, Kathleen Van den Eynde, Ivo Lambrichts, and Tania Roskams:

Histological staining;

Jeroen Van Dessel: Critical revision and statistics;

Sohaib Shujaat, and Prof. Kaan Orhan: Critical revision and approval of manuscript.

The authors are thankful to the laboratory technicians from the Research Base of West China Hospital, Sichuan University and Translational Cell and Tissue Research unit of University Hospitals Leuven, KU Leuven for their valuable help during this animal research, and to Xin Li (KU Leuven) for her help with the histological digitalization.

#### **Chapter 4:**

Dandan Song: Data collection and analysis, drafting manuscripts, critical revision and approval of manuscript;

Yan Huang: Study design, conducting animal experiment, data collection, critical revision and approval of manuscript;

Prof. Constantinus Politis, Prof. Reinhilde Jacobs: Study design;

Ivo Lambrichts: Histological staining, critical revision and approval of manuscript;

Jeroen Van Dessel: Critical revision and statistics;

Sohaib Shujaat: Critical revision and approval of manuscript.

Further acknowledgement: To the laboratory technicians from the Research Base of West China Hospital, Sichuan University and Translational Cell and Tissue Research unit of University Hospitals Leuven, KU Leuven for their valuable help during this animal research, and to Xin Li (KU Leuven) for her help with the histological digitalization.

#### **Chapter 5:**

Dandan Song: Data collection and analysis, drafting manuscripts, critical revision and approval of manuscript;

Yan Huang: Study design, conducting animal experiment, data collection;

Prof. Constantinus Politis, Prof. Ivo Lambrichts, and Prof. Reinhilde Jacobs: Study design, critical revision and approval of manuscript;

Sohaib Shujaat: Critical revision and approval of manuscript;

Karla de Faria Vasconcelos: Data analysis.

The authors are thankful to the laboratory technicians from the Research Base of West China Hospital, Sichuan University and Translational Cell and Tissue Research unit of University Hospitals Leuven, KU Leuven for their valuable help during this animal study.

#### **Chapter 6:**

Dandan Song: Data collection and analysis, drafting manuscripts, critical revision and approval of manuscript;

Yan Huang, and Ruiting Zhao: Study design, conducting animal experiment, data collection and approval of manuscript;

Eman Shaheen, Jeroen Van Dessel, Greetje Vande Velde, Ruxandra Coropciuc, and Ruben Pauwels: Conducting animal experiment and approval of manuscript;

Kaan Orhan: Data analysis , critical revision and approval of manuscript;

Prof. Constantinus Politis, and Prof. Reinhilde Jacobs: Study design, critical revision and approval of manuscript.

Further acknowledgement: To the Translational Cell and Tissue Research unit of University Hospitals Leuven, KU Leuven for their valuable help during this animal study.

## **PERSONAL CONTRIBUTION**

The author, Dandan Song, conceived the projects, collected, and managed the animal and radiological data, analyzed the data and wrote the research publications by scientific support of her promotors Prof. Dr. Reinhilde Jacobs and Prof. Dr. Ivo Lambrichts, and all the co-authors. Accordingly, Dandan Song is the first author of all the thesis chapters and corresponding research papers.

## **CONFLICT OF INTEREST**

The authors declare no conflict of interest.



## Curriculum Vitae

### Dandan Song

#### PERSONAL PROFILE

---

**Name:** Dandan Song

**Nationality:** China

**Date of Birth:** 11<sup>th</sup> of March, 1990

**Birthplace:** Lianyungang, Jiangsu

**E-mail:** dandansong9015@gmail.com

**Tel:** +32-484 198 788

**Contact Address:** Campus Sint-Rafaël, KU Leuven, Kapucijnenvoer 33, Leuven, 3000, Belgium

#### RESEARCH FIELD

---

Major in Oral & Maxillofacial Surgery and Oral & Maxillofacial Radiology. The main topic of research is to study neural and bony changes following oral implant placement based on the animal model. The purpose of the preclinical study is to investigate some efficient way to improve the osseoperception and osseointegration following the oral implant treatment.

#### PUBLICATIONS (2017-2020)

---

(\*- *corresponding author*)

- **Song D**, Zheng H, Huang Y, Ma GW, Ma XC, Liang X\*. Effect of the different implant protocols on peri-implant bone: a 6-month prospective study in beagle dogs. *Int J Artif Organs*. 2017;40(12):701-708.
- **Song D**, Ma GW, Liang X\*. One review in Chinese: Research progress on osseoperception around the dental implant. *J Dalian Med University*. DOI: 10.117.24/Jdmu:2017.03.07. (in Chinese).
- **Song D\***, Huang Y, Shujaat S, Orhan K, Lambrichts I, Jacobs R, et al. Effect of platelet-rich and platelet-poor plasma on peri-implant innervation in dog mandibles. *Int J Implant Dent*. 2019;5(40). <https://doi.org/10.1186/s40729-019-0193-3>.
- **Song D**, Liang X, Zheng H, Shujaat S, van Dessel J, Jacobs R\*, et al. Peri-implant myelinated nerve fibers: Histological findings in dogs. *J Periodontol Res*. 2020. <https://doi.org/10.1111/jre.12744>.

- **Song D\***, Shujaat S, Zhao RT, Huang Y, Orhan K, Jacobs R, et, al. In vivo quantification of mandibular bone remodeling and vascular changes in a Wistar rat model: a novel HR-MRI and micro-CT fusion technique. *Imaging Sci Dent*. 2020 Sep;50(3):199-208. doi: 10.5624/isd.2020.50.3.199.
- Orhan K, Pauwels R, Chen Y, **Song D**, Jacobs R. Estimation of the radiation dose for dental spectral cone-beam CT. *Dentomaxillofac Radiol*. 2020 Dec 22:20200372. Doi: 10.1259/dmfr.20200372.
- **Song D\***, Shujaat S, Huang Y, Politis C, Lambrichts I, Jacobs R, et al. Diagnostic accuracy of CBCT versus intraoral imaging for assessment of peri-implant bone defects. *BMC Med Imaging*. 2021;21:23. <https://doi.org/10.1186/s12880-021-00557-9>.
- **Song D\***, Shujaat S, Huang Y, Politis C, Lambrichts I, Jacobs R, et al. Effect of platelet-rich and platelet-poor plasma on 3D bone-to-implant contact: A preclinical micro-CT study. *Int J Implant Dent*. 2021;11. <https://doi.org/10.1186/s40729-021-00291-5>.

## PRESENTED WORK AND ABSTRACT

---

- Poster presentation “Effect of platelet concentration on the density of myelinated nerve fibres in the peri-implants. An experimental Study”. **Song D**, Huang Y, Lambrichts I, Shujaat S, Jacobs R. (2018). September 7-9<sup>th</sup>, 2018. European Meeting on Enhanced nature Healing in Dentistry. In Leuven, Belgium.
- Abstract “Radiographic effects of bisphosphonate (BPs) on jawbone and blood vessel in vivo micro-CT examination: A pilot study” **Song D**, Huang Y, Zhao R, Lambrichts I, Politis C, Jacobs R. The 6<sup>th</sup> EADMFR junior meeting. 3-5<sup>th</sup> Feb 2018, Istanbul, Turkey.
- Poster presentation “ Diagnostic accuracy of CBCT versus intraoral imaging for the assessment of peri-implant bone defects”. Song D, Shujaat S, De Faria Vasconcelos K, Huang Y, Politis C, Lambrichts I, Jacobs R. The 23<sup>rd</sup> International Congress of DentoMaxilloFacial Radiology. 28<sup>th</sup> April – 1<sup>st</sup> May 2021, Gwangju, South Korea.